Title
Geometry, topology, and response in condensed matter systems

Author
Varjas, Daniel

Publication Date
2016

Peer reviewed|Thesis/dissertation

Geometry, topology, and response in condensed matter systems

by

Dániel Varjas

A dissertation submitted in partial satisfaction of the

requirements for the degree of

Doctor of Philosophy

in

Physics

in the

Graduate Division

of the

University of California, Berkeley

Committee in charge:

Professor Joel E. Moore, Chair
Professor Ashvin Vishwanath
Professor Sayeef Salahuddin

Summer 2016

Geometry, topology, and response in condensed matter systems

Abstract

Geometry, topology, and response in condensed matter systems

by

Dániel Varjas

Doctor of Philosophy in Physics

University of California, Berkeley

Professor Joel E. Moore, Chair

Topological order provides a new paradigm to view phases of matter. Unlike conventional symmetry breaking order, these states are not distinguished by different patterns of symmetry breaking, instead by their intricate mathematical structure, topology. By the bulk-boundary correspondence, the nontrivial topology of the bulk results in robust gapless excitations on symmetry preserving surfaces. We utilize both of these views to study topological phases together with the analysis of their quantized physical responses to perturbations.

First we study the edge excitations of strongly interacting abelian fractional quantum Hall liquids on an infinite strip geometry. We use the infinite density matrix renormalization group method to numerically measure edge exponents in model systems, including subleading orders. Using analytic methods we derive a generalized Luttinger's theorem that relates momenta of edge excitations.

Next we consider topological crystalline insulators protected by space group symmetry. After reviewing the general formalism, we present results about the quantization of the magnetoelectric response protected by orientation-reversing space group symmetries. We construct and analyze insulating and superconducting tight-binding models with glide symmetry in three dimensions to illustrate the general result. Following this, we derive constraints on weak indices of three dimensional topological insulators imposed by space group symmetries. We focus on spin-orbit coupled insulators with and without time reversal invariance and consider both symmorphic and nonsymmorphic symmetries.

Finally, we calculate the response of metals and generalize the notion of the magnetoelectric effect to noninteracting gapless systems. We use semiclassical dynamics to study the magnetopiezoelectric effect, the current response to elastic strain in static external magnetic fields.

To my parents and grandparents.

Contents

Contents **ii**

I Introduction 1

1 Topological orders with and without symmetry 2
1.1 Symmetry and symmetry breaking . . . 2
1.2 Topological order . . . 4
1.2.1 Intrinsic topological order . . . 4
1.2.2 Symmetry protected topological order . . . 5
1.3 Topological phases of noninteracting fermions . . . 7
1.3.1 Quantum anomalous Hall effect and Chern insulators . . . 7
1.3.2 On-site symmetries and the ten-fold way . . . 9
1.3.3 Quantum spin Hall effect . . . 12
1.3.4 Three dimensional topological insulators . . . 13
1.3.5 Topological crystalline insulators . . . 13
1.3.6 Weyl semimetals . . . 14
1.4 Fractional Quantum Hall effect . . . 15
1.4.1 Bulk theory . . . 15
1.4.2 Edge theory . . . 17
1.5 Outlook . . . 18

2 Overview of dissertation 19

II Edge states of 2D quantum liquids 21

3 Edge excitations of abelian FQH states 22
3.1 Introduction . . . 22
3.2 Model and Methodology . . . 24
3.2.1 iDMRG and Finite Entanglement Scaling . . . 26
3.2.2 Obtaining the edge-exponents . . . 26

3.3 Edge universality at $\nu = 1/3, 2/5$ and $2/3$. 28
3.3.1 The $\nu = 1/3$ edge 28
3.3.2 Renormalization of edge exponents for thin strips 29
3.3.3 The $\nu = 2/5$ edge 31
3.3.4 The $\nu = 2/3$ edge 32
3.4 Edge states in the 1D picture 33
3.4.1 A Generalized Luttinger Theorem for Hall Droplets 33
3.4.2 Adiabatic continuity between Abelian edges 35
3.5 Conclusion and future directions 36
3.6 Acknowledgments 37

III Space group symmetry and topology 38

4 Geometry in band structures of solids 39
4.1 Space group symmetries 39
4.2 Bloch's theorem 40
4.2.1 Bloch's theorem and the Brillouin zone 40
4.2.2 Conventions for Bloch functions 41
4.3 Electromagnetic response of free fermions 42
4.4 Differential geometry of band structures 43
4.4.1 Overview of coordinate-free formalism 43
4.4.2 Berry curvature 44
4.4.3 Chern and Chern-Simons forms 46
4.5 BdG formalism 48
4.6 Transformation properties 49
4.6.1 Global symmetries 49
4.6.2 Space group symmetries 51
4.6.3 Magnetic space group symmetries 53

5 θ-terms and topological response with nonsymmorphic symmetries 55
5.1 Introduction 55
5.2 Magnetoelectric Coupling and $\mathbb{Z}_2$ Invariant In Mirror and Glide Symmetric Insulators 57
5.2.1 Proof of quantization of θ 58
5.2.2 Mirror symmetry 60
5.2.3 Glide symmetry 61
5.3 Topological Crystalline Superconductors in Class D 63
5.3.1 Bulk invariant and surface thermal Hall conductance 64
5.3.2 Microscopic model with glide plane in 3d 64
5.3.3 Lower dimensional topological invariants 65
5.3.4 Surface Dirac model 66

5.4 Class C superconductor with glide plane in 3d 67
5.4.1 Bulk invariant and SU(2) axion term 67
5.4.2 Microscopic model with glide plane 69
5.4.3 Surface Dirac model 70
5.5 Conclusions 71
5.6 Acknowledgements 71
Appendix 72
5.A Evaluation of Chern-Simons 3-form and second Chern-form 72
5.B Relation to earlier definition of $\mathbb{Z}_2$ index in class A 75

6 Space group constraints on weak indices in topological insulators 77
6.1 Introduction 77
6.2 Chern number and Hall conductivity (class A) 78
6.2.1 Hall conductivity of a 3D insulator 78
6.2.2 Screw symmetry enforced constraints 80
6.3 Weak TI indices (class AII) 82
6.3.1 Bravais lattice 82
6.3.2 Nonsymorphic symmetries 83
6.4 Conclusion 85
6.5 Acknowledgements 85
Appendix 86
6.A Generalization to topological superconductors 86
6.B No Constraints on Strong TI's 87

7 Zero and one dimensional invariants in TCI's 89
7.1 Topological protection with restricted equivalence 89
7.2 Space group representations and zero dimensional invariants 90
7.2.1 Representation theory of space groups 90
7.2.2 Classification at fixed filling 91
7.2.3 Representation valued invariants on simple lattices 92
7.2.4 Construction of atomic insulators 93
7.2.5 Invariants with stable equivalence on continuous space 94
7.3 Wilson loop invariants 97
7.3.1 Transformation properties of Wilson loops 97
7.3.2 TCI's from Wilson loop invariants 99
7.3.3 Derivation of the Chern number formula with C_n symmetry 99

IV Topological response in metals 101

8 Orbital magnetopiezoelectric effect in metals 102
8.1 Introduction 102

8.2 Methodology 104
8.3 Experimental feasibility 108
8.4 Conclusion 110
8.5 Acknowledgements 110
Appendix 111
8.A Vanishing of j_c^i 111

Bibliography **112**

Acknowledgments

First and foremost, I am grateful to my parents and grandparents for always encouraging my scientific curiosity, their love and continued support throughout all these years of academic pursuit. I dedicate this dissertation to you.

I am grateful to those who guided me early on as a physicist: to István Kispál for sowing the first seeds of my love for physics in high school and to Karlo Penc and Gergely Zaránd for advising me during my master's program in Budapest. Without them I would not be completing my graduate studies at Berkeley now.

I thank my collaborators, Adolfo Grushin, Roni Ilan, Fernando de Juan, Yuan-Ming Lu, Joel Moore and Mike Zaletel. Research is a cooperative endeavor, which they did not only make possible, but provided guidance, support and entertainment along the way. I also thank my fellow condensed matter theorists, Philipp Dumitrescu, Takahiro Morimoto, Sid Parameswaran, Adrian Po, Andrew Potter, Aaron Szasz and Norman Yao among many others for the enlightening discussions about physics and many other subjects.

I am grateful to my friends from Hungary and Berkeley for their support, encouragement, all the great times we had and the wonderful memories we made.

I would also like to thank Ashvin Vishwanath and Sayeef Salahuddin for serving on my dissertation committee, and James Analytis for serving on my qualifying exam committee.

Finally, I am deeply grateful to my Ph.D. advisor, Joel Moore for his mentorship throughout my graduate studies, his deep insights that guided my research, his unwavering confidence in my abilities, and his efforts to secure financial support. My discussions with him profoundly changed the way I view physics and it was a great honor to be his student.

Part I

Introduction

Chapter 1

Topological orders with and without symmetry

1.1 Symmetry and symmetry breaking

The huge success of characterizing phases of matter in the 20th century relied on Lev Landau's insight[1]: phases of matter are distinguished by the symmetry of ordering. The underlying Hamiltonian of our physical world has a large symmetry, for example continuous translation and rotation invariance. Solid state systems, however, develop a crystal structure that only retains discrete translations and rotations. The symmetry of the high temperature phase, such as gas or liquid gets spontaneously broken at lower temperatures in order to find the minimum energy configuration. This is a fight between energy and entropy, the system tries to minimize its free energy $F = E - TS$. At high temperatures a disordered phase with high entropy is favorable, that, on average, is highly symmetric. As T is lowered, energy minimization becomes dominant and a highly ordered phase with low entropy is selected.

The mathematical tool used to characterize symmetries is group theory. A symmetry operation maps one history of the system to another, this is a group element. Products of elements are formed by successive applications of the operations and every operation has its inverse by undoing it.

Most generally we say a system has a given symmetry, if a possible history is mapped onto another possible history. In the following we restrict our attention to systems invariant under continuous time translations. This allows the definition of conserved energy, and we further demand that symmetries leave the energy invariant. We say that a steady state – or equilibrium ensamble – is symmetric if it is mapped to itself. Now we see that a state with spontaneously broken symmetry is necessarily degenerate, there are symmetry operations that map it onto different states with the same energy. For example, a crystal is different from its image translated by a fraction of a lattice vector, but otherwise the two states have identical properties, as the underlying Hamiltonian has continuous translation invariance.

The symmetry breaking is characterized by a *local* order parameter, that is zero in the

symmetric phase and distinguishes the various broken symmetry states. Across a phase-transition it changes non-analytically, it is discontinuous across a first order phase transition or its derivative jumps at a second order transition. Phase transitions are also possible without symmetry breaking, such as the liquid-gas transition, but in this case the transition can be circumvented and the two phases are connected by a path where all properties change analytically.

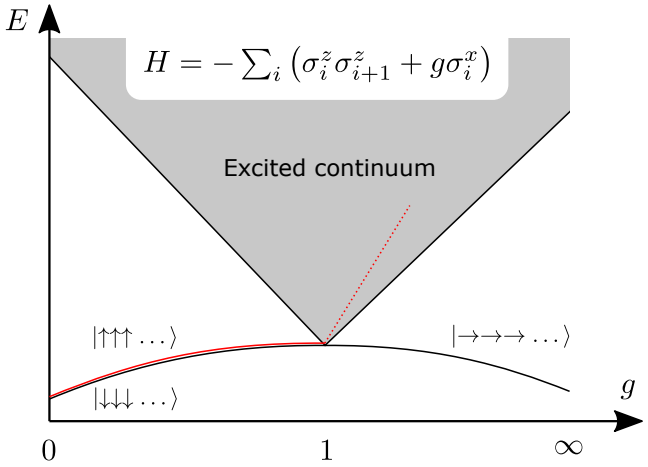

Figure 1.1: Sketch of the low energy spectrum of the transverse field Ising chain as it is tuned across the symmetry breaking transition at $g = 1$. As the degeneracy of the ground state changes across the transition, some ground states must merge into the excited continuum (red) and the gap must close at the transition.

For simplicity, in the following we only consider zero temperature gapped phases of matter. A second order symmetry breaking transition between two gapped phases necessarily comes with the closing of the gap (Fig. 1.1). This follows from the change in the ground state degeneracy: to change it, some states from the excited continuum must continuously come down to the ground state energy. In the next section we will see that such a gap closing may also be necessary even when the two ground states are both symmetric and nondegenerate, as they can be still distinguished by *topology* that cannot change continuously.

1.2 Topological order

1.2.1 Intrinsic topological order

Here we endeavor to classify local Hamiltonians with unique[1] gapped ground states by their topology. By *local* we mean the Hamiltonian is a sum of terms acting on spatially localized regions, this is necessary to make sense of the dimensionality of the system. We consider two systems to be in the same phase if their Hamiltonians can be continuously deformed into each other without closing the gap, in other words, they are *adiabatically connected*. Furthermore, to avoid distinguishing systems that only differ by some frozen degrees of freedom, we also allow adding a trivial atomic insulator, where the Hamiltonian is just a sum of strictly local, non-overlapping gapped terms, acting on the new degrees of freedom. Topological order is called *intrinsic* if it does not rely on any symmetry, so for now we allow all Hamiltonians without any symmetry restriction.

Given the dimensionality and the statistics (bosonic or fermionic) we can create a landscape of all local Hamiltonians (Fig. 1.2). It consists of connected regions with the gap open and intervening gapless areas. One of these regions contains the trivial atomic insulator, this is the trivial phase. The other phases separated from it by gapless areas have intrinsic topological order, as it is impossible to adiabatically deform them the trivial state using a path of gapped Hamiltonians.

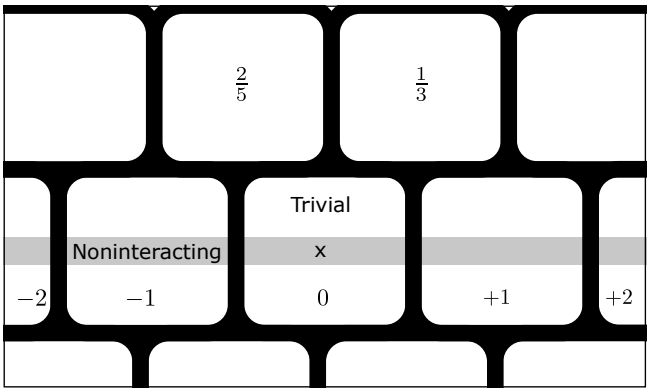

Figure 1.2: Schematic phase diagram of fermions in 2 dimensions. The white regions represent gapped topological phases, while at the black borders the gap closes. The shaded area is the space of free Hamiltonins. The atomic insulator (x) is in the trivial phase, there is an infinite series of IQH states labeled by integers, FQH states labeled by rational fractions among other possible phases.

Let us return to the question what "adding" two systems together means. It is easiest to

[1]We assume the ground state is unique in an infinite geometry. On a closed manifold with a nontrivial topology, such as a torus, a finite topological degeneracy of locally indistinguishable states may arise.

visualize in two dimensions, take the two systems as sheets and lay them on top of each other. From now on we treat them as a single 2d system and allow deformations by local terms in the Hamiltonian that couple degrees of freedom in different layers. This commutative and associative *stacking* operation maps two topological phases on a third, with the trivial phase as the unit element, defining a monoid structure on the set of topological phases. Phases are called invertible if there is an inverse phase, such that stacking the two we get a trivial phase. Thus we have a group structure on the set of invertible topological phases.

Consider for example free fermions in 2 dimensions. In a strong external magnetic field the spectrum splits into Landau-levels (LL's), when some of these are completely filled, we get an integer quantum Hall (IQH) state[2, 3]. Such states are characterized by a gapped bulk with vanishing longitudinal conductance and Hall conductance quantized in integer multiples of the conductance quantum, $\sigma_{xy} = Ce^2/h$. These states can also be mimicked using lattice models with no external magnetic field[4], termed quantized anomalous Hall (QAH) effect. The integer C is identified as the Chern number of the occupied bands[5] characterizing the nontrivial topology of the ground state wave function. C is additive under stacking, resulting in a $\mathbb{Z}$ classification of fermions in 2d. We review these phases in Sec. 1.3.1 in more detail.

Turning on interactions, gapped states can stabilize at rational fractions of the LL's filled, called fractional quantum Hall effect (FQHE)[6, 7]. These states feature fractional excitations, which carry fractions of the electric charge of the underlying fermions, as well as fractional exchange statistics. Such state is impossible in a noninteracting system, as all excitations there have the same character as the underlying fermions. For more details see Sec. 1.4.

Quantum Hall states feature one of the hallmarks of topological order: gapless edge states. One way to understand this, is to imagine a family of translation invariant Hamiltonians that interpolate between the topological bulk and the trivial vacuum. If the system has a soft edge, such that the Hamiltonian changes slowly compared to microscopic length scales, locally it looks like a translation invariant system. However, we know that any interpolation between a topological and trivial system must close the gap at some point, so there must be a gapless interface between the two phases.

1.2.2 Symmetry protected topological order

The topological classification can be refined if we restrict to Hamiltonians with a certain symmetry. Condensed matter physics deals with the low energy excitations over some already symmetry broken ground state of the very symmetric high energy Hamiltonian. But some of these symmetries are more robust than others, so it is reasonable to restrict our attention to deformations that preserve some symmetry. For example time reversal symmetry (TRS, $\mathcal{T}$) is only broken in magnetically ordered materials, which is the non-generic case. The $U(1)$ charge conservation symmetry is often implicitly assumed, even though it is broken in superconductors. The particle-hole symmetry (PHS, $\mathcal{C}$ or charge-conjugation symmetry) in superconductors is not even a physical symmetry, just a symmetry of the overcomplete

Bogoliubov-de Gennes (BdG) description, thus it can never be broken.[2]

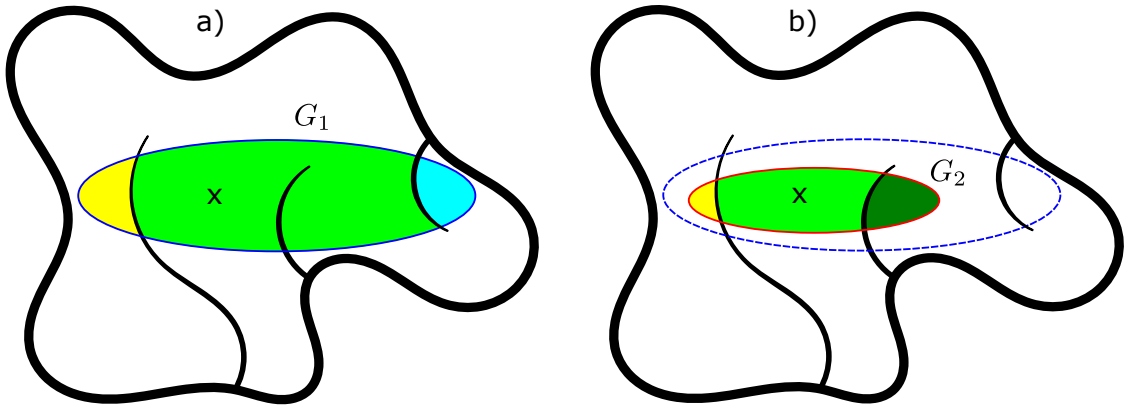

Figure 1.3: A different view of the trivial phase (black border) with the atomic insulator in it (x). Note the gapless areas proturding into the phase that can be circumvented. a) Subspace of Hamiltonians with symmetry group G_1 (blue ellipse). With the added symmetry constraint the trivial phase splits into SPT phases. b) Subspace of Hamiltonians with a higher symmetry $G_2 > G_1$ (red ellipse). With the increased symmetry some phases split into more phases, others are ruled out.

Starting from the trivial phase of the intrinsic classification, let us impose a symmetry group G_1 that constrains the possible Hamiltonians. We still demand that the ground state is unique, which implies that it is symmetric. Regions of the phase that were connected by paths breaking the symmetry, may now be separated (Fig. 1.3 a)). We term these *symmetry protected topological* (SPT) phases, with the symmetric atomic insulator defining the trivial phase.

Further increasing the symmetry to G_2 (such that G_1 is a subgroup of it) has a twofold effect on the classification (Fig. 1.3 b)). On one hand, phases that were connected in G_1 may become separated in G_2, enriching the structure of the phase diagram. On the other hand, a G_1-SPT phase may necessarily break G_2 and this phase is ruled out by the more stringent symmetry.

The classification of SPT phases admits an abelian group structure under stacking and has been extensively studied using group cohomology theory[8]. Early studies only considered on-site symmetries, that act as a product of identical commuting local operators centered at each site. These symmetries include the $\mathbb{Z}_2$ spin flip symmetry of the Ising model, time reversal, charge conservation or particle-hole symmetry. Later it was realized that translation invariance of the lattice can lead to new SPT phases[9] called *weak topological*

[2]Note that this is not the physical particle-hole symmetry of the electronic spectral function that is only approximate at low energies.

phases. Other lattice symmetries can further enrich the classification leading to *crystalline topological phases*[10].

A similar classification can be carried out for the other intrinsic phases in the presence of symmetries leading to *symmetry enriched topological order*.

1.3 Topological phases of noninteracting fermions

1.3.1 Quantum anomalous Hall effect and Chern insulators

As a basic example of a topological phase of non-interacting fermions, let us examine two dimensional insulators with only charge conservation symmetry. To further simplify the arguments we will look at translation invariant systems with only two bands (Sec. 4.2).

The Hamiltonian of such systems is a mapping $H_{\mathbf{k}}$ from the Brillouin-zone (BZ) torus T^2 to the space of 2 by 2 Hermitian matrices. The most generic such function has the form

$$H_{\mathbf{k}} = \mathbf{d}_{\mathbf{k}} \cdot \boldsymbol{\sigma} + \mu_{\mathbf{k}} \mathbb{1} \tag{1.1}$$

where $\mathbf{d}$ is a 3 dimensional vector and $\boldsymbol{\sigma}$ is the vector of Pauli matrices. The spectrum is $\epsilon^{\pm}_{\mathbf{k}} = \mu_{\mathbf{k}} \pm d_{\mathbf{k}}$ with $d = |\mathbf{d}|$. To get a gapped insulator with the lower band filled we need $d > 0$ and $|\mu| < d$, for simplicity we set $\mu = 0$ in the following. As the Hamiltonian at a fixed $\mathbf{k}$ is formally identical to that of a spin-1/2 in a magnetic field in the $-\mathbf{d}$ direction, the eigenstates $\left|u^{\pm}_{\mathbf{k}}\right\rangle$ are spins pointing parallel or antiparallel to $\mathbf{d}$ and can be represented as points on the Bloch-sphere.

As we saw, gapped Hamiltonians can be represented as maps from a torus to 3d space excluding the origin, and their ground states (the $|u^-\rangle$ band) as maps from a torus to the unit sphere. We want to study the topology of such maps, so we allow continuous deformations. The two views are equivalent, as we can project points of 3d space onto the unit sphere by continuously "flattening" it, this corresponds to continuously changing the magnitude of $\mathbf{d}$ to 1 without changing its direction.

Now we can classify the topological phases using this intuitive picture (Fig. 1.4). As the origin is excluded, a torus that does not enclose it cannot be "dragged through" this forbidden point without "breaking the surface" such that the origin is now inside. This is easy to see, considering that the former torus can be contracted to a single point, while the latter cannot. Tori that do not enclose the origin form the trivial class, as they can be deformed to any constant map. There are also two distinct directionalities in which the torus can wrap the origin together with the possibility of multiple wrappings in either direction. Mathematically, the homotopy classes of maps from the 2-torus to the 2-sphere (or the punctured 3d space) are classified by this integer wrapping number.

This classification can be extended to multiple bands using the Berry curvature and Chern-number (Sec. 4.4). To characterize geometry of the band-structure we introduce the Berry connection for the n-th band

$$\mathcal{A}^n_{i,\mathbf{k}} = \langle u^n_{\mathbf{k}} | \left(\partial_i \left| u^n_{\mathbf{k}} \right\rangle\right) \tag{1.2}$$

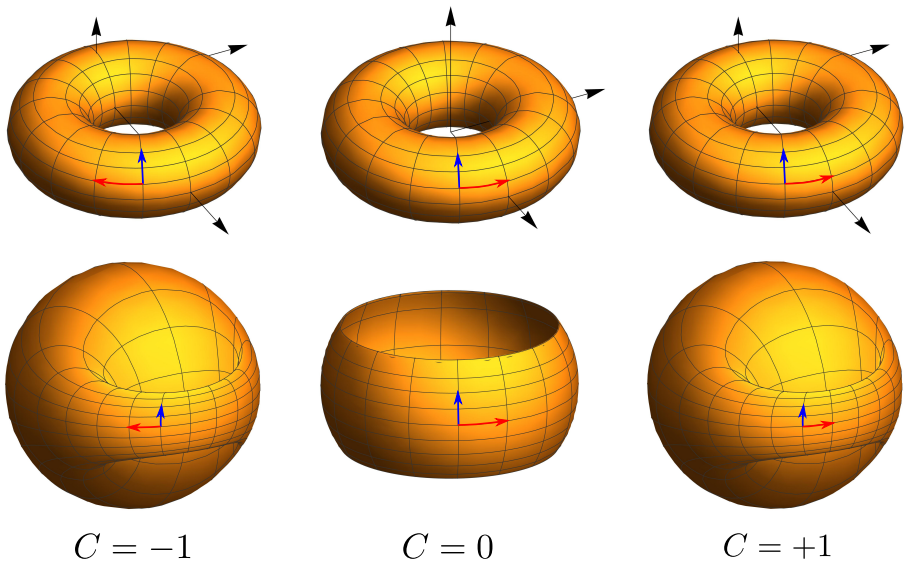

Figure 1.4: Topologically distinct embeddings of the BZ torus into the space of 2-band Hamiltonians (top row) and the corresponding maps to the Bloch sphere (bottom row) indexed by the Chern number.

where ∂_i is the derivative with respect to the i-th coordinate in $\mathbf{k}$-space. It is analogous to the electromagnetic vector potential, and we define the associated "magnetic field", the Berry curvature

$$\Omega^n_{\mathbf{k}} = \partial_x \mathcal{A}^n_{y,\mathbf{k}} - \partial_y \mathcal{A}^n_{x,\mathbf{k}}. \tag{1.3}$$

It can be visualized as a normal magnetic field penetrating the BZ torus. Its total flux for all occupied bands is quantized in integer multiples of 4π, so the Chern number is

$$C = \frac{1}{4\pi} \sum_{n \in \text{occ.}} \int_{\text{BZ}} d^2k \; \Omega^n_{\mathbf{k}}. \tag{1.4}$$

C is additive under stacking, and provides the $\mathbb{Z}$ classification for noninteracting insulators with only charge conservation symmetry. It can also be shown by studying homotopy classes of Hamiltonians[11] that this classification is complete, all the information is captured by C.

The Chern number is related to the Hall conductance as $\sigma_{xy} = (e^2/h)\, C$ [5, 12]. This behavior is similar to the IQHE, but without external magnetic field, hence the name quantum anomalous Hall effect. This effect has been experimentally observed in magnetic insulators[13].

These simple models offer an easy way to visualize the topological edge states. For example the Hamiltonian

$$H_{\mathbf{k}} = \sin k_x \sigma_x + \sin k_y \sigma_y + (\cos k_x + \cos k_y - m)\, \sigma_z \tag{1.5}$$

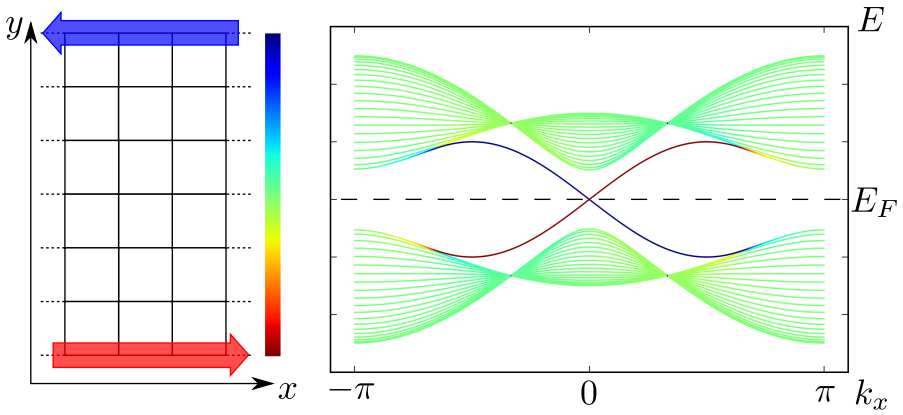

Figure 1.5: Left: Schematic view of a Chern insulator in a strip geometry with finite width in the y direction. Right: Band structure for a 20 site wide strip. The color code shows the center of mass location of the bands in the y direction.

can be realized as a nearest neighbor tight-binding model on the square lattice with two orbitals per site. Cutting a strip that has a finite L_y number of unit cells in the y direction but infinite in x reduces the system to effectively 1d. Now each unit cell has L_y sites, so we find $2L_y$ bands as a function of k_x. Most of these bands correspond to standing waves in the y direction that have near homogeneous probability density across the strip. The dispersion approximately maps out slices of the bulk 2d dispersion at evenly spaced k_y values. If the system is in the topological phase, however, we find states that are exponentially localized on one edge. In Fig. 1.5 we show the numerically calculated band structure at $m = 1$. The bulk bands are gapped and the center of mass is near the center of the strip. We find two counterpropagating modes crossing the gap that are localized on opposite edges of the strip, these are the chiral edge modes analogous to those in IQHE. We often use bandstructures in the strip (or slab in 3d) geometry to illustrate surface states in the rest of the dissertation.

1.3.2 On-site symmetries and the ten-fold way

Translation invariant systems of non-interacting fermions in other dimensions and with additional on-site symmetries can be classified using similar methods: by finding the homotopy classes and associated invariants of maps $H_{\mathbf{k}}$ from the d-dimensional BZ torus to a constrained set of Hermitian matrices. On-site symmetries act strictly locally, in an appropriately chosen basis their action can be written as a product of commuting operators that map non-overlapping compact regions onto themselves. The two most universal symmetries are time reversal ($\mathcal{T}$) and charge conjugation ($\mathcal{C}$) that combine with charge conservation and spin rotation non-trivially, and we focus on them here. Free fermions can form topological phases thanks to the Fermi exclusion principle, by completely filling bands with non-trivial

topology. Free bosons at zero temperature, on the other hand, form a gapless Bose-Einstein condensate. It is possible to force bosons to evenly fill entire bands by fine-tuning interactions or by pumping. Even though free bosons are not in a topological phase, they still show edge states in the bulk gap when in a topological band structure.

Time reversal acts as an antiunitary operator on the Hilbert space. This can be seen by looking at the time-dependent Schrödinger equation

$$i\partial_t \left|\Psi(t)\right\rangle = H(t) \left|\Psi(t)\right\rangle . \tag{1.6}$$

Besides reversing the direction of time, time reversal may also act in the Hilbert space of a given instance t in a local, norm-preserving fashion. The time reversed history of the wave funcion $\left|\Psi(t)\right\rangle$ reads $\mathcal{T}\left|\Psi(-t)\right\rangle$ and the time reversed Hamiltonain as $\mathcal{T}H(-t)\mathcal{T}^{-1}$. Substituting this into the Schrödinger equation and renaming $t \to -t$, we get

$$-i\partial_t \mathcal{T}\left|\Psi(t)\right\rangle = \mathcal{T}H(t)\mathcal{T}^{-1}\mathcal{T}\left|\Psi(t)\right\rangle = \mathcal{T}H(t)\left|\Psi(t)\right\rangle = \mathcal{T}\left(i\partial_t\right)\left|\Psi(t)\right\rangle . \tag{1.7}$$

As $\mathcal{T}$ is temporally local, it must commute with ∂_t, so the only choice is making it antiunitary such that it anticommutes with i. Any antiunitary operator can be written as a combination of a unitary and complex conjugation ($\mathcal{K}$). Furthermore, we demand that if we reverse time twice, the result is physically identical to the original state, $\mathcal{T}^2 \propto \mathbb{1}$ forming the two-element group $\mathbb{Z}_2^{\mathcal{T}}$. From the properties of $\mathcal{T}$ it follows that there are only two choices, $\mathcal{T}^2 = \pm\mathbb{1}$. For physical spin-1/2 fermions $\mathcal{T} = \sigma_y\mathcal{K}$ and $\mathcal{T}^2 = -\mathbb{1}$. The other possibility may be realized in systems without spin-orbit coupling, which allows combining $\mathcal{T}$ with a spin flip and only focusing on one spin sector. This relies on $SU(2)_c$ spin rotation symmetry, which is only approximate in a solid state system. $\mathcal{T}^2 = +\mathbb{1}$ is also possible in various effective models, or if the system is invariant under TR combined with a π spin rotation, but not under TR or spin rotations separately[14].

Charge-conjugation (or particle-hole) symmetry is somewhat more subtle. We may view it as an extra antiunitary $\mathbb{Z}_2^{\mathcal{C}}$ "antisymmetry", an operator that anticommutes with the Hamiltonian such that $\mathcal{C}H = -H\mathcal{C}$. Again, we may choose whether $\mathcal{C}^2 = \pm\mathbb{1}$.

On the other hand, in the context of the Bogoliubov-de Gennes (BdG) formalism (Sec. 4.5) it is not a physical symmetry, merely a constraint enforcing Hermiticity and Fermi-statistics in a formalism that doubly counts degrees of freedom. It is actually *the lack of* charge (or particle number) conservation. In the low energy theory of a paired superconductor charge conservation is broken, as a Cooper-pair from the condensate can break up any time and create two fermionic Bogoliubov quasiparticles, so we allow fermion bilinears of two creation or annihilation operators $c_i c_j$ or $c_i^\dagger c_j^\dagger$. If charge is conserved, only terms like $c_i^\dagger c_j$ are allowed, and the system has a global $U(1)_c$ phase symmetry: $c_i \to e^{i\phi}c_i$ (together with $c_i^\dagger \to e^{-i\phi}c_i^\dagger$).

With no symmetry only the $\mathcal{C}^2 = +\mathbb{1}$ case is realized with $\mathcal{C} = \tau_x\mathcal{K}$ where τ_x flips particle and hole-like states. To get $\mathcal{C}^2 = -\mathbb{1}$ we need to demand $SU(2)_s$ spin rotation invariance, these are the singlet superconductors.

Both $\mathcal{T}$ and $\mathcal{C}$ can be absent, or square to either of the two signs which gives 9 possibilities. If both symmetries are present, their combination $\mathcal{S} = \mathcal{C}\mathcal{T}$ is a unitary "antisymmetry"

called *chiral symmetry*. Chiral symmetry may be present without $\mathcal{T}$ or $\mathcal{C}$, it appears for example in insulators on bipartite lattices or TR invariant superconductors with $U(1)_s$ spin rotation invariance[15]. This completes the list of the 10 Altland-Zirnbauer (AZ) symmetry classes[16].

Let us briefly review the most important symmetry classes.

- **Class A** This is the class of TR breaking (magnetic) insulators. Only relies on charge conservation symmetry. The Chern insulators of the previous section represent this class in $d = 2$. The class can also be realized in TR breaking superconductors with spin-z conservation.
- **Class AII** Time reversal invariant insulators, relies on charge conservation and time reversal symmetry. The quantum spin Hall (QSH) effect in 2d[17–19] and the strong TI in 3d[9] belong to this class, both require strong spin-orbit coupling (SOC).
- **Class AI** Time reversal invariant insulators without spin-orbit coupling. Relies on full spin rotation invariance. SOC approximately vanishes in materials consisting of light elements.
- **Class D** TR breaking superconductors. This class requires no symmetry, any combination of singlet and triplet pairing is allowed. There is a residual fermion parity conservation that cannot be broken in any free (quadratic) theory.
- **Class DIII** TR invariant superconductors.
- **Class C** TR breaking superconductors without SOC. Needs full spin rotation invariance, only singlet pairing is allowed.
- **Class CI** TR invariant superconductors without SOC.

The SPT phases of systems in the ten-fold way can be classified using various techniques[11, 15] (Tab. 1.1). There is a remarkable periodicity in the classification which can be explained by the study of Clifford-algebras and K-theory. The two unitary classes (without antiunitary symmetries) repeat a pattern for changing d by 2. The 8 real classes, repeat a pattern with a periodicity of 8, these are manifestations of the Bott periodicity. A common feature of these phases is that they admit an effective long-wavelength topological field theory description[20, 21]. This guarantees stability in the presence of weak, symmetry preserving disorder and interactions. However, different non-interacting phases may be connected through strongly interacting gapped symmetric deformations [22, 23].

The classification can be easily enhanced by including additional unitary on-site symmetries that commute with the symmetries considered so far. As an on-site symmetry acts locally and identically at every $\mathbf{k}$-point, $H_{\mathbf{k}}$ can be block-diagonalized, and the above classification applied to each block separately, resulting in a *symmetry graded* classification. This can also be applied for spatial symmetries on the subspace of the BZ that is left pointwise invariant (Sec. 1.3.5).

class	$\mathcal{T}$	$\mathcal{C}$	$\mathcal{S}$	physical symmetry	d=0	1	2	3	4	5	6	7
A	0	0	0	$U(1)_{c/s}$	$\mathbb{Z}$		$\mathbb{Z}$		$\mathbb{Z}$		$\mathbb{Z}$	
AIII	0	0	1	$U(1)_s \times \mathbb{Z}_2^{\mathcal{T}}$		$\mathbb{Z}$		$\mathbb{Z}$		$\mathbb{Z}$		$\mathbb{Z}$
AI	1	0	0	$U(1)_c \rtimes \mathbb{Z}_2^{\mathcal{T}} \times SU(2)_s$	$\mathbb{Z}$				$2\mathbb{Z}$		$\mathbb{Z}_2$	$\mathbb{Z}_2$
BDI	1	1	1	$\mathbb{Z}_2^{\mathcal{T}+}$	$\mathbb{Z}$	$\mathbb{Z}$				$2\mathbb{Z}$		$\mathbb{Z}_2$
D	0	1	0	0	$\mathbb{Z}_2$	$\mathbb{Z}_2$	$\mathbb{Z}$				$2\mathbb{Z}$	
DIII	-1	1	1	$\mathbb{Z}_2^{\mathcal{T}}$		$\mathbb{Z}_2$	$\mathbb{Z}_2$	$\mathbb{Z}$				$2\mathbb{Z}$
AII	-1	0	0	$U(1)_c \rtimes \mathbb{Z}_2^{\mathcal{T}}$	$2\mathbb{Z}$		$\mathbb{Z}_2$	$\mathbb{Z}_2$	$\mathbb{Z}$			
CII	-1	-1	1	$SU(2)_s \times \mathbb{Z}_2^{\mathcal{T}+}$		$2\mathbb{Z}$		$\mathbb{Z}_2$	$\mathbb{Z}_2$	$\mathbb{Z}$		
C	0	-1	0	$SU(2)_s$			$2\mathbb{Z}$		$\mathbb{Z}_2$	$\mathbb{Z}_2$	$\mathbb{Z}$	
CI	1	-1	1	$SU(2)_s \times \mathbb{Z}_2^{\mathcal{T}}$				$2\mathbb{Z}$		$\mathbb{Z}_2$	$\mathbb{Z}_2$	$\mathbb{Z}$

Table 1.1: The periodic table of non-interacting fermions. Time reversal ($\mathcal{T}$), charge conjugation ($\mathcal{C}$) and chiral ($\mathcal{S}$) symmetry can be absent (0) or square to ± 1. We also list examples of physical symmetries that realize the classes in systems of spin-1/2 fermions. These can be time reversal ($\mathbb{Z}_2^{\mathcal{T}}$), time reversal combined with a π (pseudo)spin rotation ($\mathbb{Z}_2^{\mathcal{T}+}$), charge conservation ($U(1)_c$), spin-$z$ conservation ($U(1)_s$) or full spin rotation invariance ($SU(2)_s$). The classification is marked with the corresponding abelian group ($\mathbb{Z}_2$ or $\mathbb{Z} \simeq 2\mathbb{Z}$), no symbol means there is only one trivial phase.

In the following sections we briefly review the state of theoretical and experimental research in the most studied classes.

1.3.3 Quantum spin Hall effect

The quantum spin Hall state is the nontrivial two dimensional phase in class AII. Shortly after its prediction[17–19] it was experimentally realized[24] in HgTe quantum wells. The hallmark feature of this phase is an insulating bulk with a pair of topologically protected gapless edge modes resulting in $2e^2/h$ longitudinal conductance. The two counterpropagating modes have opposite spin polarization, which prevents backscattering even in the presence of TR invariant disorder.

Quantum spin Hall effect is in fact a misnomer, as in general these systems completely break spin rotation invariance in the bulk. A conserved spin current cannot be defined in the absence of spin conservation. In the effective low energy theory of the edge, the states at the Fermi level select a spin quantization axis. This spin component is approximately conserved and a transverse electric field drives a nonzero spin current, resulting in a spin-hall conductance of $2\frac{e}{4\pi}$. This picture is only correct in a pristine edge with translation invariance, a spatial modulation of the Fermi level causes the quantization axis to rotate.

The $\mathbb{Z}_2$ classification can also be understood using the edge states. TR invariance de-

mands that modes with opposite momentum carry opposite spin, but the spin direction can be arbitrarily twisted without leaving the phase. Combining two QSH edges, where the right movers in one system have the same spin polarization as the left movers in the other, it becomes possible to fully gap the edge.

1.3.4 Three dimensional topological insulators

Class AII hosts a nontrivial topological phase in 3d as well. Similarly to QSH systems, a material realization in strongly spin-orbit coupled Bi_2Se_3 was found[25, 26] shortly after the theoretical proposal[9]. A TR invariant surface is metallic, with a single Dirac cone. If TR invariance is broken, the surface is gapped out, but a half-integer surface Hall conductance is left behind. Both of these situations is impossible in a purely 2d system with the same symmetry, showing the topological nature of the bulk. Stacking two such surface layers, however, results in a trivial or Chern-insulator 2d system, that can arise from the details of the surface termination of a trivial bulk, resulting in a $\mathbb{Z}_2$ classification. A different view of the bulk phase comes form the half-quantized magnetoelectric effect[20, 27]. A topological $\mathbf{E} \cdot \mathbf{B}$ term is allowed in the effective electrodynamics of TR invariant crystalline systems. This results in an electric polarization response parallel to magnetic fields, and conversely a magnetic polarization in response to electric fields.

Besides the above *strong* $\mathbb{Z}_2$ index, 3d crystalline insulators have three further $\mathbb{Z}_2$ invariants[9]. These are analogues of the 2d QSH invariant for TR invariant cuts of the BZ, called *weak* indices. Insulators with only nontrivial weak indices are adiabatically connected to weakly coupled stacks of QSH layers. As explained in the previous section, these layers can pairwise couple to form trivial layers, this is only prevented if the translation invariance between the layers is preserved. Thus we see that these weak phases rely on lattice translations for symmetry protection, the simplest example of topological crystalline insulators.

1.3.5 Topological crystalline insulators

In recent years, extensions the SPT classification scheme to phases protected by space group symmetries gained much attention[14, 28–54], these phases are called *topological crystalline insulators and superconductors* (TCI/TCSC). Initially topological crystalline phases were viewed as unphysical because of the reliance on perfect crystalline order. However, further efforts then showed that weak topological phases have many robust features emerging from topology[55–59], in particular that lattice defects play a special role in these phases and topological zero modes captured by them signal SPT order in the disorder-free bulk[39, 60–62].

As a simple example we present a construction of mirror Chern insulators[28] in terms of weakly coupled Chern insulator layers[63]. Consider a layered 3d material with layers in the xy plane that has two spinful s orbitals on every site. The symmetries we impose are charge conservation (class A), lattice translations and a single mirror. A mirror $M_z : z \to -z$ acts on the spin sector as $i\sigma_z$, the two spin z eigenstates have $\pm i$ eigenvalues. Let us put the

symmetry sectors in half filled Chern-insulator states with the filled $+i$ band with Chern number $C^+ = C$ and the filled $-i$ band with $C^- = -C$.

If the layers are completely decoupled, $H_{\mathbf{k}}$ does not depend on k_z and every xy cut looks like a combination of Chern insulators. In $\mathbf{k}$-space the mirror also flips the sign of k_z, so the Hilbert spaces at $k_z = 0$ or π are mapped onto themselves. This means the mirror eigenvalue is well defined at these two mirror-invariant planes. If we turn on hopping between the layers, the symmetry prevents hybridization of the two mirror sectors at the high symmetry planes. So we see that even though the total Chern number is zero, the mirror symmetry allows the definition of the *mirror Chern number* $C^M = \frac{1}{2}(C^+ - C^-)$ at these invariant planes, signaling nontrivial topological crystalline order. A surface in the xz plane preserves the mirror symmetry, and one finds C pairs of counterpropagating chiral modes as a function of k_x at fixed $k_z = 0$ or π. All the right movers have $+i$ mirror eigenvalue, while the left movers have $-i$, preventing a gap from opening. If we move away from the symmetric k_z values, the surface bands can hybridize, opening a gap, resulting in Dirac-cones on the high symmetry lines.

1.3.6 Weyl semimetals

A different kind of topological states of matter we did not explain in detail are gapless topological phases. These phases are distinguished from trivial gapless phases by robust properties that can only be changed by large deformations[64].

A simple realization of such a phase with noninteracting fermions is a *Weyl semimetal*[65–68]. These 3d materials host pointlike crossings of two bands that are topologically protected. To see this, consider the 2-band effective Hamiltonian linearized near the band-crossing. Most generally

$$H_{\mathbf{k}} = \mathbf{k} \cdot \boldsymbol{\sigma} + \mu \tag{1.8}$$

for an appropriate (not necessarily orthogonal) basis in $\mathbf{k}$-space. The crucial fact is that such Hamiltonians exhaust the full space of 2-band Hamiltonians, an arbitrary perturbation merely shifts the Weyl-point either in momentum or energy, but cannot gap it out. Weyl semimetals are in some sense generic, as the space of 2-band Hamiltonians (ignoring the constant energy shift) is 3 dimensional, a mapping from the 3d Brillouin-zone includes the origin with a finite probability.

There are several topological aspects to this band crossing. Calculating the Berry flux for occupied bands on a sphere surrounding the Weyl-point one finds that it is quantized to ± 1. So the Weyl-node acts as a monopole for the Berry vector potential. This also implies that the total charge of Weyl-points must be zero and they can pairwise annihilate by merging. For cuts of the BZ that separate opposite charges the Berry flux is also nonzero. By analogy to Chern insulators, we expect that the projection of such a cut onto the surface BZ will cross a gapless chiral mode. By moving the surface we can map out the surface dispersion, and find *Fermi arcs* connecting the projections of Weyl-points of opposite charge. These unusual lines of gapless excitations do not enclose a Fermi surface, instead at the end of the arc the

states extend into the bulk to then emerge on the opposite surface of the sample to form the counterpart of the Fermi arc. Besides direct detection using angle-resolved photoemission spectroscopy, the presence of the arcs can also be inferred from quantum oscillations[69]. The study of responses of low symmetry (semi)metals is an active area of research. Many of these responses, such as optical gyrotropy[70, 71] and negative magnetoresistence[72, 73] are forbidden by common symmetries like time reversal and inversion, thus scarcely studied in the literature.

1.4 Fractional Quantum Hall effect

The first strongly interacting topologically ordered states that were experimentally discovered are the fractional quantum Hall (FQH) states[6]. Phenomenologically they manifest in a similar fashion to the integer effect, but with robust plateaus of the Hall conductance at rational fractions of the conductance quantum $\sigma_{xy} = \nu e^2/h$.

Electrons confined to a 2d plane a strong external normal magnetic field form Landau-levels: the single particle energy levels are highly degenerate and evenly spaced. The level spacing is given by the cyclotron energy $E_c = \hbar\omega_c = \hbar eB/m$. The degeneracy of each level is such that there is one electronic state per flux quantum penetrating the surface. This allows the definition of the *filling fraction* $\nu = (hn)\,/\,(eB)$, the number of electrons per flux quantum with the electron number density n. If ν is an integer, some LL's are completely filled, in strong enough magnetic field such that E_c is much larger than other energy scales (such as interactions or temperature) excitations to the next LL are absent and a gapped IQH state is formed. If ν is fractional, however, there is a huge ground state degeneracy in the non-interacting limit and the ground state is chosen exclusively by interactions however weak. Considering this, it is quite surprising that we find a robust gapped state and a mystery why certain fractions are preferred while others are not.

1.4.1 Bulk theory

The first theoretical proposal came from Laughlin[7] in terms of the many-particle wave function

$$\Psi\left(\{z_i\}\right) = \prod_{j<k}(z_j - z_k)^m \exp\left(-\frac{1}{4}\sum_l |z_l|^2\right) \tag{1.9}$$

where $z_i = x_i + iy_i$ are electronic coordinates and m is an odd integer indexing the principal FQH states. These wave functions have the desired properties of uniform charge density and because of the m-th order zeroes, when two electrons are close by, the electrons "avoid" each other and Coulomb energy is lowered compared to an uncorrelated state. Later it was shown by Haldane[74] that the Coulomb interaction can be expanded in terms of the relative angular momentum of the electrons (pseudopotential) and these wave functions are exact eigenstates if the series is truncated after m terms.

The appearance of fractionally charged quasiparticles can be understood at this level, using the charge pumping argument[7]. Imagine starting from a disk of the FQH state, then adiabatically inserting an infinitely thin flux tube at the middle. The changing flux induces a circular electric field, that dives a radial current as demanded by the Hall conductivity $\sigma_{xy} = \nu e^2/h$. When the flux reaches one flux quantum, the Hamiltonian is identical to the original, completing the pumping cycle. However, a total of νe charge leaves the vicinity of the flux tube, thus creating an excited state with a localized fractionally charged excitation, a quasihole. The associated wave function with a quasihole at z_0 can be written as $\Psi_{z_0}(\{z_i\}) = \prod_j (z_j - z_0)\Psi(\{z_i\})$. This picture also explains why the filling fraction and the Hall conductivity coincide. In the symmetric gauge the LL basis functions are concentric annuli. By inserting a flux through the origin, each orbital moves smoothly out, taking the place of the next one by the end of the cycle. Assuming that the structure and the uniform density of the many-body wave function does not change during this process, the charge depletion in the center is exactly given by the filling fraction.

Using the principal states as building blocks it is possible to construct a hierarchy of FQH states[74]. If there is a finite density of quasiparticles (because the filling is sufficiently detuned from $\nu = 1/m$) the quasiparticles can again form a principal state. For example the $\nu = 2/5$ state can be viewed as a $1/3$ state with a $1/5$ state of $e/3$ quasiparticles on top, since $2/5 = 1/3 + 1/3 \times 1/5$.

A different view of the hierarchy is given by the composite fermion picture[75]. A closer look at the Laughlin wave function reveals that an electron encircling another picks up $2\pi m$ phase. 2π is from the Fermi statistics (half of an encirclement amounts to an exchange that comes with a π phase) and the rest can be viewed as magnetic flux "attached" to the electrons. As the average electron density is homogeneous, this attached flux is smeared out and forms part of the external magnetic field. So attaching $m - 1$ flux quanta to each electron, we are left with composite fermions at filling $\nu^* = 1$. So in this picture a FQH state is the IQH state of composite fermions. To build the hierarchy we can go the other way, starting from an integer state at ν^* and attaching $2p$ flux quanta to each electron, for example the $2/5$ state has $\nu^* = 2$, $p = 1$.

This flux attachement argument can be made more rigorous, and after integrating out the fermions in a mean-field approximation we are left with an effective Chern-Simons (CS) gauge theory [76, 77]. A state at the nth level of the hierarchy is described in terms of an n-component statistical gauge-field $a_{I\mu}$ with the Lagrangian density

$$\mathcal{L} = -\frac{1}{4\pi\hbar}\epsilon^{\mu\nu\lambda} K_{IJ} a_{I\mu} \partial_\nu a_{J\lambda} + \frac{e}{2\pi\hbar}\epsilon^{\mu\nu\lambda} t_I A_\mu \partial_\nu a_{I\lambda} \tag{1.10}$$

where the summation over field component (I, J) and spacetime (μ, ν, λ) indices is implicit. K is an integer matrix (K-matrix) and $\mathbf{t}$ an integer vector (charge vector) characterizing the topological order and its response to external electromagnetic fields. A principal state, for example has $K = (m)$ and $\mathbf{t} = (1)$.

It is easy to see how this Lagrangian reproduces the phenomenology of the FQHE. The

current is given by

$$\frac{\delta \mathcal{L}}{\delta A_\mu} = J^\mu = \frac{e}{h} t_I \epsilon^{\mu\nu\lambda} t_I \partial_\nu a_{I\lambda}, \tag{1.11}$$

substituting this into the equation of motion

$$\frac{\delta \mathcal{L}}{\delta a_{I\mu}} - \partial_\nu \frac{\delta \mathcal{L}}{\delta \left(\partial_\nu a_{I\mu}\right)} = 0 \tag{1.12}$$

we find

$$J^\mu = \frac{e^2}{h} \left(\mathbf{t}^T K^{-1} \mathbf{t}\right) \left(\epsilon^{\mu\nu\lambda} \partial_\nu A_\lambda\right). \tag{1.13}$$

Looking at different components, we find that the charge density is proportional to the magnetic field with filling fraction $\nu = \mathbf{t}^T K^{-1} \mathbf{t}$ and the Hall conductance $\sigma_{xy} = \partial J^x / \partial E_y = \nu e^2/h$.

The theory is gapped in the bulk and the excitations are vortices of the a_I fields (with a core energy not included in the Lagrangian) corresponding to localized charged quasiparticles. Such vortices can happen in one or more of the field components, characterized by an integer vector $\mathbf{m}$ listing the vorticities. The charge of the excitation is given by $e\mathbf{m}^T K^{-1} \mathbf{t}$. Generic quasiparticles have anyonic exchange statistics, that is, under the exchange the complex phase picked up by the wavefunction is not bosonic (0) or fermionic (π) but given by $\pi \mathbf{m}^T K^{-1} \mathbf{m}$. All the states described by the K-matrix formalism are abelian, as particle exchanges commute. Other FQH states may be nonabelian[78], such that an exchange acts as a unitary operator on the space of locally indistinguishable degenerate excited states with identical quasiparticle positions.

1.4.2 Edge theory

Similar to IQHE and Chern-insulators, FQH states demonstrate gapless edge states. While the bulk is insulating, the edges have nontrivial transport properties. For example, there is nonzero resistance between contacts on the edge of a QH sample. Tunneling current[79, 80] and noise[81–83] measurements between edges separated by the FQH liquid or the vacuum provide further insights to the structure of the topological order.

The Chern-Simons theory is not gauge-invariant at the boundary, this can be fixed by restricting gauge-transformations, which makes some of the gauge degrees of freedom dynamical at the boundary. This results in the effective Chiral Luttinger Liquid (χLL) theory

$$\mathcal{L}_{\text{edge}} = \frac{1}{4\pi} \left(K_{IJ} \partial_t \phi_I \partial_y \phi_J - V_{IJ} \partial_y \phi_I \partial_y \phi_J\right). \tag{1.14}$$

The low energy excitations are waves propagating on the edge of the incompressible liquid. In general there is a different number of left and right moving excitations. If all excitations propagate in the same direction, the edge is fully chiral and backscattering is forbidden. Similar to the bulk theory, excitations are characterized by an integer vector $\mathbf{m}$. Some of

these have unit charge, electrons tunneling in through vacuum, or from a trivial metallic lead excite some combination of these modes. Tunneling through the bulk at a quantum point contact is allowed for all excitations, as the FQH liquid hosts the corresponding fractionalized quasiparticles. Using this, it is possible to verify the presence fractionally charged quasiparticles.

1.5 Outlook

One of the most promising application of topological states of matter is *topological quantum computing*[84–86]. Quantum computers process information by executing unitary operations on an entangled set of quantum states. The main obstacle to developing this technology is decoherence, interaction with the environment ruins the phase coherence of the quantum state, eventually leading to wave function collapse into a classical product state. Topological quantum computing addresses this issue by storing the quantum information non-locally. As we previously mentioned, topological states of matter may have degenerate states that are locally indistinguishable. This provides protection against local perturbations, as the locally identical states are perturbed in an identical way and the relative phase in a superposition is preserved.

Using multi-genus surfaces to harness the ground state degeneracy is practically very challenging. Instead, most attention is focused on nonabelian states, that have degeneracy on a trivial geometry when quasiparticles are present. Adiabatic braiding of nonabelian quasiparticles (nonabelions) performs unitary operations on the degenerate manifold with an error rate exponentially suppressed with their separation. Certain FQH states are thought to host nonabelions, however, no definitive experimental evidence of this is known to date.

The simplest nonabelions are *Majorana fermions*[87]. These can be thought of as "half of a fermion", representing the real an imaginary part of a fermionic zero mode. The two halves can be spatially localized and well separated, such systems are experimentally accessible in 1d superconducting heterostructures[88, 89]. These quantum wires realize the nontrivial phase in the $\mathbb{Z}_2$ classification of class D in 1d. While braiding is not well defined in strictly 1d, use of wire networks was proposed[90] to perform effective braiding. While Majoranas alone are not sufficient for universal quantum computing, it is a promising direction to realize scalable quantum computing with partial topological protection in the near future.

Further progress may be made by harnessing the effects of strong disorder on interacting topological phases. Topological order combined with many-body localization can result in phases where not only the ground state, but all excited states are short-range entangled and carry topological information[91]. This opens up the possibility to observe novel quantum effects and engineer topological quantum computers without the need of cooling near the ground state.

Chapter 2

Overview of dissertation

The dissertation is divided into three parts. In Part II we study the edge excitations of fractional quantum Hall systems. In Part III we investigate classification of non-interacting fermionic topological phases in the presence of space group symmetries. In Part IV we generalize the notion of the magnetoelectric effect to metallic systems.

Part II

- Chapter 3 presents a study of edge excitations of abelian fractional quantum Hall liquids on an infinite strip geometry. We use the iDMRG method to numerically measure edge exponents in model systems, including subleading orders. Using analytic methods we derive a generalized Luttinger's theorem that relates momenta of edge excitations. The work was completed in collaboration with Michael P. Zaletel and Joel E. Moore, published in Ref. [92].

Part III

- Chapter 4 reviews the formalism and main technical results used throughout Part III. We review concepts of space group symmetry and geometry of band structures. Then we develop the transformation properties of these geometrical objects under generic space group operations. These results were published as appendices to Refs [48] and [49], here we organized them into a separate chapter for a more transparent presentation.

- Chapter 5 presents results about the quantization of topological θ-terms protected by orientation-reversing space group symmetries. We construct and analyze tight-binding models with glide symmetry in 3d in classes A, D and C to illustrate the general result. This study was completed in collaboration with Fernando de Juan and Yuan-Ming Lu, published in Ref. [48].

- Chapter 6 presents results about constraints on weak indices imposed by space group symmetries. We focus on spin-orbit coupled insulators with and without time reversal

invariance and consider both symmorphic and nonsymmorphic symmetries. This study was completed in collaboration with Fernando de Juan and Yuan-Ming Lu, published in Ref. [49].

- Chapter 7 reviews some results about zero and one dimensional invariants. Zero dimensional invariants are obtained from studying space group representations. We develop the transformation properties of Wilson loops under space group operations and possible crystalline topological phases characterized by resulting invariants. Some of these results are unpublished, others appeared in appendices of Ref. [49].

Part IV

- Chapter 8 generalizes the notion of a topological θ-term to 3d metallic systems. We use semiclassical dynamics to study the current response to elastic strain in static external magnetic fields, an effect we call magnetopiezoelectricity. This work was completed in collaboration with Adolfo G. Grushin, Roni Ilan and Joel E. Moore and published in Ref. [93].

Part II

Edge states of 2D quantum liquids

Chapter 3

Edge excitations of abelian FQH states

We use bosonic field theories and the infinite system density matrix renormalization group (iDMRG) method to study infinite strips of fractional quantum Hall (FQH) states starting from microscopic Hamiltonians. Finite-entanglement scaling allows us to accurately measure chiral central charge, edge mode exponents and momenta without finite-size errors. We analyze states in the first and second level of the standard hierarchy and compare our results to predictions of the chiral Luttinger liquid (χLL) theory. The results confirm the universality of scaling exponents in chiral edges and demonstrate that renormalization is subject to universal relations in the non-chiral case. We prove a generalized Luttinger's theorem involving all singularities in the momentum-resolved density, which naturally arises when mapping Landau levels on a cylinder to a fermion chain and deepens our understanding of non-Fermi liquids in 1D.

3.1 Introduction

The incompressible liquids of two-dimensional electrons that underlie the fractional quantum Hall effect (FQHE) are believed to support excitations with fractional charge and anyonic statistics. For the "abelian" states, including the Laughlin states at fractional filling $\nu = 1/m$ of the lowest Landau level [7], the quasiparticles pick up an exchange phase factor that is neither bosonic nor fermionic, as allowed in two-dimensional systems.[94] Experiments on these quasiparticles typically involve edge [79, 80, 82, 95, 96] or dot [97] geometries. While it is clear that the gapless excitations at an FQHE edge are different from those of a Fermi liquid, it has been challenging to obtain quantitative agreement between microscopic models and predictions of the effective theory.

We aim to answer two long-standing questions about fractional quantum Hall edge physics by combining recent analytical and numerical advances in mapping the 2D Landau level of an infinitely long cylinder to an unusual 1D fermion chain. First, we address whether electron

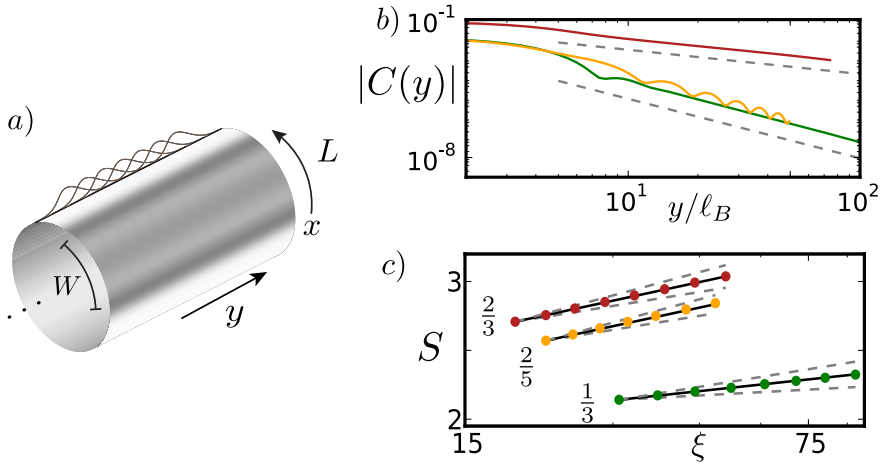

Figure 3.1: **a) Geometry:** An infinitely long cylinder of circumference L with a trapping potential $V(x)$ squeezing the fluid into a strip of width W. Coordinate x runs around the circumference, and y along the infinite length. The Landau orbitals are localized in y. **b) Real space edge correlation functions** $|C(y)| = \langle \psi^\dagger(x,y)\psi(x,0)\rangle$ for $\nu = 1/3$ (green), $\nu = 2/5$ (yellow) and $\nu = 2/3$ (red). x lies near the edge of the strip. Guiding dashed lines indicate $\eta = 3$ and $\eta = 1.14$ power laws. In the 2/5 case, oscillations are present due to two $\eta = 3$ contributions with different momenta. **c) Central charge** c **from finite entanglement scaling.** The correlation length ξ and the entanglement entropy S are measured for increasingly accurate MPS, and are found to scale as $S = \frac{c}{6}\log(\xi) + s_0$. The markers are the measured data points; the undashed lines show the scaling relation for $c = \{1, 2, 2\}$ for the $\nu = \{1/3, 2/5, 2/3\}$ states respectively; the dashed lines indicate slopes for $c \pm 1/4$.

correlation functions along an unreconstructed[98] edge have the universal behavior predicted by the chiral Luttinger liquid (χLL) theory. [77, 99] If universal, the edge correlation functions are an experimentally accessible probe of the topological order characteristic of the FQHE phase. For the interactions studied here (truncated dipolar for nu = 1/3, hollow-core for nu = 2/5 and 2/3) we find unambiguous evidence that for maximally chiral edges with excitations moving in only one direction, the equal time electron correlation functions show universal exponents resulting from the bulk topological order, while non-chiral edges have exponents depending on the intra-edge interactions. In both cases, the subleading edge exponents obey the relations obtained from χLL theory.

Second, since our method involves mapping the Landau level of a cylinder to a 1D fermion chain, we address how the critical states that arise when studying FQHE edge physics fit into standard descriptions of 1D metals. For a 1D metal, Luttinger's theorem [100] can be taken to mean that the volume of the Fermi sea, as determined by the non-analytic points in the electron occupation n_k, is not modified by interactions (though we note that there

is continuing debate over the validity of Luttinger's original formulation in the presence of non-perturbative effects[101]). Haldane conjectured [102, 103] a 'Luttinger sum rule' that extends Luttinger's theorem to FQH strips in the Abelian hierarchy, which was motivated by a simplified picture of the density profile of the hierarchy states. We unambiguously state and prove a 'generalized Luttinger's theorem' which constrains the momenta of singularities in the Greens function of any Abelian FQH state. In the K-matrix description of the χLL it takes the simple form $\mathbf{k}^T\mathbf{t} = \pi\nu_T$, where ν_T is the filling fraction of the cylinder, which agrees with Haldane's conjecture for the hierarchy states. We prove the constraint using the Lieb-Shultz-Mattis theorem, [104, 105] and confirm it numerically for some one-component and two-component edges. We then clarify why any strip of an Mth level hierarchy state is, in the 1D picture, an M-component Luttinger liquid, which implies that any two states at level M can be adiabatically transformed into each other.

We use a geometry (Fig. 3.1a) in which the edges are infinitely long, which we study using the infinite system density matrix renormalization group (iDMRG).[106, 107] Since the problem is translation-invariant along the infinite direction, the approximation in matrix product state numerics is not finite-size but rather finite matrix dimension or "finite entanglement."[108] An advantage of this geometry is that correlation functions in the long direction can be obtained over much greater lengths than possible using exact diagonalization, leading to unambiguous scaling behavior. Recent work on how entanglement scales at conformally invariant quantum critical points [108–111] also allows us to extract the central charge of the edge (Fig. 3.1c). The finite circumference does not cut off the correlation length of the edge, and we find that the edge exponents become well quantized at circumferences where there is still significant non-uniformity of the electron density of the bulk.

Tunneling experiments, which probe the frequency and temperature dependence of the edge Green's function, have measured a tunneling exponent of $\alpha \sim 2.7$ for the 1/3-edge, while the unreconstructed χLL prediction is $\alpha = 3$. [79] Numerical studies have since investigated the equal time correlation functions and made comparison with χLL theory. [112–121] There is general agreement that the 'model' wave functions obtained from a conformal field theory (CFT), such as the Moore-Read and Laughlin wave functions, must have the exponents predicted by the associated CFT.[112, 122] The situation is much less clear both for the hierarchy states and for longer range interactions. For the 1/3-edge there is some evidence, using finite sized disks, that η_3 in fact depends on the interactions (Ref. [113, 123] found $\eta_3 \sim 2.5$ for the Coulomb interaction r^{-1} and $\eta_3 \sim 2.6$ for a Yukawa interaction $r^{-1}e^{-r/\ell_B}$).

3.2 Model and Methodology

We first map the continuum problem to a translationally invariant fermion chain.[124–126] We start with an infinitely long cylinder of circumference L, (Fig. 3.1a). Letting x be the coordinate around the cylinder, and y along it, we choose the Landau gauge $\mathbf{A} = B(-y, 0)$ so that each LLL orbital $\phi_n(x, y)$ is localized in the vicinity of $y_n = na$ with $a = 2\pi\ell_B^2/L$, and can be ordered sequentially. Interactions and potentials which are translation invariant

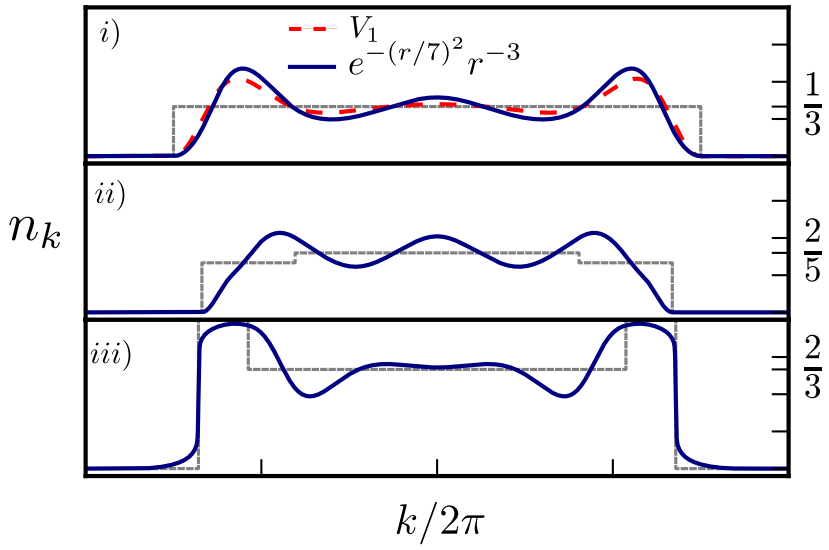

Figure 3.2: The occupation number n_k, which is the Fourier transformation of the orbital correlation function $\langle \psi_n^\dagger \psi_0 \rangle$, or equivalently, the occupation of Landau orbitals for the gauge in which they are localized in x. The gray dashed lines indicate the 'wedding cake' caricature of the hierarchy states. Three states are shown: **i**) $\nu = 1/3$ for $W = \frac{3}{4}17\ell_B$, both for the model 'hollow-core' interaction (red dashed) and for a truncated version of the r^{-3} dipole interaction (solid). **ii**) $\nu = 2/5$ at $W = \frac{5}{8}19.2\ell_B$. **iii**) $\nu = 2/3$ at $W = \frac{3}{4}20\ell_B$

.

along y result in a translation invariant Hamiltonian for the fermion chain. The interaction matrix elements are nonzero up to infinite distances, but are exponentially suppressed over a characteristic length $\mathcal{O}(L/\ell_B)$ sites. The mapping is exact, but we must truncate the interaction terms in order to use the iDMRG, which limits the economically accessible circumference to $L \lesssim 24\ell_B$.[127]

After fixing a filling fraction ν_T for the cylinder, a trapping potential $V(x)$ is projected into the LLL, resulting in hopping terms in the 1D picture. The trap squeezes the Hall fluid into a denser strip of width W. For example, to obtain the $\nu = 1/3$ strip, we set the overall filling of the cylinder to $\nu_T = 1/4$ and use a trap of width $W = \frac{3}{4}L$. Rather than realistically modeling a cleaved edge, [115] the trap potentials were chosen to stabilize the desired phases and avoid edge reconstruction, by using a box of depth t and width W convoluted with a gaussian of width $d \sim \ell_B$ to smooth the edge. For the 1/3-state, we use a truncated dipolar interaction $r^{-3}e^{-(r/7\ell_B)^2}$. For the $2/5, 2/3$-states, we use only the hollow-core Haldane pseudo-potential interaction V_1.[124, 128]

3.2.1 iDMRG and Finite Entanglement Scaling

To find the ground state we use the iDMRG method as adapted to the QH problem.[127, 129, 130] The iDMRG algorithm is a variational procedure within the space of infinite matrix product states (iMPS). An iMPS has finite bipartite entanglement, while the entanglement of the critical edges diverges logarithmically, so the iMPS ansatz cuts off the correlations at a length ξ_{MPS} depending on the dimension χ of the matrices used. The finite size effects have been removed, but 'finite entanglement' effects introduced. Analogous to finite size scaling, the finite entanglement ansatz introduces only one length scale, and a 'finite entanglement scaling' (FES) procedure has been developed for extracting critical properties. [108, 131–133] One advantage of FES is that the complexity to obtain a correlation length ξ_{MPS} scales as $\mathcal{O}(\xi_{MPS}^{3\kappa})$ for an exponent κ that depends on the central charge.[108] In contrast, to find the ground state of a disk of circumference L in exact diagonalization (ED) scales as $\mathcal{O}(\alpha^{L^2})$. We obtain states with $\xi_{MPS} \sim 200\ell_B$, an order of magnitude larger than the largest disk circumferences obtained from ED, and somewhat larger than the disk circumference obtained through composite fermion ED. For the largest simulations used here, $\chi \sim 1400$, which required about 30 cpu-hours.

The output of the iDMRG calculation is an iMPS representation of the approximate ground state, from which we can efficiently measure any desired observable.

3.2.2 Obtaining the edge-exponents

The electronic edge exponents are encoded in power-law contributions to the equal time electron correlation function $C(x;y) = e^{ixy\ell_B^{-2}}\langle\psi^\dagger(x,y)\psi(x,0)\rangle$. Here $\psi(x,y)$ is the electron operator in the FQH model, and the phase factor is chosen for convenience.

We first review the expected form of C in χLL theory. The low energy effective theory of a generic abelian FQH edge is described using the K-matrix formalism:[77]

$$S = \frac{1}{4\pi}\int dydt\left(K_{IJ}\partial_t\phi_I\partial_y\phi_J - V_{IJ}\partial_y\phi_I\partial_y\phi_J\right). \tag{3.1}$$

K specifies the topological order, while V depends on the microscopic details and sets the edge velocities and their density-density interactions. We suppress the indices in what follows. A generic quasiparticle excitation is characterized by an integer vector $\mathbf{m}$, $\psi_{\mathbf{m}}(y) = e^{i\mathbf{m}^T\phi + i\mathbf{m}^T\mathbf{k}\,y/a}$. The quantum numbers of the excitation are specified by the 'charge vector' $\mathbf{t}$ and 'momentum vector' $\mathbf{k}$. The momentum of $\psi_{\mathbf{m}}$ is $k_{\mathbf{m}} = \mathbf{k}^T\mathbf{m}$, with the convention $k \in [-\pi,\pi]$ regardless of L. The charge of $\psi_{\mathbf{m}}$ is $q_{\mathbf{m}} = \mathbf{t}^T K^{-1}\mathbf{m}$. As we only probe electronic excitations, we restrict to $q_{\mathbf{m}} = 1$.

As the bulk is gapped, the dominant long range contributions to C are power laws from each charge 1 operator in the edge theory:[77, 134]

$$C(x;y) = i\sum_{\mathbf{m}:q_{\mathbf{m}}=1} c_{\mathbf{m}}(x)e^{ik_{\mathbf{m}}y/a}\frac{1}{y^{K(\mathbf{m})}}\frac{1}{|y|^{\eta_{\mathbf{m}}-K(\mathbf{m})}} + \cdots. \tag{3.2}$$

Here $K(\mathbf{m}) = \mathbf{m}^T K^{-1} \mathbf{m}$ is an odd integer, while $\eta_{\mathbf{m}}$ is the equal time scaling exponent of the excitation $\mathbf{m}$, and depends on both K and V. A consequence of the projection into the LLL is that each $c_{\mathbf{m}}(x)$ is a Gaussian peaked at $x_{\mathbf{m}} = Lk_{\mathbf{m}}/2\pi$; hence the momenta $k_{\mathbf{m}}$ indicates the depth x at which the mode propagates.

It is easiest to perform the FES collapse in k-space. After Fourier transforming in y to obtain $C(x;k)$, the power-law behavior results in non-analytic dependence on k at the discrete set of momenta $\{k_{\mathbf{m}}\}$. To proceed we express $C(x;k)$ in the lowest Landau level. Letting ψ_n denote the field operators of the Landau orbitals, we form the Fourier transformed operators $\psi_k = \frac{1}{\sqrt{N_\Phi}} \sum_n e^{-ikn} \psi_n$, where we temporarily consider a finite number of orbitals N_Φ. Note that ψ_k are also the creation operators for orbitals in the $\mathbf{A} = B(0,x)$ gauge convention, localized at $x = Lk/2\pi$. For large L/ℓ_B, we find

$$C(x;k) = \int dy e^{-iky/a} e^{ixy\ell_B^{-2}} \langle \psi^\dagger(x,y)\psi(x,0)\rangle \tag{3.3}$$

$$= \frac{1}{\sqrt{\pi}\ell_B} n_k e^{-\ell_B^{-2}(Lk/2\pi - x)^2} \tag{3.4}$$

where $n_k \equiv \langle \psi_k^\dagger \psi_k \rangle$ is the k-space occupation number in the 1D chain. The gaussian factor implies that the correlations at x are dominated by the behavior near $k \sim 2\pi x/L$. In the vicinity of each non-analytic point n_k takes the form [124]

$$n_k \sim \theta(k - k_{\mathbf{m}}) |k - k_{\mathbf{m}}|^{\eta_{\mathbf{m}} - 1} [a_0 + a_1(k - k_{\mathbf{m}}) + \cdots] + \cdots \tag{3.5}$$

where the higher powers of k arise from more irrelevant 'descendent' operators. To determine $\eta_{\mathbf{m}}$ numerically we use a modified version of a fractional derivative defined by

$$\mathcal{D}^\nu[n_k] = \mathcal{F}[|r|^\nu \mathcal{F}^{-1}[n_k]] \tag{3.6}$$

where $\mathcal{F}$ is the Fourier transform. We expect

$$\mathcal{D}^{\eta_{\mathbf{m}} - 1}[n_k] \sim \theta(k - k_{\mathbf{m}}) [b_0 + b_1(k - k_{\mathbf{m}}) + \cdots] + \cdots \tag{3.7}$$

which can be used to check for the correct choice of $\eta_{\mathbf{m}}$.

However, the finite entanglement effects cut off the correlation functions at a scale ξ_{MPS}, and hence round out the non-analytic behavior. On dimensional grounds, the smearing must take the form

$$\theta(k - k_{\mathbf{m}}) \to s(\xi_{MPS}(k - k_{\mathbf{m}})) \tag{3.8}$$

where s is some smoothed version of a step function. For the correct choice of $\eta_{\mathbf{m}}$, we can collapse the data by plotting $\mathcal{D}^{\eta_{\mathbf{m}} - 1}[n_k]$ as a function of $\xi_{MPS}(k - k_{\mathbf{m}})$, up to irrelevant corrections and the smooth background, as can be seen in Fig. 3.3. The collapse gives a very precise measurement of both $k_{\mathbf{m}}$ (to better than one part in 10^{-5}) and $\eta_{\mathbf{m}}$ (to about one part in 10^{-2}).

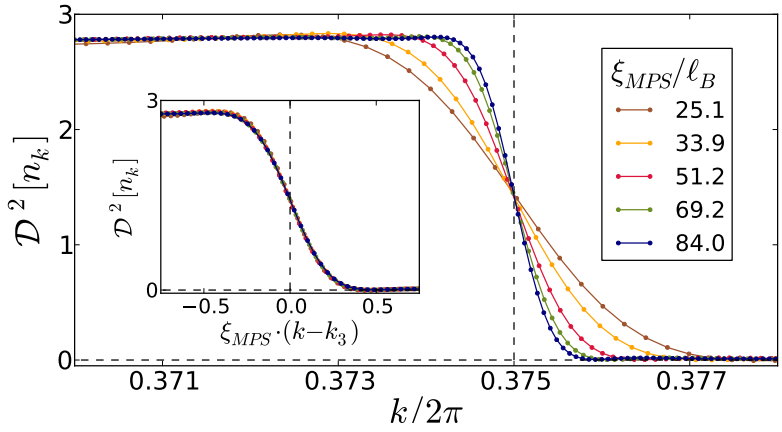

Figure 3.3: Analysis of a $\nu = 1/3$ strip of width $W = \frac{3}{4}17\ell_B$. The measured $\mathcal{D}^2[n_k]$ is plotted for increasingly accurate MPSs, parameterized by their correlation length ξ_{MPS}. The crossing of the lines at $k_3 = \frac{3}{8}\cdot 2\pi$ indicates a singularity at k_3, corresponding to the edge of the droplet. **Inset**. Scaling collapse supports a true singularity with the predicted exponent $\eta_3 = 3$. If $\eta_3 = 3$, then the singular part of $\mathcal{D}^2[n_k]$ is dimensionless near k_3, so no vertical scaling is necessary. The combination $\xi_{MPS}(k - k_3)$ is also dimensionless, so the data should collapse when plotted as a function of $\xi_{MPS}(k - k_3)$.

3.3 Edge universality at $\nu = 1/3, 2/5$ and $2/3$.

3.3.1 The $\nu = 1/3$ edge

We first study the filling $\nu = \frac{1}{3}$, a first level hierarchy state whose edge theory supports a single chiral mode. If the edge is described by a χLL, the dominant electronic edge exponent is predicted to be quantized to $\eta_3 = 3$ when the two edges of the strip don't interact.[77]

We start with a 'thick' strip of width $W = \frac{3}{4}17\ell_B$ on a cylinder of circumference $L = 17\ell_B$, with a cylinder filling fraction of $\nu_T = 1/4$. For the interaction we use truncated dipolar repulsion, $V(r) = r^{-3}e^{-(r/7\ell_B)^2}$, which was used in favor of the Coulomb interaction as a compromise between the increased numerical cost of longer range interactions and the need to ensure the interaction is significantly perturbed from the model Hamiltonian. Consequently the interaction between the two edges should be very weak. The distribution n_k is shown in Fig. 3.2i, including a comparison to the profile when only V_1 is used.

The dominant singularity of the $\nu = \frac{1}{3}$ edge is observed to occur at $|k_3| = \frac{3}{8}\cdot 2\pi \pm 10^{-6}$, corresponding to the naive 'edge' of the strip as would be obtained from assuming n_k to be a box of height $\frac{1}{3}$, an example of the Luttinger sum rule. The results of the FES collapse assuming $\eta_3 = 3$ are shown in Fig. 3.3, showing excellent agreement. To check the precision with which we can determine η_3, we repeat the collapse for various η_3 as shown in Fig. 3.4. The exponent is best fit by $\eta_3 = 3.005 \pm 0.02$.

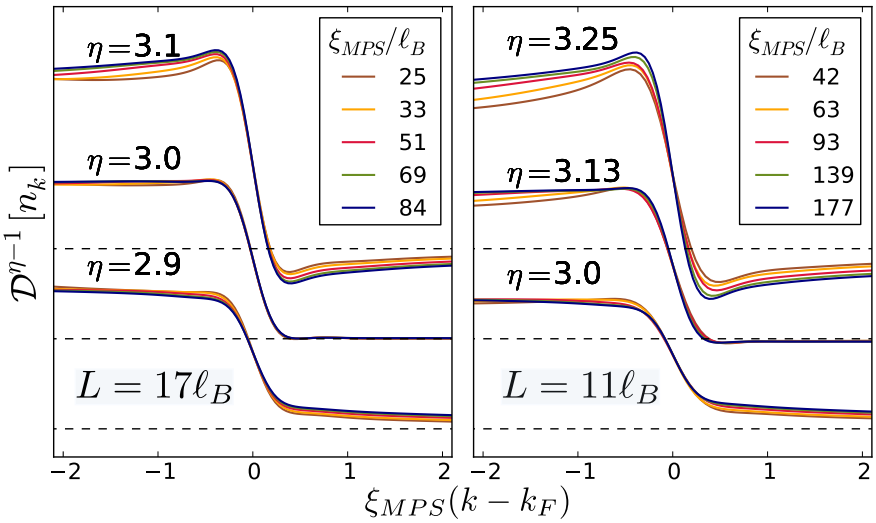

Figure 3.4: Comparing collapse of the $\nu = 1/3$ strip for different ansatz η. The correct η is distinguished by two features: the tightness of the collapse for various ξ_{MPS}, and the degree of under/overshoot to the form of a step function. The trial collapses at different η are shifted apart vertically for clarity. **Left panel**) a thick strip, $W = \frac{3}{4}17\ell_B$. We find $\eta_3 = 3.005 \pm 0.02$, consistent with no inter-edge interactions. **Right panel**) a thin strip, $W = \frac{9}{10}11\ell_B$. Because the edges are close to one another, inter-edge interactions renormalize η upwards to $\eta = 3.13 \pm 0.02$

3.3.2 Renormalization of edge exponents for thin strips

To verify that the measurement of $\eta_3 = 3$ is not a bias of the approach, we let the edges interact so that $\eta_3 = 3$ renormalizes upwards. Using the same interactions and trap profile as before, but using a $L = 11\ell_B, W = \frac{9}{10}11\ell_B$ strip, the edges now interact across the vacuum. As shown in Fig. 3.4, the exponent indeed renormalizes upwards to $\eta_3 = 3.135$.

For thin strips the 1/3-state contains multiple electron operators, which correspond to inserting, for example, charge $\frac{2}{3}e$ on one edge and $\frac{1}{3}e$ on the other, which we label $\mathbf{m} = (2,1)$. The amplitude for such a process decays as $e^{-(W/\ell_B)^2/4}$. χLL theory predicts a fixed relationship between η_3 and $\eta_{(2,1)}$ even if η_3 has renormalized away from 3, which can be derived in the K-matrix formalism.

A single edge of the 1/3 state is described by $K = (3)$, $\mathbf{t} = (1)$, but if the two edges of the strip are in proximity we cannot neglect interactions between them. The full edge theory is $K' = K \oplus (-K)$, $\mathbf{t}' = \mathbf{t} \oplus (-\mathbf{t})$, $\mathbf{k}' = \mathbf{k} \oplus (-\mathbf{k})$ and V, restricted by mirror symmetry, has two independent components. Two singularities we observe correspond to $\mathbf{m} = (3,0)$ and $\mathbf{m} = (2,1)$,[124, 135, 136] and their exponents should satisfy the relation

$$\tilde{\eta}_3 = 5\eta_{(2,1)} - 4\sqrt{\eta_{(2,1)}^2 - 1}. \tag{3.9}$$

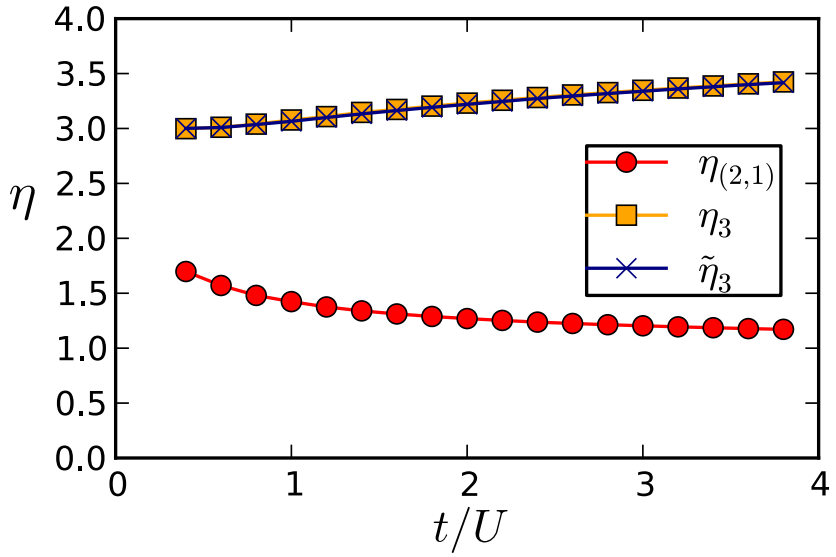

Figure 3.5: Checking the predicted χLL exponent relations as the $\nu = 1/3$ trap is squeezed. On a small enough strip (here $L = 4\ell_B$) two electronic excitations are visible, corresponding to injecting either e into one edge ($m = 3$) or $2e/3$ into one edge and $e/3$ into the other ($m = (2, 1)$). We plot the measured exponents η_3 and $\eta_{(2,1)}$ as the strength of the trap t/U is increased, as well as the predicted $\tilde{\eta}_3$ given the measured value of $\eta_{(2,1)}$ using Eq. (3.9). At low very t/U, $\eta_3 = 3$, the universal $\nu = 1/3$ value. As the trap is squeezed, the predicted relation of χLL theory is satisfied to within 0.5%. Note $\eta_{(2,1)}$ moves towards 1, the exponent of a non-interacting Luttinger liquid.

To verify Eq. (3.9) we use a thin cylinder ($L = 4\ell_B$) so that both excitations are observable. Keeping the interactions as before, we vary the strength of the trap t relative to the interaction strength U. In Fig. 3.5, for each t we extract $\eta_3, \eta_{(2,1)}$ and check their predicted relation. We find agreement with χLL theory to better than 0.5%.

In summary, the behavior of the $\nu = 1/3$ edges is well described by χLL theory, both for thick and thin strips. For thick strips the edge exponent approaches the quantized value $\eta_3 = 3$. While we have not simulated the full Coulomb interaction, the interaction is sufficient to significantly perturb the bulk density profile and measurably renormalizes the exponents when the two edges are close. It would be interesting to determine whether the quantization $\eta_3 = 3$ is nevertheless a peculiarity either of the r^{-3} interaction or its cutoff at $\sim 7\ell_B$. We leave enhancing our method to include Coulomb interaction to future work.

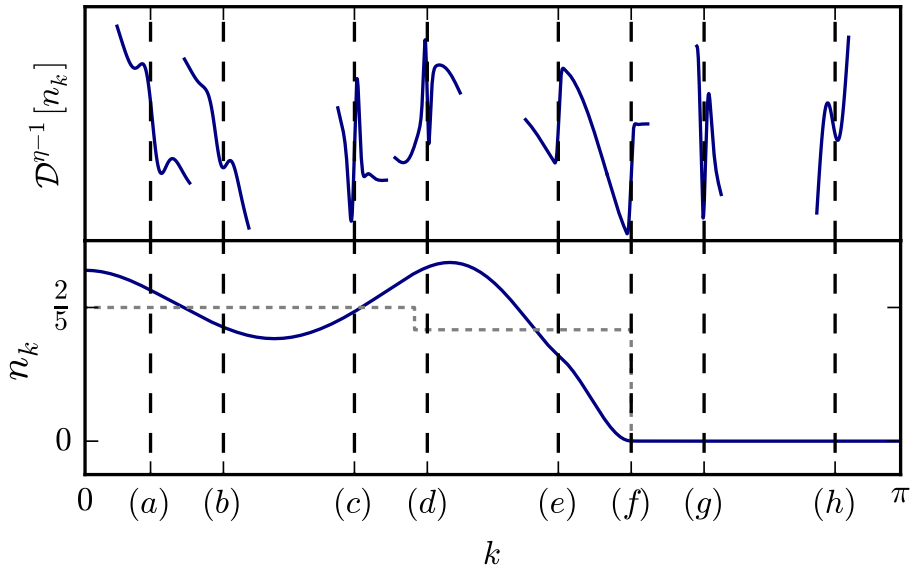

Figure 3.6: The zoo of electron excitations of a $\nu = 2/5$ strip. **Bottom panel**. Occupation number n_k; vertical dashed lines indicate locations of singularities, only some of which are directly visible in n_k. Dotted line indicates the naive wedding cake density profile. **Top panel**. After applying $\mathcal{D}^{\eta-1}$, the singularities appear as step functions. For the close-up of the mth singularity, $\mathcal{D}^{\eta_m-1}$ is applied, some of the regular background is removed, and the vertical axis is rescaled for better visibility. The two most prominent singularities (e) and (f) have exponents $\eta = 3 \pm 0.02$, consistent with no inter-edge interactions. The rest of the singularities are found at momenta predicted by the first two. Approximate η and m values for the singularities: $\eta_a = 4.8$, $\mathbf{m}_a = (2,-1,2,-2)$; $\eta_b = 5.8$, $\mathbf{m}_b = (1,1,0,2)$; $\eta_c = 5.2$, $\mathbf{m}_c = (1,2,0,1)$; $\eta_d = 4.2$, $\mathbf{m}_d = (3,-2,1,-1)$; $\eta_e = 3$, $\mathbf{m}_e = (2,1,0,0)$; $\eta_f = 3$, $\mathbf{m}_f = (3,-1,0,0)$; $\eta_g = 7$, $\mathbf{m}_g = (4,-3,0,0)$; $\eta_h = 4.2$, $\mathbf{m}_h = (3,0,-1,1)$.

3.3.3 The $\nu = 2/5$ edge

The second level hierarchy state at $\nu = 2/5$ has a rich edge structure resulting from the presence of two modes on each edge. The 2/5 edge is maximally chiral in the sense that both edge modes propagate in the same direction, so intra-edge interactions are not expected to renormalize the scaling exponents. In contrast to the $\nu = 1/3$ case, there are multiple ways of inserting charge into a single edge, which appear as a set of singularities. Using the convention

$$K^{-1} = \frac{1}{5}\begin{pmatrix} 2 & 1 \\ 1 & 3 \end{pmatrix} \qquad \mathbf{t} = \begin{pmatrix} 1 \\ 0 \end{pmatrix} \tag{3.10}$$

the two most relevant operators are $\mathbf{m}_1 = (2,1)^T$ and $\mathbf{m}_2 = (3,-1)^T$ with $\eta_1 = \eta_2 = 3$.

We simulate a strip of width $W = \frac{5}{8}19.2\ell_B$ on a cylinder of circumference $L = 19.2\ell_B$, at $\nu_T = 1/4$, using only the hollow-core V_1 pseudo-potential. Adding a small perturbing V_3 was not observed to change the exponents. Our data is consistent with negligible inter-edge interactions, but there is a small amplitude for inserting an electron as a fractional part in both edges. We can identify a number of small contributions of this type.

Over two dozen singularities are visible in n_k; a summary of the most singular exponents are included in the inset of Fig. (3.6). In all cases where the singularity is strong enough to extract η, it is consistent with the universal values predicted by the χLL theory. The dominant exponents $\mathbf{m}_1 = (2, 1)$ and $\mathbf{m}_2 = (3, -1)$ are observed to be $\eta_1 = 3.00 \pm 0.02$ and $\eta_2 = 2.995 \pm 0.015$ respectively.

The hierarchy picture of the 2/5 strip is a 1/3 droplet with an additional condensate of quasielectrons of excess density 1/15 in the interior. We cannot directly detect the singularity at the edge of the 1/15 condensate, $\mathbf{m}_3 = (0, 5)$, as the exponent $\eta_3 = 15$ is too large. Nevertheless, $\mathbf{k}$ can be determined from the momenta k_1 and k_2 of the two most relevant singularities. The locations of the remaining $k_{\mathbf{m}}$ are all in agreement with $k_{\mathbf{m}} = \mathbf{k}^T\mathbf{m}$. Assuming the unobserved 1/15 edge is at $k_3 = \mathbf{k}^T\mathbf{m}_3$, we find that $\frac{1}{3}k_2 + \frac{1}{15}k_3 = \nu_T\pi \pm 10^{-5}$. This is in agreement with the Luttinger sum rule: assuming the 2/5-state has a 'wedding cake' density profile of $n_k = \frac{2}{5}$ for $|k| < k_3$ and $n_k = \frac{1}{3}$ for $k_3 < |k| < k_2$, the total electron density is $\frac{1}{3}k_2 + \frac{1}{15}k_3 = \pi\nu_T$. If the trap potential is modified the $k_{\mathbf{m}}$ change but the constraint is always satisfied. It is quite remarkable that the naive result is correct to better than one part in 10^{-5}, as the true density profile has strong oscillations with no actual discontinuities at the $k_{\mathbf{m}}$, as shown in Fig. 3.6.

3.3.4 The $\nu = 2/3$ edge

The $\nu = 2/3$ state is also a second level hierarchy state, but the edges are not chiral, and hence the edge exponents are not universal even in the limit of a wide strip. It has been argued that disorder[137, 138] or long-range Coulomb interaction[77] makes the exponents flow to the universal Kane-Fisher-Polchinski (KFP) fixed point. Including disorder would require breaking translational invariance along the edge, which would greatly increase computational effort, thus we restrict the current study to clean edges with short-ranged interaction. Using the convention $K = \mathbf{diag}(1, -3)$, $\mathbf{t} = (1, -1)$, at intermediate intra-edge interactions the two most relevant excitations of a single edge are $\mathbf{m}_1 = (1, 0)$ and $\mathbf{m}_2 = (2, -3)$.

We simulate a $W = 15\ell_B$ strip on a cylinder of circumference $L = 20\ell_B$ at $\nu_T = \frac{1}{2}$, using only the hollow-core V_1 pseudo-potential. In agreement with χLL theory, η_1 is not observed to be quantized. In order to access different V-matrices we can change the sharpness of the edge d. Under the assumption of vanishing inter-edge interactions, η_1 and η_2 should satisfy the χLL prediction $\eta_2 = 7\eta_1 - 4\sqrt{3}\sqrt{\eta_1^2 - 1}$, which they do only to within about $\sim 10\%$, as shown in Fig. 3.7. While the disagreement is likely due to inter-edge interactions, we cannot accurately measure enough of the $\eta_{\mathbf{m}}$ to fully determine the two-edge V to check for consistency. We again observe a Luttinger sum rule $(k_1 + k_2)/3 = \pi/4$. As the trap is modified the $k_{\mathbf{m}}$ change, but the Luttinger sum rule remains satisfied to one part in 10^{-5}

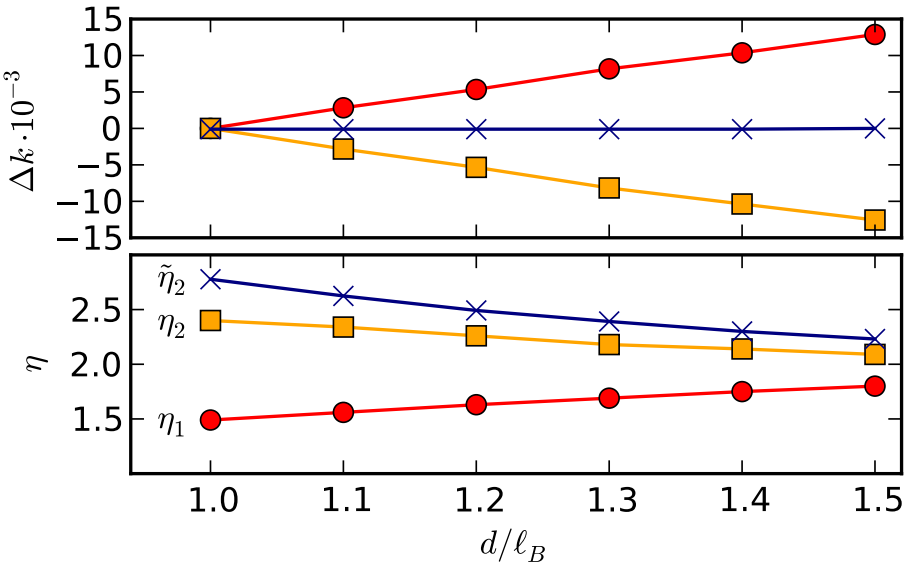

Figure 3.7: (Color online) Renormalization of edge mode momenta and exponents as a function of the edge sharpness d (large d is soft edge). **Top panel**: change of momentum k_1 (circles) and k_2 (squares) with respect to an arbitrary reference. $(k_1 + k_2)/3 - \pi/4$ (crosses) stays 0 to 10^{-5} accuracy, confirming the Luttinger sum rule. **Bottom panel**: Exponents η_1 , η_2 from iDMRG, and $\tilde{\eta}_2$ calculated from η_1 assuming χLL with no inter-edge interaction. The significant disagreement between η_2 and $\tilde{\eta}_2$ is likely due to inter-edge interactions.

accuracy, as shown in Fig. 3.7. It is interesting to note that for softer edges (large d), the exponents are observed to renormalize towards the KFP point $\eta_1 = \eta_2 = 2$ (Fig. 3.7), even with clean edges and hollow-core interaction.

3.4 Edge states in the 1D picture

Our numerics demonstrate robust χLL exponents, yet are ultimately realized in a 1D fermion chain. What can be learned from the 1D point of view? First, we apply the Lieb-Schultz-Mattis theorem to the 1D fermion chain to explain the constraint on the $k_{\mathbf{m}}$. Second, we clarify why strips of different ν, which at first seem to be different phases of matter, can in fact be smoothly deformed to each other.

3.4.1 A Generalized Luttinger Theorem for Hall Droplets

For all three filling fractions the locations of the singularities $k_{\mathbf{m}}$ obey a stringent constraint to better than a part in 10^{-5}. In the hierarchy picture, the constraint arises from a caricatured version of n_k which jumps discontinuously to a quantized filling as each level of the hierarchy

is added, though n_k looks nothing like this 'wedding cake' type profile, as can be seen in Fig. 3.2. Letting the jump in filling at the ith level of the level-M hierarchy state be $\Delta\nu_i$ at momentum k_i, the total filling fraction ν_T is observed to be

$$\nu_T = 2 \cdot \sum_{i=1}^{M} \Delta\nu_i k_i / 2\pi. \tag{3.11}$$

To our knowledge this 'Luttinger sum rule' was first conjectured by Haldane, and taken as the axiomatic starting point of a bosonized description of the excitations. [102] However, Eq. (3.11) is somewhat unsatisfactory as it appears to single out a particular set $\{\mathbf{m}_i\}$ of the edge singularities out of infinitely many. There is a natural choice for the hierarchy states, but given a generic K matrix description of an Abelian edge, what constraints are placed on the momenta $k_{\mathbf{m}}$ of the singularities?

To state the *generalized Luttinger theorem* more precisely, we show that Eq. (3.11) has the basis independent formulation $\mathbf{k}^T\mathbf{t} = \pi\nu_T$. We consider only the right edge, as the left has an identical constraint. The set of singularities $\{\mathbf{m}_i\}$ appearing in Eq. (3.11) are distinguished as a linearly independent set of M electron operators with trivial mutual statistics,

$$\mathbf{m}_i^T K^{-1} \mathbf{m}_j = \delta_{ij} D_i, \qquad\qquad \mathbf{m}_i^T K^{-1} \mathbf{t} = 1. \tag{3.12}$$

However, there are in fact *multiple* sets $\{\mathbf{m}_i\}$ satisfying this constraint, so we must show that the hypothesis is independent of the choice. Interpreting $\Delta\nu_i = D_i^{-1}$, the hypothesis reads $\sum_j D_j^{-1} \mathbf{m}_j^T \mathbf{k} = \pi\nu_T$. Since $\mathbf{m}_i^T K^{-1} \left(\sum_j^M D_j^{-1} \mathbf{m}_j \right) = 1$, while $\{\mathbf{m}_i^T K^{-1}\}$ is a linearly independent set, we must have $\sum_j^M D_j^{-1} \mathbf{m}_j = \mathbf{t}$. Hence the generalized Luttinger Theorem takes the basis independent form $\mathbf{k}^T\mathbf{t} = \pi\nu_T$.

To prove that $\mathbf{k}^T\mathbf{t} = \pi\nu_T$, we first take a 1D point of view. Temporarily consider the system on a torus, so that the edges have finite length L_y (in real space). According to Ref. [105], under conditions satisfied by our 1D fermion chain, there exists a low energy ($E \sim 1/L_y$), neutral excitation at crystal momentum $2\pi\nu_T$. The non-perturbative proof is an adaption of the Lieb-Schultz-Mattis theorem, [104] using the 'twist operator' $U = e^{2\pi i \sum_l l \hat{n}_l / N_\Phi}$, where $\hat{n}_l$ is the occupation of orbital l and N_Φ is the number of orbitals. As will become clear, we can interpret this excitation as a transfer of charge ν (the filling fraction of the strip) from the left to right edge, with $\mathbf{m}$ vector $(\mathbf{t}, -\mathbf{t})$. Accepting this interpretation gives a non-perturbative proof that $(\mathbf{k}^T, -\mathbf{k}^T).(\mathbf{t}, -\mathbf{t}) = 2\pi\nu_T$, or $\mathbf{k}^T\mathbf{t} = \pi\nu_T$. Hence Luttinger's theorem for the 1D fermion chain implies the generalized Luttinger Theorem for the Hall fluid.

To motivate the identification of the $k = 2\pi\nu_T$ excitation, we reinterpret this result in terms of the 2D continuum problem. The twist operator U acts on the real-space coordinates as translation around the circumference, $(x, y) \to (x + \ell_B^2/L_y, y)$. The interaction energy is

unchanged, but the trapping energy goes as

$$\delta V = \int dxdy \left[V(x + \ell_B^2/L_y) - V(x)\right] \rho(x, y) \tag{3.13}$$

$$\sim \frac{\ell_B^2}{2L_y} \int dx \ell_B^2 V''(x)\rho(x) = \mathcal{O}(1/L_y) \tag{3.14}$$

where we have relied on the reflection symmetry $x \to -x$. Hence the $k = 2\pi\nu_T$ neutral excitation is simply a small translation of the fluid, which transfers charge from the right to left edge. To show that the desired excitation is $(\mathbf{t}, -\mathbf{t})$ in the K-matrix formalism, recall that threading a 2π-flux through the cycle y of the torus translates the state by ℓ_B^2/L_y in x, due to the Hall response of the fluid. In the bulk, threading 2π-flux is, by definition, the excitation $\mathbf{m} = \mathbf{t}$. Since threading flux through y is equivalent to dragging a flux from the left to right edge, the excitation is $(\mathbf{t}, -\mathbf{t})$, as desired.

For bilayer states, there is a conserved $U(1)$ charge for each component a. A simple extension of the above argument leads to a constraint for each component; if $\mathbf{t}_a, \nu_{T;a}$ is the charge vector and filling of component a, then $\mathbf{k}^T\mathbf{t}_a = \pi\nu_{T;a}$.

This result is intuitively clear in the composite fermion or the parton picture. Our derivation demonstrates, however, that it is not necessary to assume a mapping to weakly interacting quasiparticles and the theorem is rigorously true whenever there is a K-matrix description of the edge states including, for example, reconstructed edges or strongly interacting composite fermions.

3.4.2 Adiabatic continuity between Abelian edges

In the χLL theory, edge theories with different K matrices (modulo an $SL(M, \mathbb{Z})$ equivalence relation) are understood to be distinct phases of matter. Viewed as a 1D problem, this would seem to imply the existence of distinct classes of metals, even at central charge $c = 1$. We clarify why this is not the case for any finite width strip; in principle all Mth hierarchy states can be adiabatically continued to one another. In the 1D picture, this implies they can all be adiabatically transformed to an M-component non-interacting metal. Microscopically, this adiabatic path might require shrinking the cylinder, as for thick strips coupling between the edges is exponentially suppressed.

The restriction to $SL(M, \mathbb{Z})$ transformations in the K-matrix formalism of a single edge is enforced to preserve the compactification lattice of the bosons, which determines the allowed excitations. On a geometry with one edge, the edge Hilbert space must contain fractional excitations because we can create a quasiparticle-quasihole pair and bring one particle to the edge while bringing the other infinitely deep into the bulk. However, if there are two edges, all excitations can be considered edge excitations, and the total topological charge of the two edges together should be trivial. The restriction to trivial topological charge means a larger class of $SL(2M, \mathbb{Z}/|K|)$ transformations can be applied, and the distinction between states at the same hierarchy level is lost.

The Laughlin states, for example, can all be deformed to the non-interacting IQH state. In the $\nu = 1/q$ phase, $K = \mathbf{diag}(q, -q)$, $\mathbf{t} = (1, -1)^T$, $\mathbf{k} = (k, -k)^T$. By applying an $SL(2, \mathbb{Z}/q)$ transformation

$$S = \frac{1}{2}\begin{pmatrix} q+1 & q-1 \\ q-1 & q+1 \end{pmatrix}, \tag{3.15}$$

we find $\tilde{K}^{-1} = SK^{-1}S^T = \mathbf{diag}(1, -1)$ while $\mathbf{k}$ and $\mathbf{t}$ are unchanged and all the original electronic excitations are spanned by $\mathbf{m} = S\tilde{\mathbf{m}}$ with $\tilde{\mathbf{m}} \in \mathbb{Z}^2$. This is the K-matrix description of a Luttinger liquid, which implies that any electronic excitation $\mathbf{m}$ at $\nu = 1/q$ can be identified as an excitation of a Luttinger liquid. For example, the usual $\mathbf{m} = (3, 0)$ excitation of the 1/3-state is the $3k_F$ excitation of a Luttinger liquid, i.e., $\mathbf{m} = (3, 0) \leftrightarrow \tilde{\mathbf{m}} = (2, -1)$. Likewise, the $\mathbf{m} = (2, 1)$ excitation of the 1/3-state is the usual k_F the of a Luttinger liquid, i.e., $\mathbf{m} = (2, 1) \leftrightarrow \tilde{\mathbf{m}} = (1, 0)$. By tuning V with the appropriate interactions, we can ensure $\tilde{V} = \mathbf{diag}(\tilde{v}, -\tilde{v})$, so that the exponents will agree with those of non-interacting electrons.

We have constructed similar explicit transformations for some second and third level hierarchy states. For certain bilayer states, a similar correspondence is possible only if we restrict to excitations with integral charge in *each layer separately*, which signifies that such states are only realized with two distinguishable species of fermions satisfying separate charge conservation conditions.

Adiabatic continuity of this form has already been demonstrated for the thin strip investigated in Fig. 3.5. For small t/U, η_3 and $\eta_{(2,1)}$ are close to their quantized $\nu = \frac{1}{3}$ values; as t/U increases and the edges interact, we find $\eta_{(2,1)} \to 1$, which is the exponent of the $(1, 0)$ excitation of a free Luttinger liquid. Throughout the deformation, the functional form of $\eta_3\left(\eta_{(2,1)}\right)$ is as predicted for the $\nu = \frac{1}{3}$ state, and is the *same* as the relation $\tilde{\eta}_{(2,-1)}\left(\tilde{\eta}_{(1,0)}\right)$ of a Luttinger liquid.

3.5 Conclusion and future directions

In the present work we demonstrated the potential of iDMRG to access the edge physics of FQH phases in a clean infinite strip geometry starting from a microscopic Hamiltonian. We calculated scaling exponents for multiple edge excitations in the $\nu = 1/3$, $2/5$ and $2/3$ states and found that the predictions of χLL theory are very accurately met, including the universality of scaling exponents in the maximally chiral $2/5$ edge and their renormalization in non-chiral edges or in the presence of inter-edge interactions.

The mapping of the Landau level Hamiltonian onto a fermionic chain offers a 1D point of view on our results. The occupation number n_k has multiple non-analytic features, which can be identified with edge excitations in the FQH picture. We demonstrated and analytically proved a long standing conjecture regarding the k-values where these features occur, the *generalized Luttinger theorem*, and demonstrated the adiabatic continuity between finite width FQH states and multicomponent Luttinger liquids.

The techniques used here suggest a number of future directions. Of particular interest would be the calculation of exponents in the presence of a point contact, the geometry relevant to interferometry experiments.[139] MPS techniques allow one to introduce a localized defect to the Hamiltonian (a constriction of the trapping potential) while maintaining the infinite boundary conditions of the gapless edge away from the defect. [127, 140] One could then calculate the inter-edge correlation functions in the presence of an interferometer. A second direction would be to investigate more exotic FHQ states, such as the Moore-Read state at filling $\nu = 5/2$, for which significant questions remain regarding the stability of the edge and the interplay between the trap potential and particle-hole symmetry breaking. [141, 142] Finally, one can apply iDMRG and FES techniques to lattice models on a strip in order to study the edge excitations of other candidate topological phases, either symmetry protected or intrinsic; currently little is known about the microscopics of such edges.

3.6 Acknowledgments

The author is grateful to Michael P. Zaletel and Joel E. Moore for the fruitful collaboration on this project. We thank S. Parameswaran, R. Mong, F.D.M. Haldane, and J. Jain for useful discussions. MPZ acknowledges support from NSF GRFP Grant DGE 1106400. DV and JEM acknowledge support from NSF DMR-1206515.

Part III

Space group symmetry and topology

Chapter 4

Geometry in band structures of solids

4.1 Space group symmetries

Symmetry of space underpins much of our understanding of physics. Just as the analysis the Poincaré group provides the foundations of high energy physics that deals with particles and fields in empty spacetime, crystallographic space group symmetry is the starting point of the study of solid state systems. The space group (SG) G consists of all isometries of the physical space under which the system is invariant. All crystallographic space groups are subgroups of the Poincaré group: the crystal defines an absolute rest frame, so it contains no boosts, and it only contains discrete translations and rotations. In a broader sense one may consider magnetic space groups which also contain operations with time reversal.

A general space group operation has the form $g = \{O|\mathbf{t}\}$ where O is an orthogonal rotation (or rotoinversion) and $\mathbf{t}$ is a vector describing the translational part. It acts on a point as $\{O|\mathbf{t}\}\,\mathbf{x} = O\mathbf{x} + \mathbf{t}$ The composition rule is

$$\{O_1|\mathbf{t}_1\}\,\{O_2|\mathbf{t}_2\} = \{O_1O_2|\mathbf{t}_1 + O_1\mathbf{t}_2\}\,. \tag{4.1}$$

Note that the operation on the right is carried out first, and we treat these as active operations that move the physical system rather than changing the basis. The form of the transformation does depend on the choice of the coordinate system. If we shift the origin by $\tilde{\mathbf{t}}$ and rotate the coordinate system by $\tilde{O}$ such that $\mathbf{x} = \tilde{O}\mathbf{x}' + \tilde{\mathbf{t}}$, a SG operation $\{O|\mathbf{t}\}$ in the new coordinate system reads $\{O'|\mathbf{t}'\} = \left\{\tilde{O}^{-1}O\tilde{O}\middle|\tilde{O}^{-1}\left(\mathbf{t} - \tilde{\mathbf{t}} + O\tilde{\mathbf{t}}\right)\right\}$.

Pure translations form a normal subgroup T of any space group, as its conjugate with any SG operation g, $g\,\{\mathbb{1}|\mathbf{t}\}\,g^{-1}$ is again a pure translation. In a crystalline system pure translations form a d-dimensional lattice, such that there is a set of primitive translations $\mathbf{t}_i$ $(i = 1 \ldots d)$ of which any translation is an integer linear combination. This requirement restricts the possible rotations to be 1, 2, 3, 4 or 6-fold. Classification of all such groups (up to group isomorphisms) yields the list of *affine space groups*, of which there is 17 in 2 and 219 in 3 dimensions. For 11 of these groups there are two distinct chiralities in which they

can act on 3d space, making the total of 230 crystallographic space groups. Including time reversal, we find 80 and 1651 magnetic groups in 2 and 3 dimensions respectively.

The *point group* of a space group G is defined as the quotient $P = G/T$, it is isomorphic to the group of orthogonal transformations that appear in the SG. Symmorphic space groups are distinguished by the property that they are a semidirect product $G = T \rtimes P$. With proper choice of origin there is a true subgroup of G isomorphic to P that consists of pure orthogonal operations $\{O|\mathbf{0}\}$. A nonsymmorpic group contains at least one symmetry operation with a fractional lattice translation irrespective of the choice of origin.

An *essential* nonsymmorpic operation[143] leaves no point in space invariant, or equivalently, contains a fractional translation for any choice of origin. There are two kinds or essential nonsymmorphic operations: a glide which is a mirror combined with a fractional translation parallel to the mirror plane, and a screw which is a rotation combined with a fractional translation parallel to the axis of rotation. Almost every nonsymmorphic SG contains at least one essential nonsymmorphic symmetry with only two exceptions: space groups 24 and 199 contain only true rotations, but no choice of origin makes them simultaneously have no fractional translation part.

4.2 Bloch's theorem

4.2.1 Bloch's theorem and the Brillouin zone

In quantum mechanics symmetries act by (anti)unitary operators on the physical Hilbert space and commute with the Hamiltonian. Every energy eigenstate can be labeled by the eigenvalue under the symmetry. If we consider a symmetry group, where operations do not necessarily commute, we label sets of states by the *irreducible representations* of the symmetry group by which they transform. A group representation is a group homomorphism $\rho : G \to U(V)$ from G to a group of unitary operators over a vector space V [1] (usually a set of finite unitary matrices). It is irreducible if no basis transformation brings all operators to the same block-diagonal form, or in other words, V has no invariant subspace under the action of the operator group. As all symmetries commute with the Hamiltonian, these irreducible subspaces of the Hilbert space are also eigensubspaces of the Hamiltonian and are degenerate in energy. The Hamiltonian has no matrix elements between subspaces that belong to different irreducible representations, hence it can be block-diagonalized in a symmetry-respecting basis.

Translations form a commutative group, so all representations are one dimensional, $\rho_{\mathbf{k}}(\{\mathbb{1}|\mathbf{t}\}) = e^{i\mathbf{kt}}$, labeled by a vector $\mathbf{k}$. We call this vector the *(crystal) momentum* of the state. For continuous translations ($T \simeq \mathbb{R}^d$) all $\mathbf{k} \in \mathbb{R}^d$ describe different representations, so the momentum space (or $\mathbf{k}$-space) is infinite. If translations are discrete ($T \simeq \mathbb{Z}^d$), there are vectors $\mathbf{G}$ such that $\rho_{\mathbf{k}+\mathbf{G}} = \rho_{\mathbf{k}}$. These vectors form a d-dimensional lattice called the *reciprocal lattice*, and a (non-unique) set of generators $\{\mathbf{G}_i\}_{i=1\ldots d}$ are *primitive reciprocal*

[1] For simplicity we only explain unitary representations here.

lattice vectors. By identifying points in **k**-space that are related by reciprocal lattice vectors, it turns into a finite d-dimensional torus. There are many choices for the fundamental domain in **k**-space, we will either use a primitive cell which is a parallelepiped spanned by a set of primitive reciprocal lattice vectors, or the Brillouin zone that consists of the points closer to the origin than to any other reciprocal lattice point. The former has the advantage of simplicity, while the latter reflects the symmetries of the lattice better.

As explained earlier, using this symmetry the Hamiltonian can be block-diagonalized in the momentum basis. The Hilbert-space splits according to the momentum representation, $\mathcal{H} = \oplus_{\mathbf{k}} \mathcal{H}_{\mathbf{k}}$ and the Hamiltonian is a direct sum of terms, each acting only at a single $\mathbf{k}$, $H = \oplus_{\mathbf{k}} H_{\mathbf{k}}$. The problem of diagonalizing H reduces to diagonalizing each $H_{\mathbf{k}}$ separately.

To use Bloch's theorem and write operators and states in **k**-space instead of real space, we have to rearrange the degrees of freedom first. A system with discrete translation invariance has the same degrees of freedom in every unit cell, periodically repeated. The crystal momentum only captures the spatial structure at the level of the lattice, but is blind to the details within the unit cell. Degrees of freedom in a unit cell are to be considered "internal", their number determines the dimensionality of the Hilbert-space $\mathcal{H}_{\mathbf{k}}$ and the number of Bloch-bands. We use the indices a, b, etc. to label the orbitals in the unit cell. If we wanted to view free space as a lattice, it would have an infinite number of degrees of freedom per unit cell, thus Bloch states would be infinite dimensional. But in a physical solid it is reasonable to restrict attention to a finite number of electronic states per unit cell: the low energy orbitals of the ions making up the crystal.

4.2.2 Conventions for Bloch functions

There are two widely used conventions to define the Bloch basis functions. When appropriate we use the convention where we define Bloch basis functions $|\widetilde{\chi}^a_{\mathbf{k}}\rangle \in \mathcal{H}_{\mathbf{k}}$ in terms of the orbitals of the unit cell

$$|\widetilde{\chi}^a_{\mathbf{k}}\rangle = \frac{1}{\sqrt{N}} \sum_{\mathbf{R}} e^{i\mathbf{k}\mathbf{R}} \left|\phi^a_{\mathbf{R}+\mathbf{r}_a}\right\rangle \tag{4.2}$$

where $\mathbf{R}$ is the unit cell coordinate, a the orbital index and $\mathbf{r}_a$ is the position of the a-th orbital in the unit cell. Note the absence of phase factors corresponding to the position of the orbitals within the unit cell, so the basis functions are strictly periodic in the BZ. While in this convention the information about the position of the orbitals is lost, thus the polarizations computed via Berry vector potential integrals do not equal the true Wannier center positions, the Bloch Hamiltonian is BZ periodic, making some derivations more transparent.

In the other convention, called the "periodic gauge"[144] we define

$$|\chi^a_{\mathbf{k}}\rangle = \frac{1}{\sqrt{N}} \sum_{\mathbf{R}} e^{i\mathbf{k}(\mathbf{R}+\mathbf{r}_a)} \left|\phi^a_{\mathbf{R}+\mathbf{r}_a}\right\rangle \tag{4.3}$$

. The two conventions are related by the operator $W_{\mathbf{k}}$ with $W^{ab}_{\mathbf{k}} = \delta^{ab} e^{-i\mathbf{k}\mathbf{r}_a}$ such that $|\chi^a_{\mathbf{k}}\rangle = \left(W^{-1}_{\mathbf{k}}\right)^{ab} \left|\widetilde{\chi}^b_{\mathbf{k}}\right\rangle$ so the coefficients of of Bloch wavefunctions transform as $n^a_{\mathbf{k}} = W^{ab}_{\mathbf{k}} \widetilde{n}^{ab}_{\mathbf{k}}$.

The basis functions are not BZ periodic, $\left|\chi^a_{\mathbf{k}+\mathbf{G}}\right\rangle = e^{i\mathbf{G}\mathbf{r}_a}\left|\chi^a_{\mathbf{k}}\right\rangle$ where $\mathbf{G}$ is a primitive reciprocal lattice vector. Consequently, states and operators expanded in this basis satisfy $n_{\mathbf{k}+\mathbf{G}} = W_{\mathbf{G}} n_{\mathbf{k}}$ and $O_{\mathbf{k}+\mathbf{G}} = W_{\mathbf{G}} O_{\mathbf{k}} W^{-1}_{\mathbf{G}}$ respectively. $W_{\mathbf{G}} : \mathcal{H}_{\mathbf{k}} \to \mathcal{H}_{\mathbf{k}+\mathbf{G}}$ is acting between the Hilbert spaces of the *coefficients* of the wavefunctions in this basis. As an example we expand the Hamiltonian in this basis:

$$H^{ab}_{\mathbf{k}} = \left\langle \chi^a_{\mathbf{k}}\right| H \left|\chi^b_{\mathbf{k}}\right\rangle = \frac{1}{N}\sum_{\mathbf{R}\mathbf{R}'} e^{-i\mathbf{k}(\mathbf{R}+\mathbf{r}_a)} \left\langle \phi^a_{\mathbf{R}+\mathbf{r}_a}\right| H \left|\phi^b_{\mathbf{R}'+\mathbf{r}_b}\right\rangle e^{i\mathbf{k}(\mathbf{R}'+\mathbf{r}_b)} =$$
$$= \frac{1}{2}\sum_{\boldsymbol{\delta}} e^{i\mathbf{k}(\boldsymbol{\delta}+\mathbf{r}_b-\mathbf{r}_a)} \left\langle \phi^a_{\mathbf{0}+\mathbf{r}_a}\right| H \left|\phi^b_{\boldsymbol{\delta}+\mathbf{r}_b}\right\rangle = \frac{1}{2}\sum_{\boldsymbol{\delta}} e^{i\mathbf{k}(\boldsymbol{\delta}+\mathbf{r}_b-\mathbf{r}_a)} H^{ab}_{\boldsymbol{\delta}} \tag{4.4}$$

Here we used the discrete translation invariance, such that the hopping matrix elements only depend on the relative separation of the unit cells $\boldsymbol{\delta}$.

This convention, using the coefficients only (e.g. $\mathcal{A}^{nm} = in^\dagger \mathrm{d}m$), is usually assumed in formulae for electromagnetic response, as the naive Peierls substitution $\mathbf{k} \to \mathbf{k} + \mathbf{A}$ only gives the correct phase factor for hopping in this case, as we explain in the next section in more detail. The two conventions give equivalent results for quantized topological indices in most symmorphic cases, provided there is a continuous, symmetry preserving deformation of the lattice, such that all the orbitals are brought to the same point in the unit cell. In nonsymmorphic lattices however, this is never possible, as the shortest orbit of a point in the unit cell under the symmetry group modulo lattice vectors is longer than one, there is no crystal with one site per unit cell obeying a nonsymmorphic symmetry. For example with an n-fold screw translating in the z direction one needs at least n lattice sites that can be arranged such that the positions are $\mathbf{r}_a = \mathbf{a}_z a/n$ for $a = 1 \ldots n$, so $W^{ab}_{\mathbf{G}_z} = \delta^{ab} e^{2\pi i a/n}$ and $W_{\mathbf{G}} = \mathbb{1}$ for perpendicular directions.

We remark that in both bases global antiunitary transformations, such as $\mathcal{T} = \mathcal{K}\sigma_y$ act as constant operators in $\mathbf{k}$-space. To switch conventions, one must transform them same as other operators, $\widetilde{\mathcal{T}} = W_{-\mathbf{k}} \mathcal{T} W^{-1}_{\mathbf{k}} = \mathcal{T}$, where we used that $W^{-1}_{\mathbf{k}} = W_{-\mathbf{k}} = W^*_{\mathbf{k}}$ as W is diagonal and proportional to the identity in spin space.

4.3 Electromagnetic response of free fermions

A wide range of experimental probes of solid state systems, ranging from DC electrical conductivity to optical measurements rely on the response to external electromagnetic fields.

A continuum theory can be coupled to an external $U(1)$ gauge-field using minimal coupling with the replacement:

$$\mathbf{p} \to \mathbf{p} - q\mathbf{A}. \tag{4.5}$$

As already mentioned, in solid state theory the tight-binding approximation is widely used, which amounts to a discretization of space, we need an analogue of the minimal coupling for these situations, called Peierls substitution.

The hopping matrix element between two orbitals is

$$H^{ll'}_{\mathbf{x},\mathbf{x}'} = \left\langle \phi^{l}_{\mathbf{x}} \right| H \left| \phi^{l'}_{\mathbf{x}'} \right\rangle . \tag{4.6}$$

For strongly localized orbitals a gauge-invariant minimal coupling is given by

$$H(\mathbf{A})^{ll'}_{\mathbf{x},\mathbf{x}'} \approx H^{ll'}_{\mathbf{x},\mathbf{x}'} \exp\left(i\frac{q}{\hbar}\int_{\mathbf{x}}^{\mathbf{x}'} \mathbf{A} d\mathbf{r} \right) \approx H^{ll'}_{\mathbf{x},\mathbf{x}'} e^{i\frac{q}{\hbar}\mathbf{A}_{1/2(\mathbf{x}'+\mathbf{x})}\cdot(\mathbf{x}'-\mathbf{x})} + \mathcal{O}\left(\partial^2 \mathbf{A}\right). \tag{4.7}$$

In the first approximation we assumed that the orbitals are strongly localized on the scale $\mathbf{A}$ varies and the integration contour is taken to be a straight line. Note that there is an ambiguity in the choice of a straight line, this approximation neglects the detailed spatial structure of the orbitals. Taking a straight line assumes that most of the overlap between the orbitals in question occurs near the line connecting their centers. This is not necessarily the case, lobes of the two orbitals may overlap at an angle, in this case the flux through the triangle spanned by the straight line and the lobes presents as an error[145]. This error is at the same order as the mixing of various orbitals on the same atom due to the magnetic field. At experimentally relevant field strengths the magnetic flux through a surface of such atomic scale is negligible compared to the flux quantum.

It is important to note that $\mathbf{x}$ is the real space coordinate of the orbital, not the position of the unit cell. When we transform to momentum space, only when the phase factors corresponding to the actual orbital coordinates are used do we find the result analogous to the continuum minimal coupling:

$$H(\mathbf{A})^{ab}_{\mathbf{k}} = \left\langle \chi^{a}_{\mathbf{k}} \right| H(\mathbf{A}) \left| \chi^{b}_{\mathbf{k}} \right\rangle = H^{ab}_{\left(\mathbf{k}-\frac{q}{\hbar}\mathbf{A}\right)}. \tag{4.8}$$

The Peierls substitution underlies many common methods of calculating electromagnetic response in solids, including the use of semiclassical formalism[144] or linear response theory using the Kubo formula. To get the correct result, this convention must be used, as otherwise the position and velocity operators are represented in an unphysical way.

4.4 Differential geometry of band structures

4.4.1 Overview of coordinate-free formalism

We present a brief overview of the coordinate-free formalism of differential forms[146] we use in the remainder of the dissertation. As all our calculations are carried out in the flat $\mathbf{k}$-space, we will not delve into mathematical subtleties and treat this as a convenient notational and computational tool.

An *r-form* is an antisymmetric tensor of type $(0, r)$, it maps r vectors of the local tangent space linearly to scalars. These "scalars" may have internal indices, only need to be scalars from a geometric point of view, as we will see later, we use matrix valued forms as well.

Given a coordinate system x^μ (we use μ, ν, ... to index spatial directions), the coordinate basis in the 1-forms is given by $\mathrm{d}x^\mu$ that transform the same way as x^μ. To construct the basis of r-forms, we define the antisymmetric *wedge or exterior product* $\wedge$ of r 1-forms:

$$\mathrm{d}x^1 \wedge \mathrm{d}x^2 \wedge \ldots \wedge \mathrm{d}x^r = \sum_P \mathrm{sgn}(P)\, \mathrm{d}x^{P(1)} \otimes \mathrm{d}x^{P(2)} \otimes \ldots \otimes \mathrm{d}x^{P(r)} \tag{4.9}$$

where the sum runs over all permutations of the indices $1 \ldots r$ and $\mathrm{sgn}(P)$ is the signature of the permutation. On a d dimensional manifold r-forms form a $\begin{pmatrix} d \\ r \end{pmatrix}$ dimensional vector space. There are no forms with $r > d$ and the space of d-forms is one dimensional.

A generic r-form ω can be expanded in this basis as

$$\omega = \frac{1}{r!}\omega_{\mu_1,\mu_2,\ldots,\mu_r}\, \mathrm{d}x^{\mu_1} \wedge \mathrm{d}x^{\mu_2} \wedge \ldots \wedge \mathrm{d}x^{\mu_r} = \omega_{\mu_1,\mu_2,\ldots,\mu_r}\, \mathrm{d}x^{\mu_1} \otimes \mathrm{d}x^{\mu_2} \otimes \ldots \otimes \mathrm{d}x^{\mu_r}, \tag{4.10}$$

where $\omega_{\mu_1,\mu_2,\ldots,\mu_r}$ is completely antisymmetric and we implicitly sum over all repeated indices.

The wedge product of a generic q-form and r-form, resulting in a $q+r$-form is

$$(\omega \wedge \xi)_{\mu_1,\ldots,\mu_{q+r}} = \frac{1}{q!r!} \sum_P \mathrm{sgn}(P) \omega_{\mu_{P(1)},\ldots,\mu_{P(q)}} \xi_{\mu_{P(q+1)},\ldots,\mu_{P(q+r)}}. \tag{4.11}$$

The prefactor comes from demanding associativity of the wedge product. Some useful general properties are: $\omega \wedge \xi = (-1)^{qp} \xi \wedge \omega$, as a result $\omega \wedge \omega = 0$ if q is odd.

The exterior derivative d generalizes the concept of gradient, divergence and curl, and maps r-forms to $r+1$-forms as

$$\mathrm{d}\omega = \frac{1}{r!} \left(\frac{\partial}{\partial x^\nu} \omega_{\mu_1,\ldots,\mu_r} \right) \mathrm{d}x^\nu \wedge \mathrm{d}x^{\mu_1} \wedge \ldots \wedge \mathrm{d}x^{\mu_r}. \tag{4.12}$$

It is nilpotent ($\mathrm{d}^2 = 0$) and acts on a wedge product as $\mathrm{d}(\omega \wedge \xi) = (\mathrm{d}\omega) \wedge \xi + (-1)^q \omega \wedge (\mathrm{d}\xi)$.

A d-form $\omega = \omega_{1,\ldots,d}\, \mathrm{d}x^1 \wedge \ldots \wedge \mathrm{d}x^d$ can be integrated over a d-dimensional region V of an orientable manifold:

$$\int_V \omega = \int_V \omega_{1,\ldots,d} dx^1 \ldots dx^d. \tag{4.13}$$

The generalized Stokes' theorem relates the integral of an r-form on the boundary ∂V of an $r+1$ dimensional region V to the integral of its exterior derivative over V:

$$\int_{\partial V} \omega = \int_V \mathrm{d}\omega. \tag{4.14}$$

4.4.2 Berry curvature

We define the *Berry connection* as

$$\mathcal{A}^{nm} = i \langle u^n | \, \mathrm{d} | u^m \rangle \tag{4.15}$$

where $|u^n_{\mathbf{k}}\rangle$ is the wave function of the nth occupied eigenstate of a Hamiltonian $H_{\mathbf{k}}$. In general the dependence is on an arbitrary parameter that takes its values from a base manifold. Here, without loss of generality we call this parameter $\mathbf{k}$. Explicitly in components

$$\mathcal{A}^{nm}_{\mu}(\mathbf{k}) = i \langle u^n_{\mathbf{k}}| \partial_{\mathbf{k}^\mu} |u^m_{\mathbf{k}}\rangle . \tag{4.16}$$

From an abstract geometric point of view, by attaching a basis of the local occupied Hilbert space to every point in the base manifold, we create a fiber bundle. The connection defines parallel transport of bases between different points in the base manifold and measures nontrivial "twists" in the bundle.

It is important to realize that there is a gauge ambiguity in the assignment of $|u^n_{\mathbf{k}}\rangle$. For once, a quantum mechanical state is only well defined up to a $U(1)$ phase, the reassignment $|u^n_{\mathbf{k}}\rangle \to e^{i\phi_n(\mathbf{k})} |u^n_{\mathbf{k}}\rangle$ does not change the physical content. But there is an even greater gauge freedom. We are only interested in the topology and it is possible to make all the $n_{\text{occ.}}$ occupied bands degenerate in energy without closing the gap. Now nothing distinguishes the bands and there is a $U(n_{\text{occ.}})$ gauge freedom $|u^n_{\mathbf{k}}\rangle \to U(\mathbf{k})^{nm} |u^m_{\mathbf{k}}\rangle$ with a unitary matrix function U. As all these transformations only amount to a change of basis, all measurable physical quantities must have gauge-invariant expressions. This gauge-freedom allows for nontrivial situations, where there is no continuous global mapping (a global section of the bundle) assigning a basis to each $\mathbf{k}$-point. Instead, we may find that the bases are mismatched by a gauge-transformation between different patches in the base manifold no matter what we do.

The gauge connection $\mathcal{A}$ takes values in the Lie-algebra of $U(n_{\text{occ.}})$, the space of $n_{\text{occ.}} \times n_{\text{occ.}}$ Hermitian matrices[2]. In the following when we omit the band indices (n, m, ...) we mean products in the sense of non-commuting matrix multiplication. The connection is not gauge-invariant, it transforms as

$$\mathcal{A} \to U^\dagger \mathcal{A} U + i U^\dagger \, \mathrm{d}U. \tag{4.17}$$

The covariant derivative ($\mathrm{D}\omega = \mathrm{d}\omega - i\,[\mathcal{A}, \omega]$) of $\mathcal{A}$ with respect to the parallel transport defined by $\mathcal{A}$ gives the *Berry curvature* (or field strength):

$$\mathcal{F} = \mathrm{D}\mathcal{A} = \mathrm{d}\mathcal{A} - i\mathcal{A} \wedge \mathcal{A}, \tag{4.18}$$

or in components

$$\mathcal{F}_{\mu\nu} = \partial_\mu \mathcal{A}_\nu - \partial_\nu \mathcal{A}_\mu - i\,[\mathcal{A}_\mu, \mathcal{A}_\nu]\,. \tag{4.19}$$

The curvature is also Lie-algebra valued and it is gauge-covariant, transforms as

$$\mathcal{F} \to U^\dagger \mathcal{F} U, \tag{4.20}$$

making its trace $\mathrm{Tr}\,\mathcal{F}$ a gauge-invariant quantity. The curvature satisfies the Bianchi-identity

$$\mathrm{D}\mathcal{F} = \mathrm{d}\mathcal{F} - i\,[\mathcal{A}, \mathcal{F}] = 0. \tag{4.21}$$

[2]We use the physicist's convention, in the mathematical literature the i is usually omitted in the definition of $\mathcal{A}$ and the matrices are skew-Hermitian.

For an abelian $U(1)$ gauge field this implies $\mathrm{d}\mathcal{F} = 0$ and in general $\mathrm{Tr}\,\mathrm{d}\mathcal{F} = 0$, making $\mathrm{Tr}\,\mathcal{F}$ a closed form.

Our treatment so far has only referenced the occupied Hilbert space. A different, less abstract view is to consider the full Hilbert space at each $\mathbf{k}$. Assuming $\dim \mathcal{H}_\mathbf{k} = N$, the band structure is a mapping onto the space of $n_{\mathrm{occ.}}$ dimensional subspaces $U(N)/U\left(n_{\mathrm{occ.}}\right)$. The precise form of $\mathcal{A}$ depends on the choice of basis. As we have seen earlier, in the physical response functions of solids it is the expansion coefficients in the $|\chi\rangle$ basis that enter (cf. Sec. 4.2.2). So in the following we will use the definition in terms of the coefficients $\mathcal{A}^{nm} = in^\dagger \mathrm{d}m$.

We introduce the projector onto the occupied bands

$$\mathcal{P}_\mathbf{k} = \sum_{n \in occ.} n_\mathbf{k} n_\mathbf{k}^\dagger. \tag{4.22}$$

It is gauge-invariant and captures all the topological properties of the Bloch-Hamiltonian: $\mathbb{1} - 2\mathcal{P}_\mathbf{k}$ is identical to $H_\mathbf{k}$ except that all the occupied bands have energy -1 and the unoccupied $+1$. $\mathcal{F}$ can be written in a gauge invariant form as

$$\mathcal{F} = i\mathcal{P}(\mathrm{d}\mathcal{P}) \wedge (\mathrm{d}\mathcal{P})\mathcal{P}. \tag{4.23}$$

In this formulation $\mathcal{F}$ is a Hermitian operator acting on $\mathcal{H}_\mathbf{k}$, but is only nonzero on occupied bands. The different definitions should not cause confusion as we can form products and extend the trace to the full Hilbert-space without changing the result. The usual gauge-dependent components can be obtained as matrix elements between occupied states in a given basis of eigenstates, $\mathcal{F}_\mathbf{k}^{nm} = n_\mathbf{k}^\dagger \mathcal{F}_\mathbf{k} m_\mathbf{k}$.

4.4.3 Chern and Chern-Simons forms

The nontrivial topology of band structures, or equivalently the nontrivial winding of fiber bundles can be assessed by computing *topological invariants*.

In even dimensions it is possible to define *Chern numbers*. Let us start with the familiar 2d case. $\mathrm{Tr}\,\mathcal{F}$ is a gauge-invariant 2-form and can be integrated over the 2d parameter space V to give the first Chern-number:

$$C = \frac{1}{2\pi}\int_V \mathrm{Tr}\,\mathcal{F} = \frac{1}{4\pi}\int dk^2 \epsilon^{\mu\nu}\,\mathrm{Tr}\,\mathcal{F}_{\mu\nu}. \tag{4.24}$$

To see that C is insensitive to continuous changes, consider adding a third "deformation" dimension, making the 3d space $V \times [0,1]$. Assuming that $\mathcal{F}$ changes smoothly between $k^3 = 0$ and $k^3 = 1$, we can use the Stokes' theorem to calculate the difference between the integrals at the two cuts:

$$\frac{1}{2\pi}\int_{V,k^3=1} \mathrm{Tr}\,\mathcal{F} - \frac{1}{2\pi}\int_{V,k^3=0} \mathrm{Tr}\,\mathcal{F} = \frac{1}{2\pi}\int_{V\times[0,1]} \mathrm{Tr}\,\mathrm{d}\mathcal{F} = 0. \tag{4.25}$$

In the last step we used that $\mathrm{Tr}\,\mathcal{F}$ is closed ($\mathrm{dTr}\,\mathcal{F}$ vanishes identically). This shows that C can only take discrete values, and it can also be proved that with this normalization $C \in \mathbb{Z}$.

The concept can be generalized to higher dimensions, in $d = 2n$ the nth Chern form

$$\mathrm{ch}_n = \frac{1}{n!}\,\mathrm{Tr}\left(\frac{\mathcal{F}}{2\pi}\right)^{\wedge n} \tag{4.26}$$

is closed, allowing the definition of the nth Chern number

$$\mathrm{Ch}_n = \int ch_n = \frac{1}{n!}\int \mathrm{Tr}\left(\frac{\mathcal{F}}{2\pi}\right)^{\wedge n} \tag{4.27}$$

were we used powers with respect to the wedge product. These integers form the $\mathbb{Z}$ classification in even dimensions in class A.

A related object is the Chern-Simons form in odd dimensions[147]. It is defined such that locally

$$\mathrm{ch}_n = \mathrm{d}(\mathrm{cs}_{2n-1})\,. \tag{4.28}$$

It can be constructed for any n, for example

$$\mathrm{cs}_1 = \frac{1}{2\pi}\,\mathrm{Tr}\,\mathcal{A}, \quad \mathrm{cs}_3 = \frac{1}{8\pi^2}\,\mathrm{Tr}\left(\mathcal{A}\wedge\mathrm{d}\mathcal{A} - \frac{2i}{3}\mathcal{A}\wedge\mathcal{A}\wedge\mathcal{A}\right). \tag{4.29}$$

Its integral over a $2n+1$ dimensional manifold $\mathrm{CS}_{2n+1} = \int \mathrm{cs}_{2n+1}$ is not a topological invariant in the absence of symmetry, it can change continuously, consistent with the trivial classification in odd dimensions in class A. Nevertheless, it has an important role for classification in odd dimensions with additional symmetries (cf. Chap. 5), so we review its properties here.

The Chern-Simons forms, unlike the Chern forms, are not locally gauge invariant. This can be checked by straightforward substitution of a gauge transformed connection. The CS integrals, however, possess a limited gauge invariance, the value is well defined modulo integers. The change is nothing but the integer winding number of the $U(N)$ gauge transformation

$$\mathrm{CS}_{2n+1}(\mathcal{A}') - \mathrm{CS}_{2n+1}(\mathcal{A}) = -\frac{n!}{(2n+1)!}\left(\frac{i}{2\pi}\right)^{n+1}\int \mathrm{Tr}\left(U^{-1}\,\mathrm{d}U\right)^{\wedge 2n+1}. \tag{4.30}$$

Another way to see this, is to add an extra cyclic dimension, $k^{2n+2} \in S^1$ and consider cyclic deformations as k^{2n+2} advances from 0 to 2π. By the definition of cs_{2n+1}, the change between the initial and final slices can be calculated using Stokes' theorem:

$$\mathrm{CS}_{2n+1}(k^{2n+2}=2\pi) - \mathrm{CS}_{2n+1}(k^{2n+2}=0) = \int \mathrm{dcs}_{2n+1} = \int \mathrm{ch}_{n+1} = \mathrm{Ch}_{n+1}. \tag{4.31}$$

The right hand side is the Chern number for the $2n+2$ dimensional compact $V \times S^1$ space, which is in general a nonzero integer. As we demanded the initial and final gauge field configurations to be the same, we see that CS is only well defined modulo integers. Note that we introduce θ in Chap. 5 with a different normalization ($\theta = 2\pi\mathrm{CS}_3$) and the ambiguity also changes to multiples of 2π.

4.5 BdG formalism

Here we summarize general results of the BdG formalism used for superconductors[15], with special emphasis to representations of symmetries in class C.

The general form of a Hamiltonian for a superconductor without any additional symmetry is

$$\begin{aligned}\mathcal{H} &= \sum_{\mathbf{k}} \begin{pmatrix} c_{\mathbf{k}}^\dagger & c_{-\mathbf{k}} \end{pmatrix} \begin{pmatrix} \epsilon_{\mathbf{k}} & \Delta_{\mathbf{k}} \\ \Delta_{\mathbf{k}}^\dagger & -\epsilon_{-\mathbf{k}}^T \end{pmatrix} \begin{pmatrix} c_{\mathbf{k}} \\ c_{-\mathbf{k}}^\dagger \end{pmatrix} = \\ &= \sum_{\mathbf{k}} \begin{pmatrix} c_{\mathbf{k}}^\dagger & c_{-\mathbf{k}} \end{pmatrix} H_{\mathbf{k}} \begin{pmatrix} c_{\mathbf{k}} \\ c_{-\mathbf{k}}^\dagger \end{pmatrix} \end{aligned} \tag{4.32}$$

where c is a vector formed of all the electron anihilation operators of the unit cell and the BdG Hamiltonian $H_{\mathbf{k}}$ is a $2N \times 2N$ block matrix with N orbitals in the unit cell. $\epsilon_{\mathbf{k}} = \epsilon_{\mathbf{k}}^\dagger$ (Hermiticity) and $\Delta_{\mathbf{k}} = -\Delta_{-\mathbf{k}}^T$ (Fermi statistics). It is customary to denote the Pauli matrices acting on the particle-hole space (the block structure of H) τ_μ. All such Hamiltonians are compatible with paricle-hole symmetry represented by $\mathcal{C} = \tau_x \mathcal{K}$ for usual electronic systems such that $\mathcal{C}^2 = \mathbb{1}$. This symmetry restricts the BdG Hamiltonian as

$$\mathcal{C} H_{\mathbf{k}} \mathcal{C}^{-1} = \tau_x H_{-\mathbf{k}}^* \tau_x = -H_{\mathbf{k}} \tag{4.33}$$

which is automatically satisfied by this form of the Hamiltonian. This transformation relates excitations with opposite energy and momentum in the doubled spectrum.

At this point we digress to discuss transformation properties of the BdG Hamiltonian under physical symmetry and gauge transformations. A general transformation on the particle-hole degrees of freedom has the form

$$\begin{pmatrix} c_{\mathbf{k}} \\ c_{-\mathbf{k}}^\dagger \end{pmatrix} \to \begin{pmatrix} U_{\mathbf{k}} & W_{\mathbf{k}} \\ W_{-\mathbf{k}}^* & U_{-\mathbf{k}}^* \end{pmatrix} \begin{pmatrix} c_{\mathbf{k}} \\ c_{-\mathbf{k}}^\dagger \end{pmatrix} \tag{4.34}$$

because we require that the transformed particle and hole-like operators are still related by hermitian conjugation. Moreover, preserving the fermionic commutation relations restricts the block matrix to be unitary.

Now we turn to the case with spin rotation symmetry. We split the c vector in 2 halves for the spin z component $c_{\mathbf{k}} = \begin{pmatrix} c_{\mathbf{k}\uparrow} & c_{\mathbf{k}\downarrow} \end{pmatrix}^T$ and rewrite the Hamiltonian in a $4N \times 4N$ block form where N is the number of orbitals not counting spin. The U(1) spin rotation invariance around the z axis requires H_4 to commute with the generator of the rotations $\sigma_z \tau_z$ which restricts it to the block-diagonal form

$$H_{4\mathbf{k}} = \begin{pmatrix} \xi_{\mathbf{k}\uparrow} & 0 & 0 & \delta_{\mathbf{k}} \\ 0 & \xi_{\mathbf{k}\downarrow} & -\delta_{-\mathbf{k}}^T & 0 \\ 0 & -\delta_{-\mathbf{k}}^* & -\xi_{-\mathbf{k}\uparrow}^T & 0 \\ \delta_{\mathbf{k}}^\dagger & 0 & 0 & -\xi_{-\mathbf{k}\downarrow}^T \end{pmatrix}. \tag{4.35}$$

Imposing spin rotation symmetry for the x axis as well (commutation with $\sigma_x\tau_z$) means $\xi_{\mathbf{k}\uparrow} = \xi_{\mathbf{k}\downarrow} =: \xi_{\mathbf{k}}$ and $\delta_{\mathbf{k}} = \delta^T_{-\mathbf{k}}$. If we now define a new set of operators $d_{\mathbf{k}\sigma} = \begin{pmatrix} c_{\mathbf{k}\sigma} & c^\dagger_{-\mathbf{k}\bar{\sigma}} \end{pmatrix}^T$ with well defined momentum and spin quantum number, we can rewrite the Hamiltonian as the sum of two $2N \times 2N$ terms for the two spin orientations

$$\mathcal{H} = \sum_{\mathbf{k}\sigma} d^\dagger_{\mathbf{k}\sigma} H_{2\mathbf{k}\sigma} d_{\mathbf{k}\sigma} \tag{4.36}$$

where

$$H_{2\mathbf{k}\uparrow} = \begin{pmatrix} \xi_{\mathbf{k}} & \delta_{\mathbf{k}} \\ \delta^\dagger_{\mathbf{k}} & -\xi^T_{-\mathbf{k}} \end{pmatrix} \tag{4.37}$$

and $H_{2\mathbf{k}\uparrow} = r_z H_{2\mathbf{k}\downarrow} r_z =: H_{2\mathbf{k}}$ with Pauli matrices r_μ acting on the space with the two components of d. The unitary relation between the two spin sectors guarantees that the spectrum is doubly degenerate, for every eigenstate there is another state with the same energy and momentum but opposite spin.

The constraints on the form of $H_{2\mathbf{k}}$ can be summarized as

$$\mathcal{C} H_{2\mathbf{k}} \mathcal{C}^{-1} = r_y H^*_{2-\mathbf{k}} r_y = -H_{2\mathbf{k}} \tag{4.38}$$

where we introduced the new particle-hole conjugation operator $\mathcal{C} = r_y\mathcal{K}$ with $\mathcal{C}^2 = -\mathbb{1}$ (in the body of the paper we use τ instead of r for this set of Pauli matrices as well). This operator relates states with opposite energy and momentum but the same spin. Note that this operator differs from the original particle-hole conjugation in that it is combined with a spin flip, the physical symmetry should also reverse spin. As the symmetry is antiunitary and squares to $-\mathbb{1}$, a zero energy eigenstate at an invariant momentum must be doubly degenerate (on top of the spin degeneracy that is always present) by the same reasoning that proves Kramers degeneracy with $\mathcal{T}^2 = -\mathbb{1}$.

4.6 Transformation properties

4.6.1 Global symmetries

First we review transformation properties under time reversal. We take the active point of view, $\mathcal{T}$ acting on a band structure produces a new band structure and we express quantities of this new state in the same basis. Time reversal on a Bloch state of system of spin-1/2 fermions acts as

$$(\mathcal{T}n)_{\mathbf{k}} = \sigma_y n^*_{-\mathbf{k}} \tag{4.39}$$

where σ_y acts on the spin degree of freedom of the unit cell Hilbert-space. With simple substitution we find for the Berry connection:

$$(\mathcal{T}\mathcal{A})^{nm}_{\mathbf{k}\mu} = i\,(\mathcal{T}n)^\dagger_{\mathbf{k}}\,\partial_\mu\,(\mathcal{T}m)_{\mathbf{k}} = \left(-in^\dagger_{-\mathbf{k}}\partial_\mu m_{-\mathbf{k}}\right)^* = \left(-in^\dagger_{\mathbf{k}}\,(-\partial_\mu)\,m_{\mathbf{k}}\right)^*_{-\mathbf{k}} = \mathcal{A}^{*nm}_{-\mathbf{k}\mu} = \mathcal{A}^{mn}_{-\mathbf{k}\mu}. \tag{4.40}$$

Here we used that $\frac{d}{dx}f(-x) = -\frac{df}{dx}(-x)$ and the Hermitian property of $\mathcal{A}$. This can be written concisely as

$$(\mathcal{T}\mathcal{A})_{\mathbf{k}} = \mathcal{A}^T_{-\mathbf{k}}. \tag{4.41}$$

Similar calculation for the Berry field strength yields

$$(\mathcal{T}\mathcal{F})_{\mathbf{k}} = -\mathcal{F}^T_{-\mathbf{k}} \tag{4.42}$$

in the gauge where the nth band at $\mathbf{k}$ is mapped to the nth band at $-\mathbf{k}$ by $\mathcal{T}$. In the gauge-invariant formalism,

$$(\mathcal{T}\mathcal{F})_{\mathbf{k}} = -\sigma_y \mathcal{F}^T_{-\mathbf{k}} \sigma_y \tag{4.43}$$

which can be seen using the transformation property of the projector

$$(\mathcal{T}\mathcal{P})_{\mathbf{k}} = \sigma_y \mathcal{P}^T_{-\mathbf{k}} \sigma_y. \tag{4.44}$$

Our treatment so far did not rely on time reversal symmetry, the expressions give the time reversed image of the band structure. Even in a TR breaking system, the image of the Bloch states are Bloch states of the time reversed system with the same energy. It is often convenient to work in a basis of spin (or total angular momentum) polarized orbitals for a TR breaking system, but the time reversed orbitals can always be put back by hand, forming unoccupied bands at high energy, not affecting the topology of the occupied bands.

As $n_{\mathbf{k}}$ is not gauge invariant, TR invariance does not imply that $n_{\mathbf{k}}$ equals $(\mathcal{T}n)_{\mathbf{k}}$. The equivalence is only true up to gauge transformations $(\mathcal{T}n)_{\mathbf{k}} = U^{nm}_{\mathbf{k}} m_{\mathbf{k}}$, characterizing the nontrivial winding of $U_{\mathbf{k}}$ underlies the Pfaffian view of topological insulators[18]. Similarly $\mathcal{A}^{nm}$ and $\mathcal{F}^{nm}$ are also gauge dependent, and we must be careful to only demand TR invariance of gauge-invariant quantities. The band projector and $\mathcal{F}$ as an operator on the full Hilbert space are gauge-invariant, so TR symmetry implies $(\mathcal{T}\mathcal{P})_{\mathbf{k}} = \mathcal{P}_{\mathbf{k}}$ and $(\mathcal{T}\mathcal{F})_{\mathbf{k}} = \mathcal{F}_{\mathbf{k}}$.

Now we are in a position to prove some properties of TR symmetric systems. $\operatorname{Tr}\mathcal{F}$ is gauge-invariant and odd under time-reversal, $\operatorname{Tr}\mathcal{F}_{\mathbf{k}} = -\operatorname{Tr}\mathcal{F}_{-\mathbf{k}}$. The Chern-number for a TR invariant slice must vanish, as contributions from opposite $\mathbf{k}$-points cancel.

We also prove the quantization of the CS form in 3d TI's:

$$\begin{aligned}
\mathcal{T}\mathrm{CS}_3 &= \frac{1}{8\pi^2}\mathcal{T}\int \operatorname{Tr}\left(\mathcal{A}_{\mathbf{k}} \wedge \mathrm{d}\mathcal{A}_{\mathbf{k}} - \frac{2i}{3}\mathcal{A}_{\mathbf{k}} \wedge \mathcal{A}_{\mathbf{k}} \wedge \mathcal{A}_{\mathbf{k}}\right) = \\
&= \frac{1}{8\pi^2}\int \operatorname{Tr}\left(\mathcal{A}^T_{-\mathbf{k}} \wedge \mathrm{d}\mathcal{A}^T_{-\mathbf{k}} - \frac{2i}{3}\mathcal{A}^T_{-\mathbf{k}} \wedge \mathcal{A}^T_{-\mathbf{k}} \wedge \mathcal{A}^T_{-\mathbf{k}}\right) = \\
&= \frac{1}{8\pi^2}\int \operatorname{Tr}\left(\mathcal{A}^T_{\mathbf{k}} \wedge (-\mathrm{d})\mathcal{A}^T_{\mathbf{k}} - \frac{2i}{3}\mathcal{A}^T_{\mathbf{k}} \wedge \mathcal{A}^T_{\mathbf{k}} \wedge \mathcal{A}^T_{\mathbf{k}}\right) = \\
&= \frac{1}{8\pi^2}\int \operatorname{Tr}\left((-\mathrm{d}\mathcal{A}_{\mathbf{k}}) \wedge \mathcal{A}_{\mathbf{k}} + \frac{2i}{3}\mathcal{A}_{\mathbf{k}} \wedge \mathcal{A}_{\mathbf{k}} \wedge \mathcal{A}_{\mathbf{k}}\right)^T = -\mathrm{CS}_3.
\end{aligned} \tag{4.45}$$

In the first step we merely substitute $\mathcal{T}\mathcal{A}$, then we switch the integration variable to $-\mathbf{k}$ taking care of the minus sign picked up by the derivative. In the third step we move the

transpose out, which comes with signs corresponding to the rearrangement of wedge products. In the last step we integrate the first term by parts using $\mathrm{d}(\mathcal{A}\wedge\mathcal{A}) = (\mathrm{d}\mathcal{A})\wedge\mathcal{A} - \mathcal{A}\wedge(\mathrm{d}\mathcal{A})$. As CS_3 is gauge invariant up to integers, this explicitly proves that it is quantized to 0 or 1/2 (mod 1).

Formally charge conjugation acts very similarly,

$$(\mathcal{C}n)_{\mathbf{k}} = \tau_x n^*_{-\mathbf{k}}. \tag{4.46}$$

However, we must remember that $\mathcal{C}$ flips the sign of the energy, mapping an occupied band onto an unoccupied one. This only allows comparison of geometric properties between the occupied and unoccupied bands:

$$(\mathcal{C}\mathcal{A}^o)_{\mathbf{k}} = (\mathcal{A}^u)^T_{-\mathbf{k}}, \quad (\mathcal{C}\mathcal{F}^o)_{\mathbf{k}} = -(\mathcal{F}^u)^T_{-\mathbf{k}}. \tag{4.47}$$

This offers a concise proof for the $\mathbb{Z}_2$ classification for class D in 1d. Consider the first Chern-Simons form for the occupied bands:

$$\mathcal{C}\left(\mathrm{CS}_1^o\right) = \frac{1}{2\pi}\mathcal{C}\int \mathrm{Tr}\,\mathcal{A}^o_{\mathbf{k}} = \frac{1}{2\pi}\int \mathrm{Tr}(\mathcal{A}^u)^T_{-\mathbf{k}} = \mathrm{CS}_1^u. \tag{4.48}$$

As we constructed the system from trivial localized orbitals, $\mathrm{CS}_1^{\mathrm{tot}}$ for all the bands must be zero modulo integers, corresponding to a trivial bundle. As $\mathrm{Tr}\,\mathcal{A}^{\mathrm{tot}} = \mathrm{Tr}\,\mathcal{A}^o + \mathrm{Tr}\,\mathcal{A}^u$, we find $\mathrm{CS}_1^o = -\mathrm{CS}_1^u = -\mathrm{CS}_1^o$ (mod 1). This implies that CS_1^o is quantized to 0 or 1/2. Similar reasoning does not apply to all higher Chern-Simons forms because of the different sign under $\mathcal{C}$ or the lack of such simple additive property.

4.6.2 Space group symmetries

First we review the representations of space group operations in $\mathbf{k}$-space[47, 48]. We use the convention with Bloch basis functions $\left|\chi^{\mathbf{x}l}_{\mathbf{k}}\right\rangle = \sum_{\mathbf{R}} e^{i\mathbf{k}(\mathbf{R}+\mathbf{x})}\left|\phi^l_{\mathbf{R}+\mathbf{x}}\right\rangle$, where we split the orbital index $a = (\mathbf{x}, l)$, $\mathbf{x}$ labels the sites of the unit cell by their real space position and l is an on-site orbital index accounting for spin, orbital angular momentum, etc. (the values l can take may depend on $\mathbf{x}$). A useful property of this basis is that it is periodic in the real space coordinate, i.e. $\left|\chi^{(\mathbf{x}+\mathbf{R})l}_{\mathbf{k}}\right\rangle = \left|\chi^{\mathbf{x}l}_{\mathbf{k}}\right\rangle$ for any lattice vector $\mathbf{R}$. We emphasize that our treatment is not specific to tight-binding models, the same can be told in the continuum, there $\mathbf{x}$ is the continuous index for position in the unit cell and l stands for the spin only. To go to the tight-binding approximation, we restrict the Hilbert-space to a finite set of orbitals per unit cell, the only assumption we make is that orbitals centered on different sites span orthogonal subspaces.

Consider a general space group operation $g = \{O|\mathbf{t}\}$ acting on one of the basis states

$$g\left|\phi^l_{\mathbf{R}+\mathbf{x}}\right\rangle = U^{ll'}_{\mathbf{x}}\left|\phi^{l'}_{g(\mathbf{R}+\mathbf{x})}\right\rangle = U^{ll'}_{\mathbf{x}}\left|\phi^{l'}_{O(\mathbf{R}+\mathbf{x})+\mathbf{t}}\right\rangle \tag{4.49}$$

where U is the site and g-dependent unitary representation on the local orbitals, a double representation if the model is spinful. Applying this to the Bloch basis functions, with simple algebra we find

$$g\left|\chi_{\mathbf{k}}^{\mathbf{x}l}\right\rangle = e^{-i(g\mathbf{k})\mathbf{t}}U_{\mathbf{x}}^{ll'}\left|\chi_{g\mathbf{k}}^{g\mathbf{x},l'}\right\rangle \tag{4.50}$$

with $g\mathbf{k} = O\mathbf{k}$ and $g\mathbf{x} = O\mathbf{x} + \mathbf{t}$ that is understood as a permutation of sites at the same Wyckoff position. Grouping indices back together, this can be written as $g\left|\chi_{\mathbf{k}}^{a}\right\rangle = e^{-i(g\mathbf{k})\mathbf{t}}U^{ba}\left|\chi_{g\mathbf{k}}^{b}\right\rangle$

The key observation is that in this basis the $\mathbf{k}$-dependence decouples as a single factor proportional to the identity. Consider the transformation of a Bloch eigenstate in the n-th band $|n_{\mathbf{k}}\rangle = n_{\mathbf{k}}^{a}\left|\chi_{\mathbf{k}}^{a}\right\rangle$. The symmetry transformation results in a state at $g\mathbf{k}$, the coefficients transform as $(gn)_{g\mathbf{k}}^{a} = e^{-i(g\mathbf{k})\mathbf{t}}U^{ab}n_{\mathbf{k}}^{b}$ or in a compact notation

$$(gn)_{\mathbf{k}} = e^{-i\mathbf{k}\mathbf{t}}Un_{g^{-1}\mathbf{k}}. \tag{4.51}$$

As g is a symmetry operation, the transformed state is again an eigenstate of the Bloch Hamiltonian with the same energy, but at $g\mathbf{k}$. As a consequence, the transformation of occupied band projector operator $\mathcal{P}_{\mathbf{k}} = \sum_{n\in\text{occ.}} n_{\mathbf{k}}n_{\mathbf{k}}^{\dagger}$ reads

$$(g\mathcal{P})_{g\mathbf{k}} = \sum_{n\in\text{occ.}} (gn)_{g\mathbf{k}}(gn)_{g\mathbf{k}}^{\dagger} = U\mathcal{P}_{\mathbf{k}}U^{\dagger}. \tag{4.52}$$

So if g is a symmetry, such that $(g\mathcal{P})_{\mathbf{k}} = \mathcal{P}_{\mathbf{k}}$, any gauge invariant quantity that can be expressed through $\mathcal{P}_{\mathbf{k}}$ is invariant if the $\mathbf{k}$-space coordinates are transformed accordingly. Examples include[48] the Berry curvature $\mathcal{F} = i\mathcal{P}\,\mathrm{d}\mathcal{P}\wedge\mathrm{d}\mathcal{P}\mathcal{P}$ and closed loop integrals of the Berry connection $\mathcal{A}$ (see below).

For completeness we derive the transformation properties of $\mathcal{A}$ and $\mathcal{F}$ under the basis change corresponding to switching between conventions and show that invariants calculated in either convention give the same result. We feel this is necessary because, while the Berry connection for the Bloch basis $|\widetilde{\chi}_{\mathbf{k}}^{a}\rangle$ vanishes and one can safely use the coefficients, for the basis $|\chi_{\mathbf{k}}^{a}\rangle$ it is nonzero, $\mathcal{A}_{\chi}^{ab} = i\left\langle\chi_{\mathbf{k}}^{a}\right|\mathrm{d}\left|\chi_{\mathbf{k}}^{b}\right\rangle = i\delta^{ab}e^{i\mathbf{k}\mathbf{t}_a}\mathbf{t}_a\,\mathrm{d}\mathbf{k}$. This means that one may worry that the formulae in terms of the components in this basis may be missing some terms coming from the derivatives of the basis vectors.

For generality, we consider a transformation $U_{\mathbf{k}}$ acting on the coefficients, it may either be a basis transformation, or a physical one and let $n'_{\mathbf{k}} = U_{\mathbf{k}}n_{\mathbf{k}}$. We find

$$\mathrm{Tr}_{occ.}\,\mathcal{A}' = \sum_{n} in'^{\dagger}\,\mathrm{d}n' = \mathrm{Tr}_{occ.}\,\mathcal{A} + i\,\mathrm{Tr}\left(\mathcal{P}U^{\dagger}\,\mathrm{d}U\right) \tag{4.53}$$

$$\mathrm{Tr}_{occ.}\,\mathcal{F}' = \mathrm{Tr}_{occ.}\,\mathrm{d}\mathcal{A}' = \mathrm{Tr}_{occ.}\,\mathcal{F} + i\,\mathrm{dTr}\left(\mathcal{P}U^{\dagger}\,\mathrm{d}U\right) \tag{4.54}$$

where $\mathrm{Tr}_{occ.}(.) = \sum_n(.)^{nn}$ is the trace over occupied bands, while $\mathrm{Tr}(.) = \sum_a(.)^{aa}$ is the trace over the entire Hilbert-space of the unit cell. We see that as long as $\mathcal{P}U^{\dagger}\,\mathrm{d}U$ is unit cell periodic, which is the case for the basis transformation $U_{\mathbf{k}}^{ab} = W_{\mathbf{k}}^{ab} = \delta^{ab}e^{i\mathbf{k}\mathbf{r}_a}$ if $\mathcal{P} = \widetilde{\mathcal{P}}$

(BZ periodic convention), the change in $\mathrm{Tr}_{occ.} \int_S \mathcal{F}$ is fully compensated by the change in $\mathrm{Tr}_{occ.} \int_{\partial S} \mathcal{A}$ in the formula for the $\mathbb{Z}_2$ invariants and vanishes for Chern-numbers.

We note that the expression for $\mathrm{Tr}_{occ.} \oint \mathcal{A}$ along a non-contractible loop in terms of the projector is modified in the $|\chi\rangle$ basis,

$$\mathrm{Tr}_{occ.} \oint \mathcal{A} = i \log \det_{+} \left(W_{-\mathbf{G}} \prod_{\mathbf{k}=\mathbf{k}_0}^{\mathbf{k}_0-\mathbf{G}} \mathcal{P}_{\mathbf{k}} \right) \tag{4.55}$$

where $\det_+$ is the pseudo-determinant of the matrix, which is defined as the product of all nonzero eigenvalues. This is equivalent to calculating the determinant of the restriction to the local occupied space at $\mathbf{k}_0$, i.e. we evaluate $-i \log \det_+$ as the sum of the complex phases of the nonzero eigenvalues. The reason $W_{\mathbf{G}}$ appears is the mismatch of the basis at $\mathbf{k}_0$ and $\mathbf{k}_0 + \mathbf{G}$. We give more details on the properties of Wilson loops in Chap. 7.

4.6.3 Magnetic space group symmetries

Magnetic space groups contain symmetries that are a combinations of time reversal and a space group operation. As TR is not a symmetry by itself, the low energy theory does not necessarily contain the TR image of all orbitals. It is always possible, however, to enlarge the unit cell Hilbert-space with the time reversed image of all orbitals. These orbitals will have a high energy, forming unoccupied bands, not affecting the topology of the occupied bands. This allows definition of $\mathcal{T}$ operator with the same properties as before, but not as a symmetry. An issue we swept under the rug so far, is that the low energy theory often contains orbitals with nonzero orbital angular momentum that also has to be reversed by $\mathcal{T}$ alongside the spin. To be the most general, consider spin-orbit coupled electronic states of isolated ions where only the total angular momentum J is a well defined half-integer. In the standard basis J_y is purely imaginary and a time-reversal operator $\mathcal{T} = e^{-i\pi J_y}\mathcal{K}$ can be defined. As required $\mathcal{T}^2 = -\mathbb{1}$ and $\mathcal{T} J_i = -J_i \mathcal{T}$ for all i. The anticommutation relation ensures that spatial rotations $e^{i\mathbf{n}\cdot\mathbf{J}}$ commute with $\mathcal{T}$, and this property is inherited by any invariant subspace. So we see that $\mathcal{T}$ with all the properties we used previously is well defined in the enlarged Hilbert-space.

Now we can combine the formalisms in the two previous two sections. The symbols for magnetic group elements are the same as for space group elements, the presence of TR in the operation is denoted by a prime:

$$\{O|\mathbf{t}\}' = \{O|\mathbf{t}\}\,\mathcal{T}. \tag{4.56}$$

$\mathcal{T}$ acts strictly locally and commutes with local rotations, so it commutes with all SG operations. The transformation properties of states and other objects are a simple product of the two operations:

$$(\{O|\mathbf{t}\}'\, n)_{\mathbf{k}} = e^{-i\mathbf{k}\mathbf{t}} U \sigma_y n^*_{-g^{-1}\mathbf{k}} \tag{4.57}$$

where σ_y is the unitary part of $\mathcal{T}$, not necessarily equal to the Pauli matrix.

Armed with this formalism it is possible to show that any magnetic group operation that reverses time but preserves orientation quantizes θ. The calculation is analogous to that presented for the TR invariant case in Sec. 4.6.1 combined with the SG case in Sec. 5.2.1. This generalizes antiferromagnetic topological insulators studied in Ref. [44] where only simple Neél-like symmetries were considered, which are combinations of TR with a pure fractional translation.

Chapter 5

θ-terms and topological response with nonsymmorphic symmetries

In this chapter we consider whether nonsymmorphic symmetries such as a glide plane can protect the existence of topological crystalline insulators and superconductors in three dimensions. In analogy to time-reversal symmetric insulators, we show that the presence of a glide gives rise to a quantized magnetoelectric polarizability, which we compute explicitly through the Chern-Simons 3-form of the bulk wave functions for a glide symmetric model. Our approach provides a measurable property for this insulator and naturally explains the connection with mirror symmetry protected insulators and the recently proposed $\mathbb{Z}_2$ index for this phase. More generally, we prove that the magnetoelectric polarizability becomes quantized with any orientation-reversing space group symmetry. We also construct analogous examples of glide protected topological crystalline superconductors in classes D and C and discuss how bulk invariants are related to quantized surface thermal-Hall and spin-Hall responses.

5.1 Introduction

The last decade has seen a major breakthrough in the search of novel phases of matter with the discovery of topological insulators and superconductors[148–150]. The original predictions of these systems have already led to many experimental realizations, in a very fruitful endeavor that continues today. The key insight underlying this discovery is that the presence of a symmetry, in this case time-reversal symmetry ($\mathcal{T}$), allows to define a new bulk topological invariant of the Bloch wave functions in the Brillouin Zone (BZ). In a gapped fermion system, this invariant cannot change unless the gap closes, defining a robust phase and protecting the existence of gapless boundary states. It was soon realized that other global symmetries in the Altland-Zirnbauer (AZ) classes[16], such as charge conjugation ($\mathcal{C}$) and chiral symmetry, also give rise to new phases, leading to the periodic table[11, 15] of topological insulators and superconductors.

The classification based on global symmetries then lead to the natural question of whether lattice symmetries can give rise to new topological phases of matter. For example, it was realized early on that in the presence of lattice translations, one may define extra topological invariants in lower dimensional slices of the Brillouin Zone [9], which lead to the concept of weak topological insulators [60, 151]. Point group symmetries such as rotations or reflections were also used to define new topological invariants and phases of matter, which were termed topological crystalline insulators[28, 29] (TCI) and superconductors (TCSC). Recent efforts in the field [14, 31, 32, 34–37, 41, 46, 152] have been devoted to classifing these phases of matter protected by lattice symmetries in addition to global ones. Most of these previous works focused on symmorphic space groups for simplicity, i.e. groups where the full group is a semidirect product of the translation part and the point group. However, in view of the strong constraints that non-symmorphic symmetries place on the Bloch wave functions, one may expect that these symmetries can lead to richer structures, an idea that has drawn a lot of attention recently [40, 42–45, 50, 51, 53, 143]. The question we consider in this paper is whether non-symmorphic symmetries, in particular glide reflections, can define a new class of topological insulators or superconductors. We will focus on the three dimensional case without time-reversal symmetry, where it has been predicted that a new TCI protected by glide symmetry indeed exists[40].

While in this work we will present explicit computations of microscopic topological invariants, our main conclusions can also be understood in a simple way by considering topological bulk responses. It is well known that a three dimensional topological insulator can be characterized by a quantized bulk electromagnetic response term of the type[20]

$$S = \frac{\theta e^2}{16\pi h} \int d^4\mathsf{x}\, \epsilon^{\mu\nu\lambda\gamma} F_{\mu\nu} F_{\lambda\gamma} = \frac{\theta e^2}{4\pi h} \int F \wedge F \tag{5.1}$$

which is known as the magnetoelectric response (because $F \wedge F \propto \mathbf{E} \cdot \mathbf{B}$) or the "axion" Lagrangian. The second equality is expressed in coordinate-free notation, which we will use from now on (see Appendix 5.A). The magnetoelectric coupling θ is defined modulo 2π, and the presence of time-reversal symmetry requires that $\theta = -\theta$. This implies that $\theta = 0$ or π, and the second case corresponds to a strong topological insulator. θ can be computed microscopically from the Chern-Simons 3-form of the Berry connection, establishing a direct correspondence with the $\mathbb{Z}_2$ index. A physical consequence of $\theta = \pi$ is the presence of an odd number of massless Dirac fermions on the surface which are protected by time-reversal symmetry.

The same line of reasoning[44, 46] implies that the magnetoelectric coupling is quantized in the presence of any symmetry that sends $\theta \to -\theta$, such as mirror reflection[10, 36] which reverses one spatial coordinate. In the presence of a surface that respects this symmetry, one must also have an odd number of Dirac cones. A three dimensional topological insulator can therefore be protected by either time-reversal or mirror symmetry. The magnetoelectric coupling in the second case can be computed microscopically from mirror Chern numbers[10] at invariant planes.

The main result of this work is that glide symmetry also gives rise to quantized magnetoelectric coupling, which exactly corresponds to the $\mathbb{Z}_2$ invariant previously defined for glide protected topological crystalline insulators[40]. This result can be simply rationalized by the fact the magnetoelectric coupling is a bulk response property which makes no reference to the lattice. Since a glide differs from a regular mirror only by a half translation, from the perspective of the bulk response both symmetries guarantee the quantization of the θ term, giving rise to a topological insulator when $\theta = \pi$. This result is explicitly proven in Appendix 5.2.1 where we show in general that θ becomes quantized in the presence of any orientation-reversing space group symmetry.

In this work we also illustrate this general result by an explicit calculation of θ via the Chern-Simons form for a particular model of a glide symmetric TI, confirming the presence of a single Dirac fermion in the surface spectrum when $\theta = \pi$. In the second part of this work, we explain how these ideas can be naturally extended to superconductors without time-reversal symmetry in classes D and C. In these classes there are analogs of the magnetoelectric coupling for the thermal and spin response, respectively, and these can also be quantized in the presence of a glide symmetry. We will also present explicit models for these classes, and show that microscopic computations of the bulk topological invariants are consistent with the surface spectra.

5.2 Magnetoelectric Coupling and $\mathbb{Z}_2$ Invariant In Mirror and Glide Symmetric Insulators

The quantized magnetoelectric response in Eq. 5.1 has been long known to be the distinguishing feature of strong topological insulators[20, 27] with time-reversal invariance. The quantized coefficient in the action is known as the magnetoelectric polarization θ, and is given by the formula

$$\theta = \frac{1}{4\pi}\int_{BZ} \mathrm{Tr}\left(\mathcal{A}\wedge \mathrm{d}\mathcal{A} - \frac{2i}{3}\mathcal{A}\wedge\mathcal{A}\wedge\mathcal{A}\right). \tag{5.2}$$

where $\mathcal{A}^{nm} = i\langle u^n|\,\mathrm{d}|u^m\rangle$ for n and m conduction bands, and the integral is only gauge invariant modulo 2π, consistent with the ambiguity in Eq. 5.1. While θ is computed in this manner for translationally invariant systems, the corresponding topological response is robust against disorder that preserves the symmetry on average and can be defined in the presence of interactions. The quantization of θ can also be protected by spatial symmetries like inversion symmetry [33, 46] and improper rotations[31], but cases where it is not possible to find a surface that preserves the symmetry lack protected gapless surface states.

The existence of a quantized magnetoelectric response in a bulk material has an important implication for the response of surface states. In the presence of a small perturbation that breaks time-reversal symmetry, the surface Dirac fermion becomes gapped, giving rise to a half-integer quantized Hall conductance[20]. This cannot happen in a pure two-dimensional

system without topological order and reflects the topological nature of the 3d bulk. This behavior can be understood by considering the surface as an interface between the bulk and the vacuum where θ changes from π to 0. The surface can thus be modeled by a spatially dependent θ

$$S = \frac{e^2}{4\pi h} \int \theta(x) F \wedge F. \tag{5.3}$$

such that $\theta(x < 0) = \pi$ and $\theta(x > 0) = 0$ for an interface between the topological and trivial regions. Since $F \wedge F$ is a total derivative, one may integrate by parts to find the effective 2+1-D surface action of the Abelian Chern-Simons form

$$S = \Delta\theta \frac{e^2}{4\pi h} \int A \wedge \mathrm{d}A \tag{5.4}$$

which implies that the effective Hall conductance of the surface, given by $\Delta\theta = \pi$ in units of $e^2/(2\pi h)$, is a half-integer value. This half-quantized topological response can serve as an additional feature to distinguish a topological phase, and as we will see, can be generalized to other types of responses.

To determine the coefficient θ and identify a topological phase, one needs to explicitly evaluate Eq. 5.2. The coefficient will be quantized in the presence of any symmetry that takes $\theta \to -\theta$, but the computation may simplify in different ways for different symmetries. For example, in the presence of both time-reversal and inversion symmetry, Eq. 5.2 can be related to the eigenvalues of the inversion operator at time-reversal invariant momenta[152]. In the presence of a mirror symmetry, the computation can be related to the mirror Chern numbers at mirror invariant planes.

In the following subsection we prove the quantization of θ in the presence of a generic orientation-reversing space group symmetry with no reference to any of these simplifying circumstances. The purpose of the rest of this section is to demonstrate the robust quantization of θ imposed by mirror and glide symmetries using microscopic tight-binding models. Starting with a brief review of crystalline insulators in class A with mirror symmetry, we show that the quantized magnetoelectric response can be obtained as the parity of the the integer-valued ($\mathbb{Z}$) topological invariant protected by the mirror. However, when the mirror symmetry is replaced by a glide[40, 42], *only* a $\mathbb{Z}_2$ invariant survives, which corresponds to the quantized $\theta = 0, \pi$.

5.2.1 Proof of quantization of θ

Here we provide a formal microscopic proof of our claim that any orientation-reversing space group (SG) operation quantizes θ using the formalism in Sec. 4.6.2.

First consider a symmorphic SG operation $g = \{O|0\}$ acting as $(gn)_{O\mathbf{k}} = Un_{\mathbf{k}}$. Note that in this convention that reproduces the microscopic expression[27] for the diagonal magnetoelectric coupling, the Berry connection is calculated using the coefficients only as $\mathcal{A}^{nm}_{\mathbf{k}} = in^\dagger_{\mathbf{k}} \,\mathrm{d}m_{\mathbf{k}}$ and we drop terms that come from the derivatives of the basis states. It

transforms under g as

$$(g\mathcal{A})^{nm}_{\mu,\mathbf{k}} = i\,(gn)^\dagger_{\mathbf{k}}\,\mathrm{d}(gm)_{\mathbf{k}} = in^\dagger_{O^{-1}\mathbf{k}}U^\dagger\,\mathrm{d}Um_{O^{-1}\mathbf{k}} = \\ = O_{\mu\nu}\mathcal{A}^{nm}_{\nu,O^{-1}\mathbf{k}}. \tag{5.5}$$

The constant U cancels and the 3d BZ integral (5.2) for θ picks up a factor of $\det O$ from the point-group rotation of $\mathbf{k}$-space, so $g\theta = (\det O)\,\theta$.

We will reduce the general case to the previous symmorphic one. Consider a continuous family of transformations represented as $(g\,(k_4)\,n)_{O\mathbf{k}} = e^{-i(O\mathbf{k}\cdot\mathbf{t})k_4}Un_{\mathbf{k}}$ where $\mathbf{t}$ is fixed and $0 \le k_4 \le 1$ is a tuning parameter, $k_4 = 1$ corresponding to the actual SG symmetry $g\,(k_4 = 1) = g = \{O|\mathbf{t}\}$. We will show that $\theta(k_4)$ calculated from a wave function transformed by $g\,(k_4)$ is independent of k_4. This is to be expected, considering the special case of $U = \mathbb{1}$ and $O = \mathbb{1}$ corresponds to a mere shift of the spatial origin by $k_4\mathbf{t}$. We can calculate the change in θ as k_4 changes from 0 to 1 by evaluating the second Chern form $\int_{\mathrm{BZ}\times[0,1]}\mathcal{F}\wedge\mathcal{F}$ with k_4 as the fourth coordinate. Using the expression (5.23), as $\mathcal{P}$ is k_4-independent, we see that θ is unchanged through this process. $g\,(k_4 = 0)$ has the same form as a symmorphic SG operation discussed above, those considerations are still valid even though $g\,(0)$ is not a symmetry.

The same result can be derived by direct substitution, but one encounters a subtlety we discuss now. Using the transformed wave function $n'_{\mathbf{k}} = e^{i\mathbf{k}\mathbf{t}}n_{\mathbf{k}}$ we find $\mathcal{A}'^{nm}_{\mu} = \mathcal{A}^{nm}_{\mu} - \mathbf{t}_\mu\delta^{nm}$, substituting it in (5.2)

$$\theta' = \theta - \frac{1}{4\pi}\int \epsilon_{\mu\nu\lambda}\,\mathrm{Tr}\,\mathcal{F}_{\mu\nu}\mathbf{t}_\lambda. \tag{5.6}$$

As $\mathbf{t}$ is constant the extra term can be expressed as a linear combination of Chern numbers in various cuts of the Brillouin zone. If the Chern numbers vanish, the correction is zero, or if $\mathbf{t}$ is a lattice vector, it is an integer multiple of 2π that does not change the value of θ modulo 2π. However, $\mathbf{t}$ can be an arbitrary vector if we interpret the above transformation as a shift of the entire crystal, or equivalently as a redefinition of the spatial origin. This shows that θ is ill defined with nonzero Chern numbers, we rationalize this observation below.

This situation is analogous to the problem of polarization in 2d Chern-insulators[153]. From a mathematical point of view, there the polarization becomes ill defined because it is not possible to choose a gauge where the wave functions are BZ periodic in the presence of nonzero Chern-number. Similarly, the Chern-Simons 3-form is not invariant under gauge transformations that are not periodic over the BZ, one needs to choose a periodic gauge to fix its value, but the Chern-number prevents this. Equation (5.23) misses the extra correction term because, while $\mathcal{P}$ stays BZ periodic throughout the deformation, $\mathcal{A}_4$ does not, to apply Stokes' theorem one has to add surface terms for $\partial\mathrm{BZ}\times[0,1]$, that exactly reproduces the correction. However this does not make a difference in the cases with vanishing Chern-numbers discussed in this paper. $\mathcal{A}_4$ fails to be periodic because the boundary conditions for the Bloch functions change throughout the deformation. To guarantee that such surface terms do not appear during the deformation to the trivial state used to calculate θ, we

prescribe that these deformations should be made keeping the lattice sites (thus the boundary condition) fixed, which is always possible.

We can continue the analogy from a physical point of view. Polarization measures surface charge, but on the surface of a Chern-insulator charge is no longer conserved due to the chiral anomaly. θ measures the fractional part of the surface Hall conductance σ^S_{xy}. However, when the bulk has a Hall conductance per transverse unit cell σ_{xy}/a_z, depending on the definition of the "surface layer" it may contribute more or less to σ^S_{xy}. We may fix the boundary of the "surface layer" and push the crystal in the z direction by t_z. The surface Hall conductance changes exactly by $t_z\sigma_{xy}/a_z$, in agreement with our formal result. We conclude that there is no natural zero for θ with nonzero Chern-number, consequently our result about the quantization of θ is only meaningful if we restrict to the case of vanishing total Chern-numbers, as we did throughout this work.

To summarize, we proved that θ transforms under a generic SG operation $g = \{O|\mathbf{t}\}$ as

$$g\theta = (\det O)\,\theta \tag{5.7}$$

meaning that θ is quantized to 0 or π by any orientation-reversing SG symmetry.

5.2.2 Mirror symmetry

In three dimensional insulators with mirror symmetry, topological invariants can be defined by considering the mirror invariant planes in the BZ, where bands have a definite mirror parity. Total and mirror Chern numbers can be thus defined for these invariant planes [10, 154]. The total Chern numbers for cuts perpendicular to the mirror plane vanish by symmetry, and for simplicity we assume they are zero in the mirror-invariant planes as well[1]. In a system with mirror symmetry reflecting the z axis, the bulk BZ has two mirror invariant planes[2] at $k_z = 0$ and π (Fig. 5.1 (a)). This allows us to label bands in these two planes by their mirror eigenvalue $\pm i^F$ ($F = 0$ and 1 for spinless and spinful fermions respectively), as no terms mixing the two sectors are allowed by symmetry. Chern numbers $C^{\pm}_{k_z}$ for the even and odd occupied bands are separately well defined for $k_z = 0$ and π. The mirror Chern number for a mirror-invariant plane ($k_z = 0, \pi$) is defined as the difference between the two sectors $C^M_{k_z} = \frac{1}{2}\left(C^+_{k_z} - C^-_{k_z}\right)$. Consider, for example the case with nonzero Chern numbers for the even and odd sectors in the $k_z = 0$ plane ($C^{\pm}_0 = \pm 1$) and vanishing Chern number for both sectors at $k_z = \pi$ ($C^{\pm}_\pi = 0$), now $C^M_0 = 1$ and $C^M_\pi = 0$.

A minimal Hamiltonian implementing this phase can be obtained starting from the 4-band model of a 3d TI with time-reversal symmetry[20, 31] $\mathcal{T} = i\sigma_y\mathcal{K}$:

$$H^{AM}_{\mathbf{k}} = t_x \sin k_x \tau_y + t_y \sin k_y \sigma_z \tau_x + t_z \sin k_z \sigma_y \tau_x + m_{\mathbf{k}} \tau_z \tag{5.8}$$

[1] In a gapped 3d insulator, the total Chern number in any parallel cut in momentum space must be the same integer, which is a 2d weak index. We omit this extra factor of $\mathbb{Z}$ in our further classification.

[2] Note that not all space groups have two mirror-invariant $\mathbf{k}$-planes. For example a tetragonal crystal only has one pointwise invariant plane with respect to a diagonal mirror. While this might affect the detailed classification with mirror symmetry, the conclusions about the quantization of θ remain valid.

with $m_{\mathbf{k}} = m - \sum_\mu \cos k_\mu$. This model is in the strong TI phase for $1 < |m| < 3$ with $\theta = \pi$. Now we can remove the time-reversal symmetry constraint and instead demand invariance under mirror $M = i^F \sigma_z$ reflecting the z direction. The Hamiltonian (5.8) formally has both symmetries, but the mirror allows different perturbations than time-reversal. It is easy to see that the two mirror sectors (with opposite σ_z eigenvalues) now have opposite Chern numbers in the $k_z = 0$ plane and vanishing Chern numbers at $k_z = \pi$. Similar to the weak indices in time-reversal invariant insulators, C_0^M and C_π^M separately rely on translational symmetry along z direction but the *strong* mirror Chern number $C_s^M = C_0^M + C_\pi^M$ is robust against translational symmetry breaking, as long as mirror symmetry is preserved. We note that, with vanishing total Chern number (*i.e.* $C_{k_z}^+ + C_{k_z}^- = 0$), the quantized magnetoelectric coupling θ is completely determined by the strong mirror Chern number, $\theta = \pi C_s^M \pmod{2\pi}$. This is seen by counting surface modes: in the invariant planes $C_{k_z}^+ = -C_{k_z}^-$ counts the number of chiral modes on the surface at $k_z = 0$ or π propagating right (left) in mirror sector $+$ $(-)$. Each pair of counterpropagating modes forms a surface Dirac-cone, so if the total number is odd, the bulk has nontrivial θ.

5.2.3 Glide symmetry

In this section we present an alternate picture to understand the glide-protected $\mathbb{Z}_2$ invariant first proposed in Ref [40] (see also Appendix 5.B), in terms of the quantized magnetoelectric polarization. Let the glide $G = \{M_z|\mathbf{t}_x/2\}$ reflect the z direction and translate along x by half of a unit cell (Fig. 5.1). $G^2 = \left\{(-1)^F \mathbb{1}|\mathbf{t}_x\right\}$ is a pure translation, with the sign depending on how a 2π rotation is represented. The eigenvalues of the glide operator are $\pm i^F e^{ik_x/2}$. As we traverse the Brillouin Zone (BZ) in the x direction on a line that is pointwise invariant under the symmetry, the eigenvalues wind into each other. In a system respecting this symmetry if we follow a band with the $+i^F e^{ik_x/2}$ eigenvalue, it is connected to band with $-i^F e^{ik_x/2}$ at the zone edge, so the boundary condition for the Bloch wave functions is constrained to $\left|u_{\mathbf{k}+\mathbf{G}_x}^+\right\rangle \propto \left|u_{\mathbf{k}}^-\right\rangle$ where $\mathbf{G}_x$ is the reciprocal lattice vector parallel to $\mathbf{t}_x$. So bands in the presence of glide symmetry come in pairs that cannot be separated by a gap, as the crossings are protected by the fact that the pairs have different eigenvalues under the symmetry. The Chern number for each single band is ill defined as one band must evolve into the other on the zone boundary, only the total Chern number for the pair is a topological invariant.

Again, for simplicity, we assume that the total Chern number for conduction/valence bands in any 2d cut parallel to the mirror plane vanishes. Nonzero values for perpendicular cuts are forbidden by mirror symmetry. The minimal model realizing the nontrivial phase[40] is analogous to the mirror-symmetric case i.e. Eq. (5.8)

$$\begin{aligned} H_{\mathbf{k}}^{AG} &= t_x \sin\left(\frac{k_x + \phi}{2}\right) \rho_x \tau_x + t_y \sin k_y \tau_y + \\ &+ t_z \sin k_z \rho_z \tau_x + m_{\mathbf{k}} \tau_z \end{aligned} \tag{5.9}$$

with the glide operator $G_{\mathbf{k}} = i^F e^{ik_x/2} \rho_x$. Here $m_{\mathbf{k}}$ has the same form as in (5.8). It is easy to see that the model is gapped for appropriate choice of parameters and band degeneracies

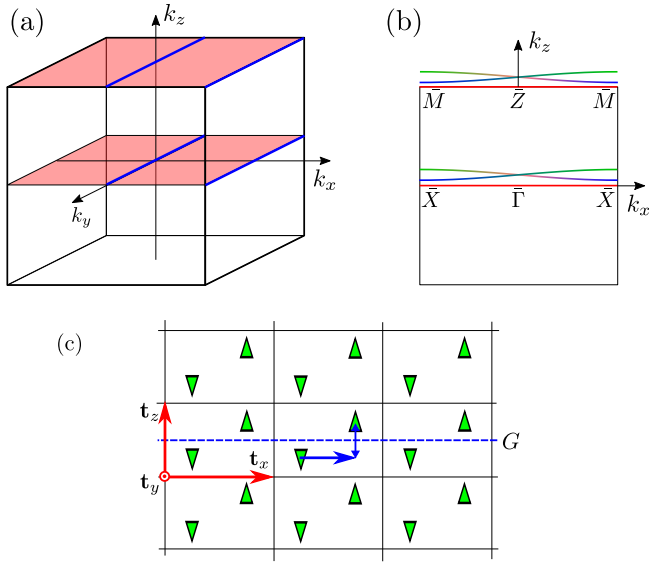

Figure 5.1: (a) Bulk BZ of a glide or mirror symmetric crystal with the two invariant planes BZ in red (shaded) and invariant lines in blue (thick) if particle-hole symmetry is also present. (b) Surface BZ for a cut normal to y with invariant lines in red (thick), labels for high symmetry points and a sketch of an occupied band pair along these lines. On the invariant planes ($k_z = 0$ and $k_z = \pi$) the glide eigenvalue (color code) distinguishes the two bands. (c) Example of a crystal with glide symmetry G that reflects the z direction and translates by half of the unit cell in the x direction, the glide operator exchanges the two sublattices ($\triangle$ and $\triangledown$). This pattern is repeated in parallell planes shifted perpendicular to the plane of the drawing.

can be removed almost everywhere in the BZ with symmetry allowed terms. Pauli matrices τ and ρ act on orbital and sublattice degrees of freedom respectively and the Hamiltonian preserves glide symmetry $G_{\mathbf{k}} H_{\mathbf{k}} = H_{M_z \mathbf{k}} G_{\mathbf{k}}$ with $M_z\,(k_x, k_y, k_z) = (k_x, k_y, -k_z)$. We used the convention where operators and Bloch wave functions are not periodic in the BZ (see Appendix **??**), and the model can be regarded as either spinless ($F = 0$) or spinful ($F = 1$) with spin-polarized electrons, such that trivial bands with opposite z-component spin S^z are pushed far over or below the Fermi level and can be omitted (note that M_z is diagonal in the S^z basis).

Regardless of the microscopic differences, in the macroscopic translational-invariant electromagnetic response theory there should be no distinction between a mirror and a glide, θ is quantized as 0 or π just like with a mirror. We numerically[155] verified that in the nontrivial phase of this model, $\theta = \pi$ is robust against symmetry preserving perturbations (Fig. 5.2, for details see Appendix 5.A). We would like to point out that starting from a mirror symmetric TCI (for example (5.8)) one can double the unit cell and weakly break down separate mirror and half translation symmetries to a glide without closing the gap or

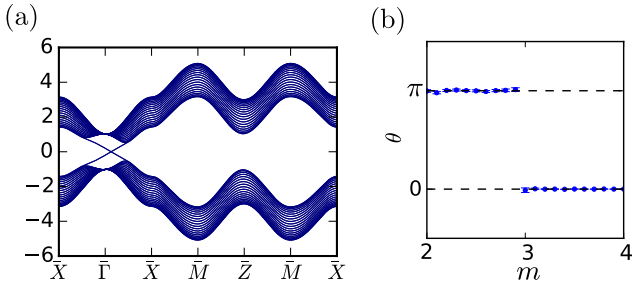

Figure 5.2: (a) Band structure in slab geometry with 20 unit cells in the y direction for glide protected class A topological insulator. We use H^{AG} with $t_\mu = 1$, $m = 2$ and $\phi = 0.4$. The surface Dirac cone is at a generic momentum on the high symmetry line, the left and right moving branches are distinguished by their glide eigenvalues and cannot gap out. (b) Evolution of θ from numerics while tuning across the transition from the topological to the trivial phase without breaking the glide symmetry. The error bars indicate two standard deviations (95% confidence interval) of the Monte Carlo estimates.

changing the value of θ. While the mirror Chern numbers are no longer well defined, the $\mathbb{Z}_2$ invariant defined by θ survives. We emphasize that θ is a macroscopic response quantized by macroscopic mirror symmetry, so it is robust against symmetry preserving interactions and disorders which preserve the symmetry on average[156], both in the case of glide and mirror symmetry. To summarize, we provided a physical understanding of the $\mathbb{Z}_2$ invariant introduced in Ref. [40] in terms of quantized magnetoelectric coupling.

5.3 Topological Crystalline Superconductors in Class D

In the previous section we have shown how the magnetoelectric coupling in insulators can be quantized in the presence of symmetries other than $\mathcal{T}$, in particular a mirror or a glide. We now show how these considerations can also be applied to superconductors in three dimensions where $\mathcal{T}$ is broken. In this section we consider a superconductor with no other local symmetry but the particle-hole symmetry of the Bogoliubov-de Gennes Hamiltonian, which belongs to class D. We will show that the presence of an additional glide symmetry protects the existence of a topological crystalline superconductor with a single Majorana cone at the surface. In section 5.4 we will consider the analogous problem in the presence of SU(2) spin rotation symmetry.

5.3.1 Bulk invariant and surface thermal Hall conductance

The reason why a glide can protect a topological superconductor in three dimensions without time reversal symmetry is that this phase is also characterized by θ term that is quantized with any orientation-reversing symmetry. The reasoning is analogous to the one used for insulators. We first consider the case of a superconductor with time-reversal symmetry, in class DIII. In three dimensions, class DIII has an integer topological invariant $\nu \in \mathbb{Z}$ which counts the number of Majorana cones at the surface. In the same way as the insulator, in the presence of a weak perturbation that breaks time reversal symmetry, the surface becomes gapped and each Majorana cone contributes half of the minimal thermal Hall conductance of a 2d superconductor (that is half of the minimal value for a 2d insulator)[21, 157]:

$$\frac{\kappa_{xy}}{T} = \frac{(\pi k_B)^2}{3h}\frac{\nu}{4}. \tag{5.10}$$

Formally, a class D superconductor is the same as an insulator with an extra antiunitary particle-hole symmetry $\mathcal{C}$ that anticommutes with the Hamiltonian and squares to $+\mathbb{1}$, because a particle-hole symmetric Bloch Hamiltonian for insulators has the same form as the Bogoliubov-de Gennes (BdG) Hamiltonian for superconductors. The only important difference is that only half of the degrees of freedom in the BdG Hamiltonian are physical, since all negative energy states correspond to the annihilation operators of the positive energy excitations over the BdG ground state. This is why the surface Dirac cones in insulator case reduce to surface Majorana cones in the superconductor case.

The fact that the insulator and superconductor problems are formally the same allows us to use the BdG Hamiltonian the same way as the Bloch Hamiltonian to calculate θ from the band structure of a glide-symmetric superconductor, which must be quantized to $0, \pi$ by the same reason as in the insulator case. When $\theta = \pi$, this implies an odd number of surface Majorana cones, and a half-integer thermal Hall conductance when the glide symmetry is broken. This is not allowed in a purely two-dimensional gapped superconductor with no ground state degeneracy, where κ_{xy}/T is always quantized in integer multiples of $(\pi k_B)^2/(6h)$.

5.3.2 Microscopic model with glide plane in 3d

The explicit model for a glide symmetric superconductor in class D is very similar to the insulator in Eq. (5.9), but with an extra particle-hole symmetry $\mathcal{C}^2 = \mathbb{1}$. Again we consider a glide plane reflecting the z direction and translating along x, $G = \{M_z|\mathbf{t}_x/2\}$. We represent charge conjugation as $\mathcal{C} = \tau_x\mathcal{K}$ where $\mathcal{K}$ is the complex conjugation operator and the τ act on the particle-hole degree of freedom. As charge conjugation acts locally, it has to commute with the glide as $G_{-\mathbf{k}}\mathcal{C} = \mathcal{C}G_{\mathbf{k}}$. The Hamiltonian (5.9) with $\phi = 0$ possesses these symmetries for spinless fermions, however, such systems do not naturally appear as superconductors and require fine tuning as insulators. For the rest of this section we assume the physical case of spinful fermions, for which the appropriate choice of the glide representation is $G_{\mathbf{k}} = ie^{ik_x/2}\rho_x\tau_z$ (see Appendix **??** for details about symmetry representations in BdG systems).

A simple Hamiltonian respecting these symmetries is:

$$H^{DG}_{\mathbf{k}} = t_x \cos\frac{k_x}{2}\rho_y\tau_x + t_y \sin k_y\rho_z\tau_x + t_z \sin k_z\tau_y + m_{\mathbf{k}}\tau_z. \tag{5.11}$$

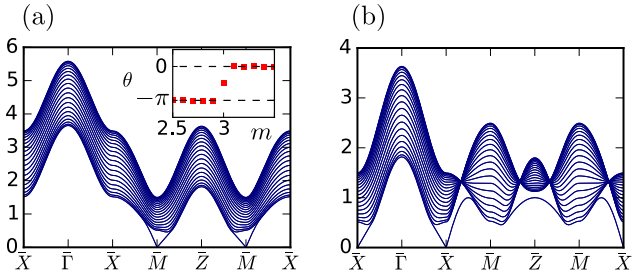

Figure 5.3: Band structures in slab geometry for glide protected class D topological superconductor. We use H^{DG} with $t_\mu = -1$. (a) with $m = 2.5$ the surface Majorna cone is at $\bar{M}$, while (b) with $m = 0.5$ at $\bar{X}$. The left and right moving branches are distinguished by their glide eigenvalues on the invariant lines and cannot gap out. Inset: Evolution of θ while tuning across the transition from the topological ($m < 3$) to the trivial ($m > 3$) phase from numerics. Note that at $m = 3$ the gap closes and θ takes on an intermediate value not allowed in a gapped system. The error bars for the Monte Carlo results are smaller than the symbols.

For appropriate choice of parameters (see Fig. 5.3) the model is in its topological phase with gapless excitations on symmetry preserving surfaces and numerical evaluation confirms that $\theta = \pi$ (Appendix 5.A). Fig. 5.3 (a) and (b) shows surface spectra with single Majorana cones pinned by particle-hole symmetry to different high symmetry points. As will be explained later, in fact the Majorana cone can only appear at $\bar{X}$ or $\bar{M}$, but not $\bar{\Gamma}$ or $\bar{Z}$ in the surface BZ (shown Fig. 5.1 (b)). This is an important difference compared to the insulator case.

5.3.3 Lower dimensional topological invariants

The structure of the surface modes in the particular case of class D can be further understood from the presence of lower dimensional topological invariants (known as weak invariants or indices) associated to glide-invariant lines and planes in the Brillouin Zone. While our model has been chosen such that all 1d and 2d invariants associated to particle-hole symmetry are trivial, the presence of a mirror or glide enables new lower dimensional invariants.

First we review the case of mirror symmetry[36, 37]. The classification for TCSCs in class D depends on the square of mirror operator i.e. $M_\pm^2 = \pm\mathbb{1}$. In particular, no nontrivial TCSCs exist with M_-, this means, while θ is quantized, only $\theta = 0$ is allowed by symmetry. On the other hand, with the choice of M_+, we find a rich structure with both 1d and 2d weak

invariants. Similarly to class A, there is an integer-valued 2d index (mirror Chern number) in mirror-invariant planes. Besides, there are 1d mirror $\mathbb{Z}_2$ invariants along the high symmetry bulk lines in y direction (blue lines in Fig. 5.1 (a)). These mirror $\mathbb{Z}_2$ invariants guarantee the presence of a pair of surface zero modes of opposite parity at the corresponding surface high-symmetry momentum, which split for any other momenta generating a Majorana cone. Therefore, these 1d mirror indices determine the parity of the number of surface Majorana cones on the surface projections of the mirror invariant lines (Fig. 5.1 (b)). This leads to a $\mathbb{Z}_2^4$ index in the case of M_+ mirror symmetry, as long as translation symmetry is preserved.

The case of a glide can be understood as a combination of the above two cases as we argue below. Mirror Chern numbers cannot be defined with a glide for the same reason that applies in class A. However, the smaller symmetry group with glide symmetry poses weaker constraints on the band structure compared to mirror M_-, allowing $\theta = \pi$ as illustrated by our model. 1d indices can still be defined, but the square of the glide operator is different for high symmetry points since it changes with k_x, unlike for a mirror. For the lines at $k_x = 0$ we have $G_0^2 = -\mathbb{1}$, but for $k_x = \pi$, $G_\pi^2 = \mathbb{1}$. This difference is key because for $G_0^2 = -\mathbb{1}$, no mirror index exists[36, 37], while for $G_\pi^2 = \mathbb{1}$ there is a $\mathbb{Z}_2$ index at each high symmetry point. Therefore, surface Majorana fermion can only be found at high-symmetry points with $k_x = \pi$, i.e. the $\bar{X}$ or $\bar{M}$ points. Two cases with a single Majorana cone at $\bar{X}$ or $\bar{M}$ are realized in our proposed model for $m = 0.5$ and $m = 2.5$, as seen in Fig. 5.3, in both cases $\theta = \pi$ as it is determined by the parity of the total number of Majoranas.

5.3.4 Surface Dirac model

An alternative approach to demonstrate the protection of a topological phase by a symmetry is to consider how symmetries are implemented in a generic surface theory. For example, for a regular topological insulator, the presence of time-reversal symmetry protects a single Dirac cone to be gapless. If a single Dirac cone is found at the surface, it cannot be removed until the symmetry is broken or the bulk gap closes. Two surface Dirac cones can however be gapped without breaking the symmetry.

We consider how the glide symmetry is implemented in a generic Dirac Hamiltonian at a high-symmetry point, offering an alternative explanation of the results in the previous section. As mentioned earlier, as a result of particle-hole symmetry a single Majorana cone can only appear at a high symmetry surface momentum, we will discuss the case of more Majoranas later. In a 2-band model G_0 that squares to $-\mathbb{1}$ can be chosen $i\sigma_i$ for $i = x, y, z$, but since σ_x and σ_z behave the same under complex conjugation we only need to consider σ_x or σ_y. Charge conjugation is represented as $\mathcal{C} = U_\mathcal{C}\mathcal{K}$ with real unitary $U_\mathcal{C}$. A 2-band gapless Dirac Hamiltonian has the form

$$H = k_x\Gamma_x + k_z\Gamma_z \tag{5.12}$$

where the Γ's are hermitian, anticommuting, with ± 1 eigenvalues and $[\Gamma_x, G_0] = \{\Gamma_z, G_0\} = [\Gamma_i, \mathcal{C}] = 0$. If we choose $G_0 = i\sigma_y$, $[U_\mathcal{C}, G_0] = 0$, so $U_\mathcal{C} = \mathbb{1}$, Γ_x cannot be chosen to satisfy all

commutation and anticommutation relations. Similarly if $G_0 = i\sigma_x$, $\{U_\mathcal{C}, G_0\} = 0$, $U_\mathcal{C} = \sigma_z$ and again no Γ_x is allowed. Therefore it is impossible to write a Dirac Hamiltonian with particle-hole symmetry and $G_0^2 = -\mathbb{1}$. This shows that a single surface Majorana cone is forbidden at the $\bar{\Gamma}$ and $\bar{Z}$ points of the surface BZ (see Fig. 5.1 (b)) in the presence of a glide.

On the other hand with $G_\pi^2 = +\mathbb{1}$ we can choose $G_\pi = \sigma_x$, $U_\mathcal{C} = \mathbb{1}$, $\Gamma_x = \sigma_x$ and $\Gamma_z = \sigma_z$. Now a single Majorana cone is allowed, but it cannot be gapped out, for that we would need a mass term $m\Gamma_0$ such that $\{\Gamma_0, \Gamma_i\} = \{\Gamma_0, \mathcal{C}\} = [\Gamma_0, G_\pi] = 0$. One can check that a mass term is not allowed for any valid choice of a 2×2 representation, single Majorana cones are allowed and protected at $\bar{X}$ and $\bar{M}$.

Finally, we may also consider a system with a pair of cones at opposite surface momenta. Similarly to class A[40], a pair of surface Majorana cones with different glide eigenvalues at one high symmetry point are locally protected, but can symmetrically move around the BZ and gap each other out at another point where their eigenvalues are the same. This shows that only the number of cones modulo 2 at each of $\bar{X}$ and $\bar{M}$ is stable against symmetry-preserving perturbations. The classification with full translation invariance is thus $\mathbb{Z}_2^2$, while allowing terms doubling the unit cell in the z direction reduces the classification to $\mathbb{Z}_2$ counting the parity of the total number of surface Majorana cones. Such a $\mathbb{Z}_2$ index is given by the Chern-Simons 3-form in Eqn. (5.2).

5.4 Class C superconductor with glide plane in 3d

In this last section we consider how a singlet superconductor with SU(2) spin rotational symmetry in three dimensions may also have a topological phase. This type of superconductor belongs to class C. After appropriate rearrangement of the degrees of freedom (see Appendix **??**) the Hamiltonian can be block-diagonalized in the spin-S^z basis where the two blocks are unitarily related with identical spectra and topological properties. In the reduced problem charge conjugation is combined with a spin rotation acting as $\mathcal{C} = \tau_y\mathcal{K}$, with $\mathcal{C}^2 = -\mathbb{1}$, which is the main difference compared to class D.

To understand the emergence of the topological phase protected by a glide in class C, it is instructive to first consider the more familiar case of an SU(2) invariant superconductor with time-reversal symmetry, which belongs to class CI, and the anomalous response of the surface after breaking time reversal symmetry. After this, we argue how the θ term is also quantized in a class C superconductor with a glide, present an explicit model for this, and also argue how the protection of the surface states can be seen directly from the surface theory.

5.4.1 Bulk invariant and SU(2) axion term

In class CI, topological superconductors are characterized by a topological invariant ν, which counts the number of pairs of surface Majorana cones. The SU(2) spin rotation symmetry

allows the definition of spin Hall conductance[158]. Once the surface is gapped by breaking time-reversal symmetry (but not SU(2) spin rotational symmetry), the surface spin quantum Hall conductance is given by[14]

$$\sigma_{xy}^{S} = \frac{(\hbar/2)^2}{h}\frac{\nu}{2} \tag{5.13}$$

where ν is an even integer. Note that when $\nu = 2$ the above σ_{xy}^{S} is only half of that of a $d + \mathrm{i}d$ singlet superconductor in 2d[158]. Therefore this anomalous half-integer surface spin quantum Hall conductance serves as a probe to characterize the nontrivial 3d phase. It should be noted that the thermal Hall conductance κ_{xy} is well defined, but it is not sufficient to characterize the topological phase.

This half-integer response can be related to an analog SU(2) bulk θ term, in an analogous way to a 3d topological insulator. To see this, we first consider the effective SU(2) continuum gauge theory that describes the spin quantum Hall superconductor in 2+1 dimensions, which captures the response of the SU(2) spin rotation invariant system coupled to a SU(2) gauge field. While this gauge field is fictitious, this treatment is useful to derive the response to an external Zeeman field[159]. This system is described by the effective action[159]

$$S = \frac{1}{4\pi}\frac{(\hbar/2)^2}{\hbar}C\int A^z \wedge \mathrm{d}A^z \tag{5.14}$$

where A^z is the z component (in spin space) of the SU(2) gauge field, which we identify as the z component of an external Zeemann field $A^z = B^z$. $C = \int \mathcal{F} \in 2\mathbb{Z}$ is the Chern-number of the negative energy bands in one spin sector, which is an even integer in class C. This is analogous to the quantum Hall effect, but as we are interested in spin currents, the electric charge e is replaced by $\hbar/2$ in the coupling (we take the g-factor $g = 1$). The spin current is

$$J^i = \delta S/\delta A_i^z = \frac{(\hbar/2)^2}{h}C\epsilon_{ij}\partial_j B^z, \tag{5.15}$$

so the spin Hall conductance is $\sigma_{xy}^{s} = \frac{(\hbar/2)^2}{h}C$. To get a proper SU(2) gauge theory, we promote A to a nonabelian SU(2) gauge field by $A = \sigma_i A_\mu^i$, the action compatible with the previous one is given by the nonabelian Chern-Simons 3-form

$$S = \frac{1}{4\pi}\frac{(\hbar/2)^2}{\hbar}\frac{C}{2}\int \mathrm{Tr}\left(A \wedge \mathrm{d}A - \frac{2i}{3}A \wedge A \wedge A\right), \tag{5.16}$$

where an extra 1/2 appears to compensate for the trace. As we see, compared to the U(1) gauge theory, the coefficient is only half of the Chern number for one spin sector.

In analogy to Eq. (5.1), an SU(2) axion action can be defined in 3+1 dimensions in the following way:

$$S = \frac{1}{4\pi}\frac{(\hbar/2)^2}{\hbar}\frac{\theta}{2}\int \mathrm{Tr}\, F \wedge F \tag{5.17}$$

where F is the nonabelian field strength tensor and θ is the Berry Chern-Simons 3-form (Eq. (5.2)) for the occupied bands in one spin species. The ambiguity in θ is now 4π because

of the extra factor of 1/2. One can also check that a spatial domain wall of 4π in theta gives rise to a surface with the minimum allowed value of the spin Hall conductance in a 2d system, corresponding to $C = 2$ in one spin sector. As we argued in class A, if the system has a symmetry on average that flips an odd number of spacetime dimensions, θ is quantized to 0 or 2π modulo 4π, leading to a $2\mathbb{Z}_2$ classification. The reason why the ambiguity in θ calculated from the band structure changes to 4π is quite subtle[159]. It comes from the gauge fixing requirement that the band structure can be continuously deformed to the trivial band structure in the trivial gauge without breaking $\mathcal{C}$. We refer the interested reader to Appendix 5.A for details.

5.4.2 Microscopic model with glide plane

Following the same logic as for classes A and D, we now consider how the presence of a glide symmetry can protect an SU(2) invariant topological superconductor in the absence of time-reversal symmetry, i.e. in class C. As in the previous classes, the presence of an orientation reversing symmetry is sufficient to guarantee the quantization of the θ term (now to either 0 or 2π), which is the topological invariant that characterizes the phase. This phase has formally the same properties as a CI topological superconductor with $\nu = 2$, namely a pair of Majorana surface cones and a half-quantized spin Hall conductance upon breaking the glide symmetry on the surface.

To show this, we now consider a microscopic model in class C with a glide symmetry, demonstrating the presence of protected surface modes and computing the value of θ explicitly. In the original full Hilbert space the natural representation of the glide is $G_{\mathbf{k}} = ie^{ik_x/2}\rho_x\tau_z\sigma_z$, but because of the full SU(2) spin symmetry we can cancel the spin rotation part by attaching $-i\tau_z\sigma_z$ to our definition, so we may use $G_{\mathbf{k}} = e^{ik_x/2}\rho_x$. For this operator $G_{\mathbf{k}}^2 = +e^{ik_x}\mathbb{1}$, showing the "spinless" nature of the problem. A Hamiltonian for one spin component with these symmetries can be constructed as

$$\begin{aligned} H_{\mathbf{k}}^{CG} =& \Delta_{xy}\sin k_y \sin\frac{k_x}{2}\rho_x\tau_x + \Delta_{xz}\sin k_x \sin k_z\rho_z\tau_x + \\ &+ \Delta_0(\cos k_x - \cos k_y + \alpha)\tau_y + m_{\mathbf{k}}\tau_z. \end{aligned} \tag{5.18}$$

For appropriate choice of parameters (Fig. 5.4) this Hamiltonian realizes a nontrivial topological phase with an odd number of pairs of surface Majorana cones (not counting the spin degeneracy). Class C is similar to class A as it has a $2\mathbb{Z}$ index in 2d without symmetry, corresponding to an even total Chern number in xy cuts which vanishes in our model and we restrict our further discussion to this case. Again, no integer-valued mirror Chern number can be defined in glide-invariant planes, but a $2\mathbb{Z}_2$ index still survives due to the bulk quantization of θ, which we have computed explicitly (Fig. 5.4 inset).

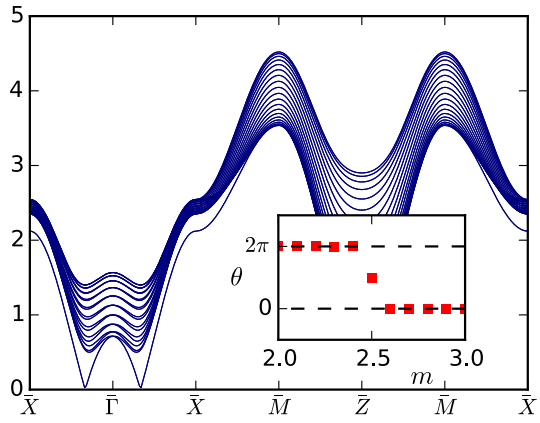

Figure 5.4: Band structure in slab geometry for glide protected class C topological superconductor. We use H^{CG} with $\Delta_{xy} = \Delta_{xz} = \Delta_0 = 1$, $\alpha = 0.5$ and $m = 1.5$. Note the symmetric pair of surface Majorana cones at a generic momentum, the left and right moving branches are protected from gapping out by different glide eigenvalues. This is the spectrum for one spin sector, for the full system there is an additional spin degeneracy. Inset: Evolution of θ while tuning across the transition from the topological to the trivial phase from numerics. Note that at $m = 2.5$ the gap closes and θ takes on an intermediate value not allowed in a gapped system. The error bars for the Monte Carlo results are smaller than the symbols.

5.4.3 Surface Dirac model

The fact that an odd number of pairs of Majorana cones is protected in class C with a glide can be shown explicitly by considering the surface Hamiltonian of a pair of Majorana cones with $\mathcal{C}^2 = -\mathbb{1}$. It is instructive to show first the known case of class CI. The Hamiltonian in the vicinity of a high symmetry surface momentum (Fig. 5.1 (b)) is

$$H = \sigma_x k_x + \sigma_z k_z \tag{5.19}$$

where the Dirac matrices are 4×4 and spanned by σ_i, τ_j, the identity is implicit. The particle-hole operator is $\mathcal{C} = i\tau_y\mathcal{K}$ and the time-reversal operator is $\mathcal{T} = \sigma_y\tau_y\mathcal{K}$ with $\mathcal{K}$ complex conjugation. There are four possible mass terms for this Hamiltonian, $\sigma_y\tau_x, \sigma_y\tau_y, \sigma_y\tau_z, \sigma_y$. The first three masses are forbidden by $\mathcal{C}$, and the last one, σ_y, is forbidden by $\mathcal{T}$. Therefore, a single pair of Majorana cones cannot be gapped out at the surface in class CI.

In class C, when time reversal symmetry is broken, both a mirror or a glide can still protect the presence of a single pair Majorana cones, because as we now show, both of these symmetries forbid the σ_y mass as well. In the presence of a mirror, we consider a reflection $z \to -z$, with operator $M_\pm$ that satisfies $M_\pm^2 = \pm\mathbb{1}$. In the presence of a glide, we would have $G_{\mathbf{k}}^2 = e^{ik_x}$, but since the Majorana cones must be at opposite momenta due to $\mathcal{C}$, their

annihilation can only occur at $k_x = 0, \pi$ and we only need to consider these two cases with $G_0^2 = +\mathbb{1}$ and $G_\pi^2 = -\mathbb{1}$, same as the situation of regular mirrors. We now discuss the two cases of $M_\pm$, which apply to both mirror and glide.

In the M_+ case, for the two eigenstates of σ_x with positive eigenvalues, the mirror eigenvalues are the same and equal to 1, while the other two are equal to -1, as would happen if M were the glide operator at $k = 0$. The operator doing this is simply $M_+ = \sigma_x$. In the M_- case, for the two eigenstates of σ_x with positive eigenvalues, the mirror eigenvalues are $\pm i$, as would happen if M were the glide operator at $k = \pi$. This is achieved with $M_- = i\sigma_x\tau_z$. Note both $M_\pm$ anticommute with σ_z because M reverses k_z. Also note both $M_\pm$ commute with $\mathcal{C}$ as we want.

Once we have the operators for $M_\pm$, it is easy to see that both operators forbid the mass σ_y. Since the other three masses are already forbidden by $\mathcal{C}$, a pair of Majorana cones is protected in the presence of $\mathcal{C}^2 = -\mathbb{1}$ and the additional mirror/glide symmetry $M_\pm$.

5.5 Conclusions

In this work we classified 3d topological insulators and superconductors protected by nonsymmorphic glide symmetry in classes A, D and C and presented lattice models for these phases. Our results, however, are more general. As our arguments only rely on symmetries of the effective long-wavelength response theory, the $\mathbb{Z}_2$ classification is also robust if mirror symmetry, or any symmetry reversing an odd number of spatial coordinates, is preserved on average. The cases with glide symmetry illustrate that these macroscopic considerations are insensitive to the fractional translation that accompanies the mirror operation, and identify the most robust topological invariants that are also defined (among others) with simple mirror symmetry. Glide symmetry is present in over a hundred of the 230 crystallographic space groups, and all but the 65 chiral groups contain orientation-reversing operations, so our results should be widely applicable to experimentally and numerically detect topological crystalline insulators and superconductors without time-reversal symmetry.

5.6 Acknowledgements

The author is grateful for the efforts of Fernando de Juan and Yuan-Ming Lu in this collaboration. We thank Joel Moore, Philipp Dumitrescu and Takahiro Morimoto for helpful conversations. This work is supported by NSF Grant No. DMR-1206515 (D.V., F. de J.) Office of Science, Basic Energy Sciences, Materials Sciences and Engineering Division, Grant No. DE-AC02-05CH11231 (F. de J.) and startup fund at Ohio State University (Y.-M. L.).

Appendix

5.A Evaluation of Chern-Simons 3-form and second Chern-form

In this section we review the calculation of the magnetoelectric coupling. The magnetoelectric coupling is defined in terms of the Chern-Simons 3-form:

$$\theta = \frac{1}{4\pi}\int_{BZ} \mathrm{Tr}\left(\mathcal{A}\wedge \mathrm{d}\mathcal{A} - \frac{2i}{3}\mathcal{A}\wedge\mathcal{A}\wedge\mathcal{A}\right). \tag{5.20}$$

The main difficulty about evaluating this expression is that one has to find a (patchwise) smooth gauge in the occupied band space, which is a complicated task in numerical studies. To circumvent this, we instead find a gapped deformation to a trivial state with constant Hamiltonian using a tuning parameter k_4, such that $\theta(k_4 = 0) = 0$, and calculate the change in θ by the 4 dimensional second Chern form[20, 27] that is locally gauge invariant:

$$\theta(\pi) - \theta(0) = \frac{1}{4\pi}\int_{BZ}\int_{k_4=0}^{\pi} \mathrm{Tr}\left(\mathcal{F}\wedge\mathcal{F}\right) \tag{5.21}$$

where $\mathcal{F} = \mathrm{d}\mathcal{A} - i\mathcal{A}\wedge\mathcal{A}$, the nonabelian Berry curvature in the 4 dimensional space spanned by $\mathsf{k}_\mu = (\mathbf{k}, k_4)$. (Note that in the convention we use $\mathcal{F}\wedge\mathcal{F} = \frac{1}{4}\epsilon_{\mu\nu\gamma\lambda}\mathcal{F}_{\mu\nu}\mathcal{F}_{\gamma\lambda}$.) We realize that $\mathcal{F}$ can be written in a gauge invariant form as $\mathcal{F} = i\mathcal{P}(\mathrm{d}\mathcal{P})\wedge(\mathrm{d}\mathcal{P})\mathcal{P}$ using the projector onto occupied bands $\mathcal{P}_\mathsf{k} = \sum_{n\in occ.} |u^n_\mathsf{k}\rangle \langle u^n_\mathsf{k}|$, which is also gauge invariant. In this formulation $\mathcal{F}$ is an operator acting on the full Hilbert-space of the unit cell, but only nonzero on occupied bands, so we can extend the trace to the full Hilbert-space without changing the result. The usual components can be obtained as matrix elements between occupied states in a given basis, $\mathcal{F}^{nm}_\mathsf{k} = \langle u^n_\mathsf{k}| \mathcal{F}_\mathsf{k} |u^m_\mathsf{k}\rangle$. So we arrive at the locally gauge-invariant expression

$$\begin{aligned} &\theta(\pi) - \theta(0) = \\ &= -\frac{1}{4\pi}\int_{BZ}\int_{k_4} \mathrm{Tr}\left(\mathcal{P}(\mathrm{d}\mathcal{P})\wedge(\mathrm{d}\mathcal{P})\mathcal{P}\wedge(\mathrm{d}\mathcal{P})\wedge(\mathrm{d}\mathcal{P})\right) \end{aligned} \tag{5.22}$$

that we numerically evaluate using adaptive Monte Carlo integration[155]. In order to get physical result, one must use the Bloch formalism where the orbital positions are taken into

account (Sec 4.2.2 and 5.2.1), the interpolating Hamiltonians in classes A and D can be written as

$$H_{\mathsf{k}}^{AG} = \frac{1}{2}(1-\cos k_4)H_{\mathbf{k}}^{AG} + \\ + \sin k_4 \sin(k_x/2)\rho_y + \frac{1}{2}(1+\cos k_4)\tau_z \tag{5.23}$$

$$H_{\mathsf{k}}^{DG} = \frac{1}{2}(1-\cos k_4)H_{\mathbf{k}}^{DG} + \\ + \sin k_4 \sin(k_x/2)\rho_x\tau_x + \frac{1}{2}(1+\cos k_4)\tau_z \tag{5.24}$$

with $H_{\mathbf{k}}^{AG}$ and $H_{\mathbf{k}}^{DG}$ given in (5.9) and (5.11) respectively. We find that θ is quantized to 0 or $\pi \pmod{2\pi}$ to high accuracy, a result that is robust against symmetry allowed perturbations of the final Hamiltonian and deformations of the interpolation as long as the bandgap does not close (Fig. 5.A.1 (a)).

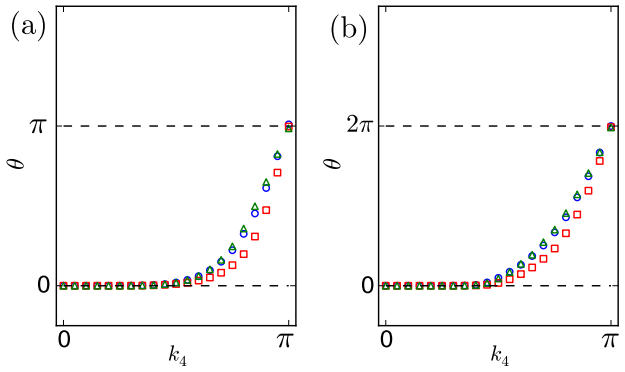

Figure 5.A.1: (a) Evolution of θ during the gapped deformation H_{k}^{AG} from the trivial to the topological phase while breaking glide symmetry in class A. We use parameters $t_\mu = 1$, $\phi = 0.4$ and $m = 2$ (circles) or $m = 2.5$ (squares) and we also show a deformation with $m = 2$ but with the symmetry allowed perturbation $\beta\tau_y$ with $\beta = 0.5$ added to $H_{\mathbf{k}}^{AG}$ (triangles). (b) Same plot for class C using H_{k}^{CG} with $\Delta_{xy} = \Delta_{xz} = \Delta_0 = 1$, $\alpha = 0.5$ and $m = 1.5$ (circles) or $m = 2$ (squares) and $m = 1.5$ with symmetry allowed perturbation $\beta\tau_x$ with $\beta = 0.5$ added to $H_{\mathbf{k}}^{CG}$. The error bars are smaller than the symbols.

In class C we have to reconcile the change of ambiguity in θ from 2π to 4π from the band structure point of view. A natural gauge choice for a class C system is the requirement that $|u_{\mathbf{k}}^o\rangle = i\tau_y \left|u_{-\mathbf{k}}^u\right\rangle^*$ that relates unoccupied states at $\mathbf{k}$ with occupied states at $-\mathbf{k}$. Gauge transformations preserving this condition satisfy $\tau_y U_{\mathbf{k}}^o = (U_{-\mathbf{k}}^u)^*\tau_y$ where $U^{o/u}$ act on the occupied/unoccupied bands. This constraint is not sufficient to remove the 2π gauge

ambiguity in θ coming from the winding number of $U^o_{\mathbf{k}}$, as any $U^o_{\mathbf{k}}$ is allowed as long as it is accompanied by the appropriate $U^u_{\mathbf{k}}$.

So how can we define a proper bulk invariant? The idea is to prove that for a cyclic gapped deformation of the band structure (with k_4 as the tuning parameter) the second Chern form

$$\frac{1}{4\pi}\int \mathrm{Tr}\,\mathcal{F}\wedge\mathcal{F} \tag{5.25}$$

is quantized to multiples of 4π as long as particle-hole symmetry in any 3d cut is preserved (as opposed to multiples of 2π without symmetry). This is proved in Ref. [160], for our case $D = 3$ is the dimension of k-space and $\delta = 1$ the dimension of real space, for us this is k_4, the tuning parameter that is not affected by particle-hole symmetry. The result is, for $D - \delta = 2$ in class C the classification is $2\mathbb{Z}$, proving our conjecture.

Now, if we find a gapped particle-hole symmetric deformation from the trivial band structure to the glide symmetric one, we can calculate the difference $\Delta\theta = \theta(\pi) - \theta(0)$ in the 3d Chern-Simons forms between the initial and final states using the locally gauge invariant expression of the second Chern form in terms of the band projector. 2π will be different from zero, as the ambiguity introduced by different deformations is 4π. Such deformation to the trivial state always exists, as there are no nontrivial phases in 3d class C without any other symmetry. Note that the formula in terms of $\mathcal{F}$ requires a continuous gauge choice throughout the deformation and $\theta(0)$ is only zero in the trivial gauge. We can view this as a nontrivial gauge fixing condition demanding that the band structure is continuously deformable to the trivial state in the trivial gauge, in this gauge the Chern-Simons 3-form in the final state gives the same result. However, we know of no method of checking whether this condition is satisfied other than explicitelly constructing a deformation. On the other hand, the formula with the projector is completely gauge-invariant, insensitive to discontinuous large gauge changes that would add extra 2π's to the formula with $\mathcal{F}$, so we do not have to worry about the band structure satisfying any gauge condition using this method of computation.

For the specific model in equation (5.18) we use the deformation preserving $\mathcal{C} = \tau_y\mathcal{K}$:

$$\begin{aligned} H^{CG}_{\mathsf{k}} =& \frac{1}{2}(1-\cos k_4)H^{CG}_{\mathbf{k}} + \\ &+ \sin k_4 \sin(k_x/2)\rho_y\tau_x + \frac{1}{2}(1+\cos k_4)\tau_z. \end{aligned} \tag{5.26}$$

Our numerical results give $\theta = 0$ and $2\pi \pmod{4\pi}$ to a high accuracy for the trivial and topological phases respectively (Fig. 5.A.1 (b)).

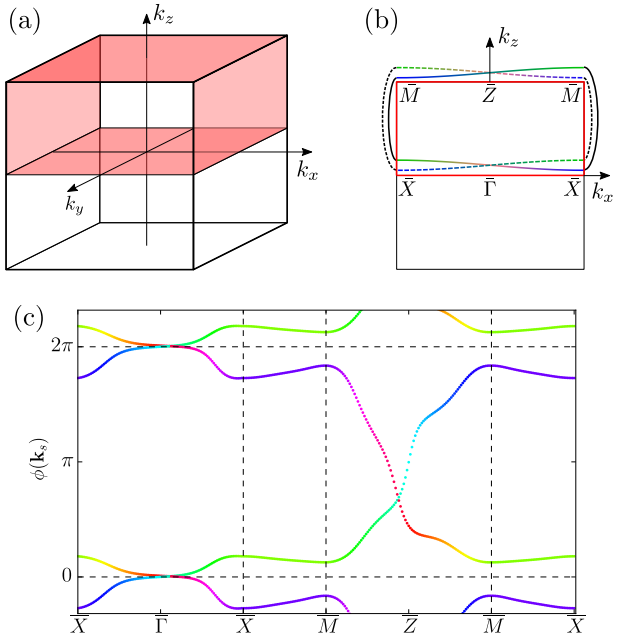

Figure 5.B.1: Illustration of our definition of the glide Chern number. (a) Bulk BZ of a glide symmetric crystal with a possible choice of the "bent" BZ in red (shaded). The glide Chern number is calculated by integrating the Berry flux following a single band around this torus. (b) Surface BZ for a cut normal to y with projection of the "bent" BZ in red (thick) and a sketch of an occupied band pair along this loop. On the invariant planes ($k_z = 0$ and $k_z = \pi$) the glide eigenvalue (color code) distinguishes the two bands. On the non-symmetric part (other values of k_z) bands are generically nondegenerate. The glide Chern-number is calculated by counting the winding number of $\phi(\mathbf{k}_s)$ following a single band (solid or dashed) around the $\bar{X} - \bar{\Gamma} - \bar{X} - \bar{M} - \bar{Z} - \bar{M} - \bar{X}$ loop. (c) Value of $\phi(\mathbf{k}_s)$ around the loop for the minimal model in the nontrivial phase. Color code indicates glide eigenvalue in the invariant planes. Note that following one band around, the phase winds 2π, indicating that the glide Chern-number is odd.

5.B Relation to earlier definition of $\mathbb{Z}_2$ index in class A

Here we review the alternate definition of the $\mathbb{Z}_2$ index in class A introduced in Ref. [40]. There are two planes in the 3d BZ that are invariant under a mirror or glide, at $k_z = 0$ and π, in the rest of the BZ glide does not act locally, bands do not have a well defined eigenvalue and symmetry allowed perturbations generically destroy most degeneracies. A 2×2 Hamiltonian without any symmetry constraints only has pointlike degeneracies between occupied bands in 3d (Weyl nodes), which allows us to choose a surface in the BZ that connects the $k_z = 0$

and π planes such that the all the bands are nondegenerate. We will choose a constant k_x surface for simplicity and show later that the result is insensitive to this choice or the assumption that there are only pointlike degeneracies.

Now we can choose a surface in the bulk BZ that includes the two invariant planes plus a surface connecting them traversing half the BZ, say at $k_x = 0$ (see Fig.5.B.1 (a)). We can follow a band around this surface (Fig.5.B.1 (b)), this is possible because of the well defined glide eigenvaue in the invariant planes and the generic lack of degeneracies in the connecting surfaces. We can compute the "glide Chern number" corresponding to one such band on the "bent BZ"[32] by counting the winding number of the Berry-connection integral integrals in the y direction

$$\phi(\mathbf{k}_s(t)) = \int_0^{2\pi} \mathcal{A}^y(\mathbf{k}) dk_y. \tag{5.27}$$

where $\mathcal{A}^\mu(\mathbf{k}) = i \langle u_\mathbf{k} | \partial^\mu | u_\mathbf{k} \rangle$ and the curve $\mathbf{k}_s(t) = (k_x(t), k_y(t))$ encloses half of the surface BZ (Fig.5.B.1 (b)). In the case when there are multiple pairs of conduction bands with we naturally sum the Chern numbers for bands with the same glide eigenvalue. This quantity (mod 2) is a well defined topological invariant because pushing a Weyl node across one of the connecting surfaces can only change the winding by 2. A definition that does not rely on distinguishing the two bands in the nonsymmetric region is obtained realizing that the winding number (mod 2) is the same as the parity of crossings regardless of direction of an arbitrarily set branch cut by $\phi(t)$ throughout the invariant planes and one copy of the connecting plane[40]. Even when the bands are degenerate, phases of eigenvalues of the nonabelian Wilson loop operators along the y direction give equivalent quantities. This definition, while in principle well defined, still suffers from problems of distinguishing crossings from anticrossings in a many-band model at finite $\mathbf{k}$-space resolution[161].

The fact that the Berry flux through a closed surface for a set of bands that are separated from all other bands on this surface is nonzero signals the presence a Weyl-node inside the bounded region connecting this set of bands to some other bands. This Weyl-node connects valence/conduction bands among themselves, the systems we consider are fully gapped. This Weyl-node is also present in mirror symmetric insulators with different mirror Chern-numbers in the two invariant planes (sec. 5.2.2). We can think of the 3d band structure as an interpolation of 2d systems in the k_xk_y cuts as the tuning parameter k_z evolves from 0 to π. To interpolate 2d systems between the two cuts, we have to close and open a Dirac node between the occupied bands connected to different mirror sectors to transfer Berry flux, which corresponds to a Weyl node inside the half 3d BZ. This Weyl node is topologically protected and must exist somewhere in the half BZ, mirror symmetry at the high symmetry planes prevents it from locally annihilating with its opposite chirality mirror image that lives in the other half of the BZ.

Chapter 6

Space group constraints on weak indices in topological insulators

Lattice translation symmetry gives rise to a large class of "weak" topological insulators (TIs), characterized by translation-protected gapless surface states and dislocation bound states. In this chapter we show that space group symmetries lead to constraints on the weak topological indices that define these phases. In particular we show that screw rotation symmetry enforces the Hall conductivity along the screw axis to be quantized in multiples of the screw rank, which generally applies to interacting systems. We further show that certain 3D weak indices associated with quantum spin Hall effects (class AII) are forbidden by the Bravais lattice and by glide or even-fold screw symmetries. These results put a strong constraints on candidates of weak TIs in the experimental and numerical search for topological materials, based on the crystal structure alone.

6.1 Introduction

The discovery of topological insulators and superconductors is one of the most important breakthroughs of condensed matter physics in the past decades[148–150]. The key principle underlying the existence of these novel topological phases is that the presence of a symmetry, such as time reversal symmetry ($\mathcal{T}$), can lead to a quantized bulk topological invariant and robust gapless surface states. In a gapped fermion system, this invariant cannot change unless the gap closes, defining a stable quantum phase and protecting the existence of gapless boundary states. After the discovery of three dimensional topological insulators, which are protected by $\mathcal{T}$, it was shown that other global symmetries in the Altland-Zirnbauer (AZ) classes[16], such as charge conjugation ($\mathcal{C}$) and spin rotational symmetries, also give rise to topological phases, leading to the periodic table[11, 15] of topological insulators and superconductors.

It was realized early on that additional topological phases can be obtained from invariants defined on a lower dimensional slice of the Brillouin Zone [9] (BZ). Since this definition

requires the discrete translational symmetry of the lattice, it was initially thought that these phases would not survive generic disorder and thus termed "weak" topological insulators. The lower-dimensional topological invariants are therefore known as weak indices. However, further efforts then showed that weak topological phases have many robust features emerging from topology[55–58], in particular the fact that lattice dislocations host protected gapless modes that originate from the weak indices[60–62]. Recently it was also proposed that strong interactions can lead to novel topological orders on the surface of weak TIs[59, 162]. Most of these theoretical predictions remain untested due to the difficulty of finding materials realizing these weak topological phases[163], though several candidates have been predicted in ab-initio studies[164–167]

The consideration of a perfect lattice with translational symmetry immediately raises the question of whether the space group symmetries of this lattice may also have an impact on the topological properties. The addition of space group often leads to the emergence of novel phases, generally termed topological crystalline insulators[14, 31, 35–37, 39–45, 47, 48, 152], with different properties from weak TIs. Here we address a complementary question: what are the restrictions brought by space group symmetries on possible topological phases, in particular, the weak topological phases?

In this work, we show that the nonsymmorphic elements of the space group lead to unexpected constraints for the weak indices beyond those derived from the point group. First, we show that for three dimensional (3D) magnetic insulators in class A there is nontrivial quantization condition of Hall conductivity tensor in the presence of nonsymmorphic screw symmetry. We derive this condition from band theory, and then provide a general proof of its applicability to interacting systems. Second, we turn to time-reversal-invariant insulators in class AII and show how nonsymmorphic screw and glide symmetries can make the weak indices vanish in a particular direction. While enumerating every AZ symmetry class and dimensionality is beyond the scope of this paper, we present the necessary formalism to generalize our results to topological superconductors with a few examples in Appendix 6.A.

6.2 Chern number and Hall conductivity (class A)

6.2.1 Hall conductivity of a 3D insulator

A simplest example of weak indices in a three dimensional system is the quantized Hall conductivity of an insulator, which in proper units is given by integer-valued Chern numbers of 2D slices of the BZ. As off-diagonal elements of the conductivity tensor, these Chern numbers transform like an axial vector under point group operations. Here we show that a nonsymmorphic screw symmetry further imposes an important constraint on the integer-valued Hall conductivity. This constraint holds generally for interacting and disordered systems, as long as the ground state is a non-fractionalized 3D insulator which preserves the screw symmetry.

In a 2D system, the Hall conductance (or conductivity) σ_{xy} characterizes the transverse

current response to an in-plane electric field: $j_x = \sigma_{xy} E_y$. Using the Kubo formula one finds[5, 168] that the Hall conductivity in unit of e^2/h is given by the integral of Berry curvature for the occupied bands over the BZ:

$$\sigma_{xy} = \frac{e^2}{h}\mathcal{C}, \quad \mathcal{C} = \frac{1}{2\pi}\int_{\mathrm{BZ}} \mathrm{d}^2\mathbf{k}\,\mathrm{Tr}_{occ.}\,\mathcal{F}_{\mathbf{k}} \tag{6.1}$$

where $\mathrm{Tr}_{occ.}$ is the trace over occupied bands and $\mathcal{F}$ is the Berry curvature matrix. In an insulator with a bulk gap between valence and conduction bands, the total Berry flux over the BZ is quantized to be an integer, known as the Chern number $\mathcal{C}$, and hence σ_{xy} is also quantized.

In a 3D insulator the Hall conductivity becomes an antisymmetric tensor and can be cast in terms of an axial vector[168] $\mathbf{\Sigma}$ in the form of

$$\sigma_{ij} = \frac{e^2}{2\pi h}\epsilon_{ijl}\Sigma_l, \quad \Sigma_i = \frac{\epsilon_{ijl}}{4\pi}\int_{\mathrm{BZ}} \mathrm{d}^3\mathbf{k}\,\mathrm{Tr}_{occ.}\,\mathcal{F}^{jl}_{\mathbf{k}} \tag{6.2}$$

where repeated indices are summed over implicitly. In band insulators this "Hall vector" is always a reciprocal lattice vector[169] and can be expressed as $\mathbf{\Sigma} = \sum_{i=1}^{3} \mathbf{G}_i \mathcal{C}_i$ where $\mathbf{G}_i$ are an independent set of primitive reciprocal lattice vectors, and $\mathcal{C}_i \in \mathbb{Z}$ is the Chern-number for a cut of the BZ oriented towards $\mathbf{G}_i$ and spanned by the other two reciprocal lattice vectors. The weak topological invariant associated with 3D insulators in symmetry class A is such a "Chern vector" $\vec{\mathcal{C}} \in \mathbb{Z}^3$.

The "Hall vector" as defined in Eqn. (6.2) may be cast in a coordinate free form, as

$$\mathbf{\Sigma} = \frac{1}{2\pi}\int \mathrm{Tr}\,\mathcal{F} \wedge \mathrm{d}\mathbf{k}. \tag{6.3}$$

To see that it is equal to $\sum_{i=1}^{3} \mathbf{G}_i \mathcal{C}_i$, it is sufficient to check that $\mathbf{a}_i \cdot \mathbf{\Sigma}$ is the same in the two cases for all lattice vectors. Simple substitution shows that this vector transforms as an axial vector under all SG operations, i.e. even under inversion, $\mathbf{\Sigma} \to (\det O)\, O\mathbf{\Sigma}$).

This shows that lattice symmetry severely constrains the allowed values, as it has to stay invariant under every orthogonal transformation in the point group. Nonzero values are only allowed with low enough symmetry, two intersecting axes of (improper) rotations is sufficient to force vanishing Hall conductance[31].

For a finite 3D insulator with lattice translational symmetry, the Hall conductance normal to a certain direction $\hat{m}$ is given by

$$\epsilon_{mnl}\sigma_{nl} = \frac{e^2}{2\pi h}\mathbf{\Sigma}\cdot(L_m\hat{m}) = \frac{e^2}{h}\sum_i \frac{L_m \hat{m}\cdot\mathbf{G}_i}{2\pi}\mathcal{C}_i \tag{6.4}$$

where L_m is the linear size of the periodic system along $\hat{m}$ direction. If this 3D system has a gapped bulk, its Hall conductance must also be an integer in units of e^2/h along any direction. Adding one extra unit cell along $\mathbf{G}_i$ direction will increase the Hall conductance

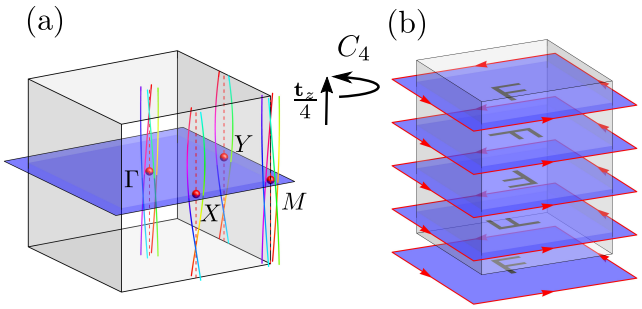

Figure 6.1: (a) Brillouin zone of an insulator with 4-fold screw symmetry. The perpendicular plane through the BZ center (blue) contains four high symmetry points (red spheres), we use the formula relating the chern number to rotation eigenvalues at these 4 points. In the direction of the screw, along the four invariant lines (dashed red) the screw eigenvalues evolve into each other, illustrated by spirals and color code. Note that at lines that are only invariant under twofold screw there are only two different eigenvalues, but the total number of occupied bands is still a multiple of 4. (b) Intuitive real space picture of the screw symmetric insulator as a stack of integer Chern insulator layers related by the screw. The unit cell contains four layers, so the Hall conductance per transverse unit cell is a multiple of 4.

along $\mathbf{G}_i$ direction by exactly the Chern number $\mathcal{C}_i$ in units of e^2/h. In an anisotropic limit the 3D insulator can be viewed as a stack of 2D layers with a quantized Hall conductance σ_{xy}^L each. Therefore the Hall conductivity tensor (6.2) is nothing but the Hall conductance per unit cell layer, σ_{xy}^L, which can be defined as the difference between the Hall conductance of N_z and $N_z + 1$ layers along a certain direction. As will become clear later, this difference σ_{xy}^L does not depend on N_z as long as N_z is much larger than the correlation length, so we adopt this definition for our interacting proof.

In the following we show that, with a nonsymmorphic n-fold screw symmetry, the Hall conductance per unit cell layer along the screw-axis direction cannot be an arbitrary integer (in units of e^2/h) for a gapped 3D insulator without fractionalization. Instead it must be a multiple of n, as enforced by the screw symmetry.

6.2.2 Screw symmetry enforced constraints

Below we will show the Chern number for a cut perpendicular to an n-fold screw axis is quantized to a multiple of n. Consider an essential n-fold screw in the z direction, by essential screw we mean a SG operation that leaves no point in space invariant up to lattice translations[143]. We assume that the translation part is $1/n$ of the primitive lattice vec-

tor parallel to the n-fold rotational axis[1], $g = \{C_n|\mathbf{a}_z/n\}$. We invoke results[31, 47] (see Sec. 7.3.3) that allow calculation of the Chern number in the presence of n-fold rotational symmetry in 2D as a product of rotation eigenvalues of occupied bands at high symmetry points of the BZ. For example with C_4 symmetry (Fig. 6.1 (a))

$$\exp\left(2\pi i\frac{C}{4}\right) = \prod_{m\in\text{occ.}} \xi_m^{\Gamma}\left(C_4\right)\xi_m^{M}\left(C_4\right)\xi_m^{X}\left(C_4^{-2}\right) \tag{6.5}$$

where $\xi_m^{\mathbf{k}}(O)$ is the rotation eigenvalue of O in band m at momentum $\mathbf{k}$. Similar formulae can be derived for rotations C_2, C_3 and C_6.

When restricted to the 2D cut of the BZ through Γ, a screw acts the same way as a symmorphic C_n rotation, so the formula can be applied. Now consider the screw-invariant lines in BZ, parallel to the screw axis (dashed vertical lines in FIG. 6.1 (a)). As the n-th power of the screw $g^n = (-1)^F\{\mathbb{1}|\mathbf{a}_z\}$ is a pure translation up to fermion parity, the eigenvalues of screw g take values of $\exp(i\mathbf{k}\cdot\mathbf{a}_z/n + 2\pi im/n + \pi iF/n)$ for $m \in \mathbb{Z}_n$. When restricted to the perpendicular plane with $\mathbf{k}\cdot\mathbf{a}_z = 0$ the eigenvalues are simply the n-th roots of fermion parity $(-1)^F$. Increasing k_z by 2π will change g eigenvalue by a factor of $e^{2\pi i/n}$, leading to a n-multiplet of occupied bands at each screw-invariant momentum. This shows that the product of screw eigenvalues at high-symmetry points is always 1 for every allowed configuration. This immediately proves that

$$\frac{\sigma_{xy}^L}{e^2/h} = \mathcal{C}_z \equiv 0 \mod n. \tag{6.6}$$

In the following we show that this result is not a peculiarity of band theory for free electrons, but holds for any gapped unique ground state preserving n-fold screw symmetry, even in the presence of interactions and disorders. The proof is based on the following cut and glue procedure. We start with a slab containing $N_z + m/n$ unit cells along the z direction which is parallel to the screw axis. While this number of unit cells is not integer, screw symmetry allows us to identify the top and bottom surfaces using a boundary condition twisted by a C_n rotation[50], which results in a screw symmetric bulk without boundaries (Fig. 6.2 (a)). To take the thermodynamic limit we assume the size of the system is much larger than the correlation length of the gapped bulk. To define the Hall conductance σ_{xy} in this geometry we invoke the Streda formula[170], whereby the Hall conductance is given by the charge bound to a localized 2π flux threaded through the system. Unless the charge captured is an integer, the system is fractionalized and has a non-unique ground state, contradicting our initial assumption.

Next we cut the system open in the z direction. During this process we change the Hall conductance by a surface contribution of $-\sigma_{xy}^S$. σ_{xy}^S can depend on the thickness, but should saturate to a thickness-independent constant, as long as N_z is much larger than the

[1]Space groups with such screw axes are usually denoted by international symbols containing 2_1, 3_1, 4_1 or 6_1.

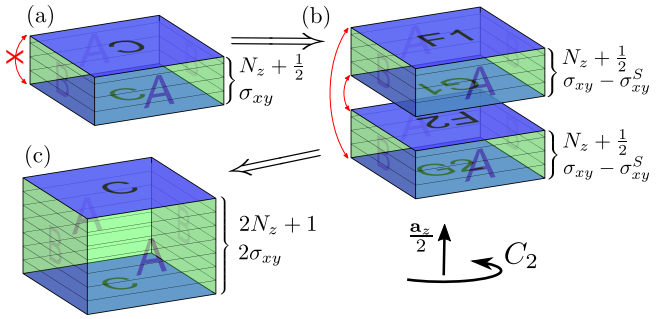

Figure 6.2: The process used in the general proof for the Hall conductance constraint (6.6), illustrated in the case of a 2-fold screw. (a) A thick slab with half-integer thickness and twisted periodic boundary condition in the z direction. As we open the boundary condition in the z direction, the Hall conductance may change by a surface contribution $-\sigma^S_{xy}$. (b) We combine two slabs, the screw axis allows to arrange these such that the interfaces are guaranteed to be identical, a top surface (F) meets a bottom surface (G) with the same orientation. Glueing the two interfaces together each contributes $+\sigma^S_{xy}$. (c) The resulting system has periodic boundary conditions in all three directions with odd thickness while the Hall conductance is an even multiple of the conductance quantum.

correlation length of the gapped bulk. We then take n copies of this open system and arrange them along the z direction related by C_n rotations such that all the interfaces are symmetry related (Fig. 6.2 (b)). Gluing the surfaces together by restoring the screw symmetric bulk Hamiltonian changes the Hall conductance by σ^S_{xy} at each interface, as the separation between them is much larger than the bulk correlation length. The resulting system (Fig. 6.2 (c)) has periodic boundary conditions in all three directions with a thickness of $nN + m$ unit cells and Hall conductance of $n\left(\sigma_{xy} - \sigma^S_{xy}\right) + n\sigma^S_{xy} = n\sigma_{xy}$. Thus we proved that a sample with arbitrary integer thickness has a Hall conductance which is a multiple of n times the conductance quantum.

6.3 Weak TI indices (class AII)

6.3.1 Bravais lattice

Point group symmetry can put stringent constraints on the allowed values of the weak indices. To calculate the weak $\mathbb{Z}_2$ invriants we evaluate[9]

$$\nu_i = \frac{1}{2\pi}\,\mathrm{Tr}_{occ.}\left(\int_{\frac{1}{2}T^2}\mathcal{F}_{\mathbf{k}}\mathrm{d}^2\mathbf{k} - \oint_{\partial\frac{1}{2}T^2}\mathcal{A}_{\mathbf{k}}\cdot\mathrm{d}\mathbf{k}\right) \mod 2 \tag{6.7}$$

where $\mathcal{A}$ and $\mathcal{F}$ are the Berry curvature and connection and the integral is over the interior and boundary of half of the time-reversal invariant 2D cut of the BZ spanned by the two

reciprocal lattice vectors other than $\mathbf{G}_i$ and displaced from the Γ point by $\mathbf{G}_i/2$. This defines a $\mathbf{k}$-space vector characterizing the weak indices, pointing to one of the 8 TR invariant momenta:

$$\mathbf{G}^\nu = \frac{1}{2}\nu_i \mathbf{G}_i. \tag{6.8}$$

This vector is independent of the choice of the unit cell[44] and transforms under space group operations as $\mathbf{k}$-space vectors (see Appendix 5.2.1). One can enumerate the allowed values of $\mathbf{G}^\nu$ by inspecting tables for Wyckoff-positions of the reciprocal space groups: $\mathbf{G}^\nu$ can only take values at points with half-integer Miller indices that are invariant under the point group up to reciprocal lattice vectors. This means that a face-centered cubic lattice (for example the common cubic diamond structure[171]) can not support nontrivial weak indices without breaking point group symmetries. To see this, consider the body-centered cubic (bcc) reciprocal lattice and note that there is no maximal symmetry $\mathbf{k}$-point other that the Γ point that represents trivial weak indices. The constraints only depend on the type of Bravais lattice[2], listed in Table 6.1.

These results can also be rationalized from the band inversion point of view. To get a weak TI, we need an odd number of band inversions among the four TR invariant momenta located on one plane offset from Γ. But point group symmetry relates some of these TR invariant momenta, and band inversion can only occur simultaneously on all symmetry related points. For example in the bcc reciprocal crystal TR invariant momenta are symmetry equivalent in such a fashion that there is an even number of related points in any of the offset planes, explaining the lack of nontrivial weak TI's. On the other hand, a strong TI is possible with any SG, as the Γ point is always of maximal symmetry and it is possible to have a band inversion only at Γ (see Appendix 6.B).

6.3.2 Nonsymorphic symmetries

The presence of nonsymmorphic symmetries leads to further constraints on the weak indices. We now show that in the presence of an essential twofold screw in the z direction, the weak index must be trivial in this direction. First we note that a 2-fold screw $\{C_2|\mathbf{a}_z/2\}$ with $\mathbf{a}_z$ a primitive lattice vector, squares to $\{-\mathbb{1}|\mathbf{a}_z\}$, represented at $k_z = \pi$ as $+\mathbb{1}$, which commutes with $\mathcal{T}$. Note that a diagonal[3] twofold screw is never essential and the Bravais lattice constraint already rules out a nontrivial weak index in the screw direction. So we can assume the other two primitive lattice vectors are perpendicular to $\mathbf{a}_z$ and in the $k_z = \pi$

[2] A priori the constraints depend on the *arithmetic crystal class* that is determined by the point group (geometric crystal class) and its action on the translations (Bravais lattice). Direct enumeration[172–174] reveals that the result in fact only depends on the Bravais lattice. This can be rationalized noting that a Bravais lattice contains arithmetic crystal classes that have a large enough point group to force certain relations among lattice vectors by mapping them to each other. As $\mathbf{G}^\nu$ takes values on the same reciprocal Bravais lattice with half the spacing, the constraints are the same for every arithmetic crystal class in a Bravais lattice.

[3] By *diagonal* screw/glide (rotation/mirror) we mean that there is no choice of a generator set of translations such that they are all parallel or perpendicular to the axis/plane.

Table 6.1: Constraints on possible weak indices based on the Bravais lattice in time reversal invariant insulators. The allowed values of $\mathbf{G}^\nu$ are labeled as in ITA[172], "all" means all the 8 possible values are allowed.

Crystal system	Centering	Allowed values of $\mathbf{G}^\nu$
Triclinic	P	all
Monoclinic	P	all
	C	Γ, Y, A, M
Orthorhombic	P	all
	C	Γ, Y, T, Z
	I	Γ, X
	F	Γ, Y, T, Z
Tetragonal	P	Γ, Z, M, A
	I	Γ, M
Trigonal	P	Γ, A
	I	Γ, T
Hexagonal	P	Γ, A
Cubic	P	Γ, R
	I	Γ, H
	F	Γ

plane the screw it acts like a proper inversion in a 2D system. We use the known result to evaluate the weak index by counting inversion eigenvalues[152], it is given by the total number of occupied Kramers pairs with -1 inversion eigenvalue at the four TR invariant momenta modulo 2. In this plane Kramers partners have the same screw eigenvalues, as required.

However, this situation in a 3D system with screw is different from a 2D system with a symmorphic inversion symmetry in that the screw requires an equal number of both screw eigenvalues below the gap, as shown earlier. Specifically at $k_z = \pi$ at each high symmetry point the number of occupied $+1$ and -1 eigenvalues must be equal, and as the number of occupied bands is constant, the total number of occupied -1 bands is a multiple of 4, leading to a trivial $\mathbb{Z}_2$ index in this plane.

In general a weak vector in the presence of an essential screw $\{C_2|\mathbf{a}_z/2\}$ is only allowed if

$$\mathbf{G}^\nu \cdot \mathbf{a}_z \equiv 0 \mod 2\pi. \tag{6.9}$$

We analogously argue[36, 37] that an essential glide forbids nontrivial weak index in the direction parallel to the the translational part of the glide. Again, a diagonal glide is never essential and is covered by our earlier constraints. In general, an essential glide with in-plane translation $\mathbf{a}_z/2$ only allows a weak vector if $\mathbf{G}^\nu \cdot \mathbf{a}_z \equiv 0 \pmod{2\pi}$, consistent with the analysis of the "hourglass" surface states[43, 47].

6.4 Conclusion

In summary, we derived a set of constraints on weak topological indices in 3D insulators from nonsymmorphic and symmorphic space group symmetries. We show that in the presence of n-fold screw rotation, Hall conductivity must be quantized as a multiple of n for any 3D non-fractionalized insulator preserving screw symmetry. This condition is generally proved for interacting systems. We also show that certain weak indices for 3D TIs (class AII) can be ruled out considering the Bravais lattice, glide and even-fold screw symmetries. These results put strong constraints on the candidates for weak topological phases in the ongoing experimental and numerical efforts to find physical realizations of these novel topological phases.

6.5 Acknowledgements

The author thanks Fernando de Juan and Yuan-Ming Lu for the continued collaboration on this project. We are grateful to Takahiro Morimoto and Hoi Chun Po for helpful conversations. This work is supported by NSF Grant No. DMR-1206515 (D.V. and F. de J.), DMR-1507141 (D.V.), the European Research Council Advanced Grant (Contract No. 290846) (F. de J.) and startup funds at Ohio State University (Y.-M. L.).

Appendix

6.A Generalization to topological superconductors

Weak indices are also present in other symmetry classes[60, 175] and we extend our considerations to other cases with $d-1$ dimensional weak indices. In 3D there are analogous 2D $\mathbb{Z}$ and $2\mathbb{Z}$ indices in classes D and C respectively, these are Chern numbers of the Bogoliubov-de Gennes Hamiltonians and the same reasoning applies as in class A. In other cases, however, the presence of charge conjugation symmetry ($\mathcal{C}$) has a more important role, in the following we review one example and present the relevant formalism.

In class D we have 1D $\mathbb{Z}_2$ indices that serve as $d-1$ dimensional weak indices in a 2D system:

$$\nu_i = \frac{1}{\pi}\oint \mathrm{Tr}\,\mathcal{A} \pmod 2 \tag{6.10}$$

where the integration contour is along an invariant line on the edge of the BZ $\mathbf{G}_i/2 + t\epsilon_{ij}\mathbf{G}_j$, $t \in [0,1]$. Similarly to the weak $\mathbb{Z}_2$ in 3D TI's, the value ν_i' on a parallel invariant line through the Γ point is not independent, it is related through the 2d strong index $C \in \mathbb{Z}$ such that $C \equiv (\nu_i + \nu_i') \pmod 2$. It can be shown that the weak vector $\mathbf{G}^\nu = 1/2\nu_i\mathbf{G}_i$ again transforms as $\mathbf{k}$-space vectors under space group operations, showing that rhombic and square lattices only allow $(1/2, 1/2)$ (in primitive basis) and 3 or 6-fold rotational symmetry does not allow any nontrivial weak vector.

In order to prove the transformation properties of the 1d weak $\mathbb{Z}_2$ indices in class D, we have to switch to the BZ periodic convention, as $\mathrm{Tr}_{occ.}\oint \mathcal{A}$ is only quantized in a periodic basis and gauge. A space group operation g in this basis is represented as $U^{ab} = U_0^{ac}\delta^{cb}e^{-i\mathbf{k}\delta\mathbf{R}_b}$ where $\delta\mathbf{R}_a$ is the lattice vector of the unit cell in which site a of the unit cell with at $\mathbf{R} = 0$ ends up after the application of g. U_0 is $\mathbf{k}$-independent and we set it to the identity without loss of generality. The set $\delta\mathbf{R}_a$ depends on the choice of the unit cell, and a basis transformation redefining the unit cell has the same form with $\delta\mathbf{R}_a$ showing the change of unit cell position to which site a is assigned. Now we are in a position to prove two things at once: the 1D $\mathbb{Z}_2$ indices in class D transform in a simple fashion under SG operations and are insensitive to the choice of the real space unit cell.

We introduce the band-flattened Hamiltonian, $\mathcal{Q} = \mathbb{1} - 2\mathcal{P}$, it has the same properties as H except all particle/hole-like bands have energy ± 1. Charge conjugation symmetry $\mathcal{C} = \tau_x\mathcal{K}$ imposes $\mathcal{Q}_\mathbf{k} = -\tau_x\mathcal{Q}^*_{-\mathbf{k}}\tau_x$, for $\mathcal{P}$ it means $\mathcal{P}_\mathbf{k} = \mathbb{1} - \tau_x\mathcal{P}^*_{-\mathbf{k}}\tau_x$. The particle and

hole-like states are related by Hermitian conjugation, this in general implies $U_{\mathbf{k}} = \tau_x U^*_{-\mathbf{k}} \tau_x$, for the diagonal form we use this means every $\mathbf{R}_a$ has to appear twice. This is a consequence of double-counting degrees of freedom, the creation and annihilation operators of the same state must live one the same lattice site. We emphasize that this assumption is not always valid in insulators with effective particle-hole symmetry[175]. We find

$$i \oint_0^{\mathbf{G}} \mathrm{Tr}\left(\mathcal{P} U^\dagger \, \mathrm{d}U\right) = -\frac{i}{2} \oint_0^{\mathbf{G}} \mathrm{Tr}\left(U^\dagger \, \mathrm{d}U\right) = \tag{6.11}$$

$$= -\frac{1}{2} \oint_0^{\mathbf{G}} \sum_a \mathrm{d}\mathbf{k} \delta \mathbf{R}_a = -\frac{1}{2} \sum_a \mathbf{G} \delta \mathbf{R}_a \tag{6.12}$$

where $\mathbf{G}$ is the reciprocal lattice vector along which the integration contour for $\mathrm{Tr}_{occ.} \oint \mathcal{A}$ is oriented. Because of the doubling of orbitals the right hand side of the equation is always an integer multiple of 2π. Comparing with (4.53) we see that a change of the unit cell or a space group operation (with the appropriate transformation on $\mathbf{k}$-space) does not change the value of $\mathrm{Tr}_{occ.} \oint \mathcal{A}$ which is only defined modulo 2π.

6.B No Constraints on Strong TI's

In general, a topological phase from Kitaev's periodic table, protected by a global symmetry of the 10 AZ classes is robust against breaking lattice symmetry, such as strong TI in 3D. If a phase is compatible with a group G, then it is also compatible with any space group that is a subgroup of G. This is simply true because the topological protection doesn't rely on G, all the symmetry restrictions in G can do is to rule out certain phases in the original classification. A subgroup can't rule out more phases, as it poses less restrictions. Of course it is possible to have phases that are protected by G (and the global symmetry), then breaking G down to a subgroup can either allow more phases or protect less. For example, as we saw, nonsymmorphic symmetry can give interesting results about weak indices, as they rely on the translation part of the space group for protection.

As every crystallographic space group is a subgroup of either SG #229 (Im3m) or #191 (P6/mmm), finding examples of strong TI's in both of these crystal structures proves that crystal symmetry cannot forbid strong TI's: starting from either of these maximally symmetric examples weakly breaking some of the lattice symmetries one can produce a system with any SG without leaving the strong TI phase.

In our tight-binding examples we have a single site per unit cell with two orbitals, four bands in total. One of the orbitals is a spinful s-orbital, transforming under rotations with the canonical SU(2) representation and even under inversion. The other orbital transforms the same way under proper rotations, but odd under inversion, such orbitals naturally arise through crystal-field splitting of p-orbitals in a spin-orbit coupled ion. We introduce the Pauli matrices τ to act on the space of the two orbitals, now proper rotations by angle $\mathbf{n}$ are represented as $\exp\left(\frac{i}{2}\mathbf{n}\cdot\boldsymbol{\sigma}\right)$, inversion as τ_z and time-reversal as $\mathcal{T} = \sigma_y \mathcal{K}$. Both minimal

models have the same form that guarantees that they are invariant under the full symmetry group:

$$H(\mathbf{k}) = \sum_{\boldsymbol{\delta}} \left\{ \sin\left(\mathbf{k}\cdot\boldsymbol{\delta}\right)\left(\boldsymbol{\delta}\cdot\boldsymbol{\sigma}\right)\tau_x + \left(m - \cos\left(\mathbf{k}\cdot\boldsymbol{\delta}\right)\right)\tau_z \right\} \tag{6.13}$$

where the sum runs over nearest neighbor vectors. By tuning m we can enter the strong TI phase, this can be easily checked by counting inversion eigenvalues.

This result is expected based on the band inversion picture, the Γ point is always of maximal symmetry, it is possible to have a band inversion only at the Γ point, resulting in a strong TI with trivial weak indices. We can also rationalize this result from the effective field theory point of view. The strong TI phase is characterized by the topological θ term in the long wavelength electromagnetic action, a theory that possesses continuous translation an rotation symmetries. While a microscopic theory with full Galilean invariance is not possible, we showed that the maximally symmetric crystal structures are all compatible with this emergent behavior.

Chapter 7

Zero and one dimensional invariants in TCI's

7.1 Topological protection with restricted equivalence

The topological phases we considered so far were all defined modulo the addition of trivial bands. We use the term *stable equivalence* borrowed from the mathematical literature for this construction. The reason for this definition is that it allows comparison between physical systems with Hilbert spaces of very different structure, for example different number and location of the degrees of freedom. This view, however, may seem too general to study phases of condensed matter systems. It allows for an infinite set of frozen, trivial low energy degrees of freedom that can be freely added or subtracted. In real systems the Hamiltonian is bounded from below, there is only a finite number of fermions (even considering core electrons and nucleons) per unit cell. When studying a phase transition in a given material, the number of electrons never changes.

This leads us to consider a finer division of topological phases:

- One possibility is to consider a fixed lattice and classify phases living on this given discretized space up to stable equivalence[31, 32, 39]. Here we only mod out atomic insulators (AI's) that live on the same lattice, but not those on different lattices compatible with the same symmetry.

- Alternatively, we may insist on a given number of electrons per unit cell, or equivalently a given number of filled bands. This will produce new classes at low fillings[50–52, 176], in the large filling limit we expect no difference from the stable equivalence classification. From the stable equivalence point of view these phases may be "too-few-band-models" that are only distinct from the trivial case because the low dimensionality of the occupied space restricts deformations.

The latter scheme looses the abelian group structure of the classification, as the addition of two band structures changes the filling, and there is no way to compare systems with different

filling. Phases in these classifications may be stably equivalent to atomic insulators, thus host no surface states on generic interfaces with the vacuum or other materials. On the other hand, the nontrivial nature may still be observed at crystallographic defects. If no impurity is present, these defects can be viewed as unusual boundary conditions for the same material. Another situation where this classification proves useful are domain walls between different symmetry breaking phases in a single crystal. Polyacetilene[] is an example of this, where a domain wall is between two regions that both have inversion symmetry with two sites per unit cell, but are staggered in opposite ways. A similar scenario may explain the recently observed metallic domain walls in all-in-all-out pyrochlore magnets[177, 178]. The important feature here, is that both domains have exactly the same residual symmetry, but the breaking of the higher symmetry occurs in distinct ways. This leads to topologically different mass terms on the two sides of the domain wall, resulting in topological zero modes.

In the remainder of this chapter we review the representation theory of space groups and the resulting one dimensional invariants. We also address the question (without fully answering it), which of these phases survive stable equivalence. Following this, we also present results about Wilson loops and speculate about further topological crystalline phases that are characterized by unusual patterns of Wilson loop eigenvalues.

7.2 Space group representations and zero dimensional invariants

7.2.1 Representation theory of space groups

Here we briefly review the representation theory of space groups. We already reviewed Bloch's theorem for representing translations, this can be extended to the full space group action. As translations form a normal subgroup, we can use Wigner's little group trick. In symmorphic space groups at each $\mathbf{k}$ point we attach an irreducible representation (irrep) of the subgroup of the point group $P_{\mathbf{k}} \leq P$ that leaves $\mathbf{k}$ invariant, the little group of $\mathbf{k}$: $P_{\mathbf{k}} = \{O \in P : O\mathbf{k} = \mathbf{k} \pmod{\mathbf{G}}\}$.

In nonsymmorphic space groups the situation is more complicated and we need to use projective representations. The reason for this is that nonsymmorphic operations, while their orthogonal parts satisfy some relation, it will only be satisfied by the full operation up to lattice translations. We already saw an example of this with an essential nonsymmorphic operation $g = \{O|t_i/n\}$ where $O^n = \mathbb{1}$ but $g^n = \{\mathbb{1}|t_i\}$. The product rule for space group operations is $\{O_1|\mathbf{t}_1\}\{O_2|\mathbf{t}_2\} = \{O_1O_2|\mathbf{t}_1 + O_2\mathbf{t}_2\}$, this has to be obeyed by the representation of the little group $P_{\mathbf{k}}$. Elements of the little group are representatives of each class of operations that only differ by pure lattice translations $\{O_g|\mathbf{t}_g\}$ ($g \in P_{\mathbf{k}}$) where $\mathbf{t}_g$ is usually chosen to be the fractional part of the translation. Pure lattice translations $\{\mathbb{1}|\mathbf{t}\}$ are represented as $e^{i\mathbf{kt}}$, so given a set of little group elements whose product is a pure translation ($gh\ldots = e$) for the representatives we have $\{O_g|\mathbf{t}_g\}\{O_h|\mathbf{t}_h\}\ldots = \{\mathbb{1}|\mathbf{t}(g,h,\ldots)\}$ where the translation $\mathbf{t}(g,h,\ldots)$ is defined by the multiplication rule of space group operations. This

means, that the projective representation of $P_{\mathbf{k}}$ must obey the set of relations

$$D_{\mathbf{k}}(g)\, D_{\mathbf{k}}(h) \ldots = e^{i\mathbf{k}\mathbf{t}(g,h,\ldots)} \beta(g,h,\ldots)\mathbb{1} \tag{7.1}$$

where the signs $\beta(g,h,\ldots)$ keep track of the 2π rotation for half integer spins. This set of relations unambiguously defines the factor system of the projective representation[179].

Projective representations may be equivalent to a linear one by attaching phase factors. For certain factor systems, however, projective representations cannot be obtained this way. Without TR invariance all point groups have one dimensional representations, but projective representations must be at least two dimensiona. This forces band degeneracies of the dimensionality of the smallest irrep at the high symmetry momentum. At points in the interior of the BZ projective representations of $P_{\mathbf{k}}$ are equivalent to linear representations with $D_{\mathbf{k}}(g) = e^{i\mathbf{k}\mathbf{t}_g} D'_{\mathbf{k}}(g)$ where $D'_{\mathbf{k}}$ is a linear (double) representation of $P_{\mathbf{k}}$.

If a high symmetry line or plane is connected to a higher symmetry point, the representation must obey compatibility conditions. If the the representation at the higher symmetry manifold is decomposed with respect to the lower symmetry group, it must yield the representation on the lower symmetry manifold. As points with the same little groups may have different factor systems and irreps, it is possible that the minimal dimension irrep at a BZ boundary point is incompatible with any representation of the same dimension at another high symmetry point connected with a high symmetry line, adding more protected band crossings[180, 181].

7.2.2 Classification at fixed filling

These considerations naturally lead to a classification with fixed filling. One can construct all the consistent band representations at a given filling[1], as representations are a discrete set, the representation content can only change through gap closings. This classification is rather fine, even atomic insulators with orbitals transforming under different representations may fall in different classes. Consider for example the case of inversion symmetry only at one electron per unit cell. The representation which is even at every invariant $\mathbf{k}$ is distinct from the one that is everywhere odd, even though both can result from AI's, with one filled orbital per site that is even or odd under inversion respectively.

The most striking of these phases are *filling enforced quantum band insulators* (feQBI)[50–52]. These are band structures that occur in TR invariant nonsymmorphic systems at fillings that do not support any atomic insulators (see Sec. 7.2.4). Because of this, feQBI's are clearly topologically distinct from any atomic insulator with the same filling and inherently short-range entangled in nontrivial ways. It is still unclear, however, whether these phases are stable with respect to adding atomic insulators, as it is possible to add AI's and arrive at a filling that is compatible with AI's. We leave the search for stable topological invariants that characterize feQBI's to future work.

[1] Care must be taken about topological obstructions, see Sec. 7.2.3.

7.2.3 Representation valued invariants on simple lattices

We rephrase the ideas in Ref. [39] in the more general terms of irreducible representations. We fix a simple symmorphic lattice with the microscopic degrees of freedom living at the centers of the Wigner-Seitz cells (WSC). Given a gapped Hamiltonian we have a representation $D_{\mathbf{k}}$ on the occupied bands that decomposes at each point as:

$$D_{\mathbf{k}} = \oplus_i N^i_{\mathbf{k}} D^{(i)}_{\mathbf{k}} \tag{7.2}$$

where the direct sum runs over the set of irreps $D^{(i)}_{\mathbf{k}}$ of $P_{\mathbf{k}}$ and $N^i_{\mathbf{k}}$ is the multiplicity of irrep $D^{(i)}_{\mathbf{k}}$. We want our classification to be insensitive to addition of trivial bands, which are in the atomic limit with noninteracting atoms at the WSC centers, meaning that every point in the BZ obeys the same representation. We take the Γ point as reference, decompose the representation there according to all the lower symmetry little groups $D^o_\Gamma = \oplus_i m^i_{\mathbf{k}} D^{(i)}_{\mathbf{k}}$ and subtract it, yielding the set of numbers:

$$n^i_{\mathbf{k}} = N^i_{\mathbf{k}} - m^i_{\mathbf{k}}. \tag{7.3}$$

These numbers are not independent for every $\mathbf{k}$, obviously $n^i_\Gamma = 0$, $n^i_{\mathbf{k}} = 0$ if $P_{\mathbf{k}}$ is trivial, $n^i_{\mathbf{k}} = n^i_{\mathbf{k}'}$ if $\mathbf{k}$ and $\mathbf{k}'$ are symmetry related and as the total number of occupied bands is fixed throughout the BZ, $\sum_i n^i_{\mathbf{k}} \dim(D^i_{\mathbf{k}}) = 0$ for every $\mathbf{k}$. If a high symmetry line or plane is connected to a higher symmetry point, the representation must obey the compatibility conditions that unambiguously fix it as the decomposition of the representation at the high symmetry point in the lower symmetry subgroup. We may worry that the representation, while staying unitarily equivalent on these submanifolds, performs some nontrivial twist hiding some topological information. This is not the case in dimensions not greater than 3, as SU(N) is simply connected and all the point groups that leave a plane pointwise fixed are commutative. So we only need to consider representations at points (or lines or planes if the symmetry is sufficiently low) of the BZ that are of highest symmetry locally, moreover if two such points are connected by a nontrivial lower symmetry line their representations must be compatible giving rise to the same representation on this line.

This classification naturally has an Abelian group structure, upon adding two systems with the same symmetry the invariants add up as natural numbers, this is obvious in the limit when we superimpose two systems without any coupling.

To elucidate this abstract reasoning we apply it to cyclic groups C_n, $n = 2, 3, 4, 6$ in 2 dimensions[31, 33, 39]. As C_n is commutative, all irreps are one dimensional, characterized by the eigenvalue of the sates under an n-fold rotation R_n, the generator of C_n, a state at the Γ point transforming under irrep D^p_Γ ($p = 0 \dots n-1$) has eigenvalue $e^{2\pi p/n}$ (for simplicity we use the single representatoin for spinless electrons). In the $n = 4$ case we have two points with full symmetry, Γ and M and two symmetry related points X and Y with C_2 symmetry with irreps D^p_X (p = 0,1) that decompose the irreps at Γ as $D^p_\Gamma = D^{(p \mod 2)}_X$. There are no high symmetry lines, so we face no constraints aside from those that come from the total

number of bands being constant, so the four independent invariants are:

$$n_M^p = N_M^p - N_\Gamma^p \quad \text{for } p = 1, 2, 3 \tag{7.4}$$
$$n_X^1 = N_X^1 - N_\Gamma^1 - N_\Gamma^3 \tag{7.5}$$

resulting in a $\mathbb{Z}^4$ classification.

We note that there may be topological obstructions to realizing all representation patterns satisfying the compatibility relations. A simple example is given in Refs. [33, 46] in terms of a 3d TR breaking inversion symmetric system. Following the same reasoning would give $\mathbb{Z}^7$ classification by counting the difference in the number of odd representations at the seven high symmetry points compared to Γ. It can be shown (Sec. 7.3.3) that the parity of the Chern number for a cut of the BZ is determined by the inversion eigenvalues in that plane. As the Chern number cannot change between parallel cuts without closing the gap, this restricts the allowed patterns.

This recipe classifies point group symmetric insulators with only unitary space group symmetries. There are two possible directions if we want to include time reversal. One can consider magnetic space groups, where time reversal is not a symmetry on its own, but only when combined with some space group operation, representatoins of magnetic space groups are known and a similar program can be carried out. The other possibility is when time reversal is a global symmetry, giving rise to so-called co-representations at high symmetry points[182, 183]. The allowed representations are intertwined with the Z_2 index and only the simplest cases have been investigated so far[33, 152]. In superconductors the charge conjugation symmetry relates states in the "occupied" band to those in the"empty" band, the representations of such symmetry related pairs are complex conjugates posing additional constraints[39].

The same recipe can be applied to more complex lattices that have multiple inequivalent sites per unit cell. Intuitively, if we include a large number of sites at different locations the classification becomes identical to that in continuous space. First we review the construction of all possible kinds of atomic insulators.

7.2.4 Construction of atomic insulators

Before addressing the question of stable equivalence on continuous space, we must clarify what exactly we mean by atomic insulators. On generic nonsymmorphic lattices it is not obvious how to enumerate all atomic insulator representations compatible with the symmetry group, here we propose a scheme for this.

First choose a Wyckoff position (WP) on which the atoms are located. A WP is defined as the set of points in the unit cell that is visited by some starting point under the action of all space group elements modulo lattice vectors. The multiplicity of the WP is the number of points in this set. Symmorphic space groups are distinguished by the existence of a position of multiplicity 1, usually this point is chosen as the origin. A given point in the WP is left invariant under a subgroup of the space group, this is the site symmetry group of the WP, or

the point group of the site. The starting point may be continuously moved without affecting the symmetry properties of the WP, more generally these families are also called Wyckoff positions. In general there may be atoms on multiple WP's, but as these are not symmetry related, we may use single WP atomic insulators as building blocks.

Next, choose an irreducible representation of the site's point group, including possible on-site antiunitary symmetries. While the site symmetry groups have isomorphic group structures for all inequivalent sites in the Wyckoff position, the orientations of the space group operations may differ and the representations are identical only up to unitary equivalence. This ambiguity is fixed by considering the operations relating different sites. Let us fix a basis of space (or spacetime for magnetic groups) on site 1 and map it onto the other sites using some set of symmetry operations and repeat the pattern in every unit cell. To get a consistent representation, for every operation mapping site i to j we compare the image of the basis at i to the basis at j and assign the representation of site symmetry group element relating the two bases to the off-diagonal block between the Hilbert-spaces of sites i and j.

Given this real space representation $U(\{O|\mathbf{t}\})$, it is straightforward to construct the corresponding $\mathbf{k}$-space representation. For the interior of the BZ all we need to do is to attach a phase factor to get $D_{\mathbf{k}}(\{O|\mathbf{t}\}) = e^{-i\mathbf{kt}}U(\{O|\mathbf{t}\})$. At high symmetry points on the surface of the BZ $\mathbf{k}$ and $O\mathbf{k}$ may only be equivalent up to reciprocal lattice vectors, and the Hilbert spaces are related by $W_{\mathbf{k}-O\mathbf{k}}$. At these points a local representation is obtained by $D_{\mathbf{k}}(\{O|\mathbf{t}\}) = e^{-i\mathbf{kt}}W_{\mathbf{k}-O\mathbf{k}}U(\{O|\mathbf{t}\})$. Note that for a point inside the BZ $\mathbf{k} = O\mathbf{k}$ for all little group elements, so this formula is applicable to the generic situation as well and produces continuously changing representations when moving on a lower symmetry line to a high symmetry point. Such atomic insulators do not generally have irreducible representations at all $\mathbf{k}$-points, one can decompose these representations and obtain a list of the irreps appearing at all inequivalent $\mathbf{k}$-points for all possible atomic insulators.

As the construction shows, in nonsymmorphic crystals atomic insulators cannot realize arbitrarily low filling. If the minimal multiplicity of a Wyckoff position is n, an AI without TR invariance cannot have less than n bands. With TRI the bound is $2n$ because of the Kramers degeneracy. These bands are degenerate in the atomic limit, and cannot be separated by gaps with weak hopping. For generic band structures the minimal number of bands that can be separated by a gap from all others (but not among each other) is called nonsymmorphic rank[143, 184], a simple upper bound for this number is provided by the above AI result. It can be proved[143] that this bound is exact for spinless fermions without TRI, but as already mentioned, feQBI's realize lower filling than any TR invariant AI.

7.2.5 Invariants with stable equivalence on continuous space

Placing the degrees of freedom to the cell centers is not the only option, most crystals have multiple equivalently high symmetry Wyckoff positions, for example on a square lattice the corners also possess the full symmetry (Fig. 7.1 (b)). A quick calculation shows that an atomic insulator placed at the cell corners would fall into a nontrivial phase with respect to the classification on a lattice with sites in the centers. This is not surprising considering

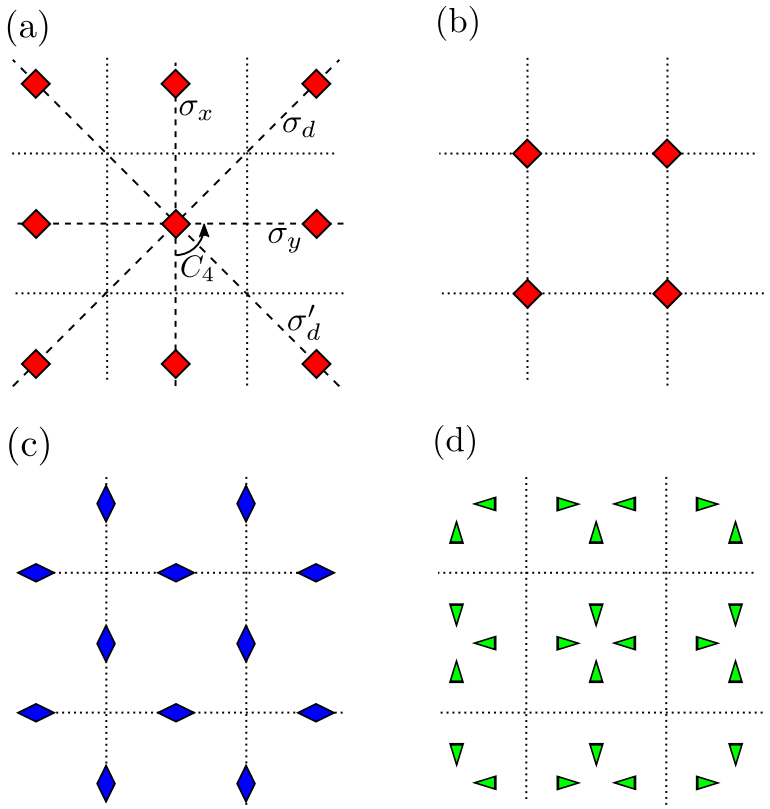

Figure 7.1: Various atomic insulators on the square lattice with C_4 or C_{4v} symmetry. Dotted lines delimit the Wigner-Seitz cells, symmetry operations are shown on subfigure (a). Every symbol represents an atom with electonic orbitals transforming by an irreducible representation of the local point group. (a), (b) and (c): three inequivalent atomic limits. Note that it is impossible to deform a single copy of (a) into (b) or a single copy of (c) into two copies of (a) or (c) without breaking the symmetry. (d): a trivial insulator with atoms at general positions in the interior of the WSC, it interpolates between four type (a) and two type (c) atomic limits.

that there is no way to continuously deform the lattice located at the corners into the one in the centers while preserving the symmetry. An alternative way of viewing this distinction is to consider the electric polarization[185] $\mathbf{P}$, it can be shown[31, 38] that $\mathbf{P}$, defined up to lattice translations, transforms as real space vectors under point group operations, so the two allowed values are $\mathbf{P} = (0, 0)$ and $\left(\frac{1}{2}, \frac{1}{2}\right)$. For a tight-binding model living at the cell centers the former is trivial, while for one on the corners the latter, there is a phase transition for a fixed microscopic model.

We shall ask the question, what if we want to classify systems living on the combined lattice that has inequivalent sites at the cell centers and corners or, going even further, where

degrees of freedom can be located anywhere in *continuous space*? The natural answer in the spirit of topological order is, we have to factor out *all* the trivial insulators. For example on the square lattice with C_4 or C_{4v} symmetry there are three distinct atomic limits with atoms located at the center, corner or two edge centers of the WSC (Fig. 7.1 (a)-(c)). It is easy to see that sites located in the interior of the WSC or at generic points of the boundary (Fig. 7.1 (d)) the representation is always reducible to multiple copies of the trivial insulator at the center, the only complications arise at locally maximal symmetry points of the WSC boundary. Without going into too much detail, we can construct representations of these new trivial insulators taking special care about the fact that the sites are only invariant up to lattice translations using methods explained in the previous section.

One may object that cases (a) and (b) in Fig. 7.1 are equivalent because they only differ by the choice of spatial origin. This is true with respect to a system with full translational invariance, like the vacuum, but they are inequivalent if compared to another system with discrete space group symmetry, like each other. If we were to consider the two cases equivalent, when adding two square lattice insulators we would have to specify whether we want to place the sites on top of each other or in the plaquette centers, thus loosing the group structure of our classification. That is why we fix the spatial origin, noting that two systems related by a shift of the origin have the same properties (such as surface states) when compared to the vacuum.

The simplest example is an inversion symmetric insulator in 1D, here, with a fixed centered lattice there are two phases, the trivial one where $D_0(I) = D_\pi(I)$ and nontrivial if $D_0(I) = -D_\pi(I)$. However, for an atomic insulator at WSC edge, because inversion moves the site by one lattice vector, we get $D_0(I) = -D_\pi(I)$, the nontrivial case is equivalent to a different atomic limit. Extending the argument to 3 dimensions it can be shown[46] that the only nontrivial topological indices are the Chern numbers and the quantized magnetoelectric polarizability (θ). For a C_4 symmetric insulator explicit calculation shows, with this extended set of equivalence relations, the only invariant is the Chern number C (mod 4), while if we include reflections (C_{4v}) that forbid nonzero Chern number there is no nontrivial index. This shows that in these symmetry classes without any global symmetry the only topological invariants are Chern numbers and quantized magnetoelectric polarizability. A natural extension of this statement (for which we do not have a rigorous proof) is that, in this stricter sense, all the topological properties of space group symmetric insulators can be expressed in terms of strong and weak invariants that only rely on global symmeties (such as Chern numbers, weak $\mathbb{Z}_2$ invariants and the quantized magnetoelectric coefficient), or their symmetry graded versions on lower dimensional subspaces of the BZ that are pointwise invariant under a subgroup, such as the mirror Chern numbers. All the space group can do is restricting the values of these invariants. A systematic study of this conjecture is left to future work.

7.3 Wilson loop invariants

7.3.1 Transformation properties of Wilson loops

Here we review symmetry properties of Wilson loop (WL) eigenvalues. As a natural consequence of our formalism we find constraints SG symmetry imposes on WL eigenvalues and resulting new topological invariants in topological crystalline insulators. Similar results were obtained in Refs [30, 31], those we generalize for all SG symmetries.

We define Wilson line operators as maps from the unit cell Hilbert space at the start of line $\mathcal{C}$ at $\mathbf{k}_0$ to the end at $\mathbf{k}_1$, $\mathcal{W}_\mathcal{C} : \mathcal{H}_{\mathbf{k}_0} \to \mathcal{H}_{\mathbf{k}_1}$. We use the definition in terms of an ordered discretization of $\mathcal{C}$, $\{\mathbf{k}_i\}_{i=1}^N$ with $\mathbf{k}_1 = \mathbf{k}_0$ and $\mathbf{k}_N = \mathbf{k}_1$:

$$\mathcal{W}_\mathcal{C} = \lim_{N\to\infty} \prod_{i=N}^{1} \mathcal{P}_{\mathbf{k}_i}. \tag{7.6}$$

We use the projector operators $\mathcal{P}$ expanded in the $|\chi\rangle$ convention, as in this convention it contains all the information about the positions of the sites in the unit cell and is invariant under the choice of the unit cell besides some other useful properties we will prove later. Note that $\mathcal{W}_\mathcal{C}$ only takes nonzero values on the occupied subspace at $\mathbf{k}_0$ and its image is the occupied space at $\mathbf{k}_1$. Its restriction to the local occupied spaces is unitary, this is seen by checking that $\mathcal{W}_\mathcal{C}^\dagger \mathcal{W}_\mathcal{C} = \mathcal{W}_{\mathcal{C}^{-1}} \mathcal{W}_\mathcal{C} = \mathcal{P}_{\mathbf{k}_0} + O(dk)$ with $dk \to 0$ the typical distance between the discretized $\mathbf{k}$ points. This means that all of its eigenvalues are either zero or a unit magnitude complex number, with the number of nonzero eigenvalues equal to the number of occupied bands. Moreover, Wilson loop operators restricted to the local occupied spaces form a unitary representation of the groupoid of curves under concatenation as $\mathcal{W}_{\mathcal{C}_2}\mathcal{W}_{\mathcal{C}_1} = \mathcal{W}_{\mathcal{C}_1+\mathcal{C}_2}$ where the end point of $\mathcal{C}_1$ is the same as the starting point of $\mathcal{C}_2$.

This definition is consistent with the definition in terms of the Berry connection as

$$\sum_{n,m\in \text{occ.}} \left(P \exp\left(i \int_\mathcal{C} \mathcal{A} \right) \right)^{nm} n_{\mathbf{k}_0} m^\dagger_{\mathbf{k}_1} = \mathcal{W}_\mathcal{C} \tag{7.7}$$

where $n_\mathbf{k}$ is the coefficients of an orthonormal set of occupied eigenstates in the $|\chi\rangle$ convention at $\mathbf{k}$[30, 31]. In general $\mathcal{W}_\mathcal{C}$ is gauge-dependent, however, as we show in the following, for a closed loop its spectrum $\sigma(\mathcal{W}_\mathcal{C})$ (with multiplicities) is well defined.

For a closed loop $\mathcal{C}$ we define

$$\mathcal{W}_\mathcal{C} = W_{-\mathbf{G}} \left(\prod_{\mathbf{k}=\mathbf{k}_0}^{\mathbf{k}_0-\mathbf{G}} \mathcal{P}_\mathbf{k} \right) \tag{7.8}$$

where $\mathbf{G}$ is a nonzero reciprocal lattice vector if the loop is non-contractible and the overall displacement along it is $\mathbf{G}$. We use this definition to make $\mathcal{W}_\mathcal{C}$ a mapping from $\mathcal{H}_{\mathbf{k}_0}$ onto itself, as in our convention the Hilbert spaces at $\mathbf{k}$ and $\mathbf{k}+\mathbf{G}$ are not identical, but related

through the unitary mapping $W_{\mathbf{G}}$. Using the groupoid property we can check that with this definition Wilson loops along the same oriented loop but with different starting points are unitarily related. Furthermore, a gauge transformation or a shift by a reciprocal lattice vector also acts as a unitary transformation, showing that the spectrum is insensitive to these choices, meaning we can consider closed loops $\mathcal{C}$ as directed curves on the BZ torus in the following. Finally, consider a shift of the real space origin by $\mathbf{t}$ acting on the coefficients as $e^{i\mathbf{kt}}$. $\mathcal{P}$ does not change, but the BZ boundary condition changes $W_{\mathbf{G}} \to W_{\mathbf{G}} e^{i\mathbf{Gt}}$, resulting in $\mathcal{W}_{\mathcal{C}} \to \mathcal{W}_{\mathcal{C}} e^{-i\mathbf{Gt}}$, meaning a simple shift in all the phases of the nonzero eigenvalues, $\{\phi_{\mathcal{C}}\} \to \{\phi_{\mathcal{C}} - \mathbf{Gt}\}$ with $\{\phi_{\mathcal{C}}\} = -i \log\left(\sigma\left(\mathcal{W}_{\mathcal{C}}\right) \setminus 0\right)$. This result is easily understood if we regard the curve $\mathcal{C}$ as the BZ of a 1d system with isolated bands. The phases of the Wilson loop eigenvalues can be identified as the Wannier center positions for occupied bands, and as we showed they indeed transform as real space coordinates in the $\mathbf{G}$ direction under a shift of the spatial origin.

In the following we establish some symmetry properties of the WL operators, starting with the well known case of time-reversal symmetry. TR symmetry with $\mathcal{T} = \sigma_y \mathcal{K}$ implies $\mathcal{P}_{\mathbf{k}} = \mathcal{T}\mathcal{P}_{-\mathbf{k}}\mathcal{T}^{-1} = \sigma_y \mathcal{P}^*_{-\mathbf{k}} \sigma_y$, plugging this in (7.8) for a TR invariant line (such that $-\mathcal{C} = \mathcal{C}^{-1}$) we find

$$\mathcal{W}_{\mathcal{C}} = \left(W_{2\mathbf{k}_0}\mathcal{T}\right) \mathcal{W}_{\mathcal{C}}^{\dagger} \left(W_{2\mathbf{k}_0}\mathcal{T}\right)^{-1} \tag{7.9}$$

where we used the fact that $W_{\mathbf{k}}$ is a diagonal unitary that commutes with σ_y. The antiunitary operator $\left(W_{2\mathbf{k}_0}\mathcal{T}\right)$ squares to $-\mathbb{1}$ same as $\mathcal{T}$, direct calculation shows that the eigenvectors $|\lambda\rangle$ and $\left(W_{2\mathbf{k}_0}\mathcal{T}\right)|\lambda\rangle$ are orthogonal, both with eigenvalues λ, proving the Kramers-degeneracy of WL eigenvalues.

Next we move on to the action of SG symmetries on WL operators, in particular we consider SG operation $\{O|\mathbf{t}\}$ represented by $R_{\mathbf{k}} = e^{-i(O\mathbf{k})\mathbf{t}} U : \mathcal{H}_{\mathbf{k}} \to \mathcal{H}_{O\mathbf{k}}$. As we did so far, we keep track of the absolute (not BZ reduced) positions, and transition to a BZ reduced convention when necessary. Using the symmetry property $\mathcal{P}_{O\mathbf{k}} = U\mathcal{P}_{\mathbf{k}}U^{\dagger}$ of the projector we see for any open Wilson line operator

$$\mathcal{W}_{O\mathcal{C}} = U\mathcal{W}_{\mathcal{C}}U^{\dagger} \tag{7.10}$$

where $O\mathcal{C}$ is the image of $\mathcal{C}$.

As discussed before, the great advantage of our formalism is that the atomic positions are encoded in the boundary conditions obeyed by operators and symmetry operators take the above simple form. Symmetry operators satisfy the same boundary conditions leading to consistency relations. Consider $R_{\mathbf{k}+\mathbf{G}} : \mathcal{H}_{\mathbf{k}+\mathbf{G}} \to \mathcal{H}_{O(\mathbf{k}+\mathbf{G})}$, leading to $R_{\mathbf{k}+\mathbf{G}} = W_{O\mathbf{G}} R_{\mathbf{k}} W_{\mathbf{G}}^{-1}$ which imposes the constraint on the constant unitary part $e^{-i(O\mathbf{G})\mathbf{t}} U = W_{O\mathbf{G}} U W_{\mathbf{G}}^{-1}$. As a result, for closed Wilson loops

$$\mathcal{W}_{O\mathcal{C}} = e^{i(O\mathbf{G})\mathbf{t}} U \mathcal{W}_{\mathcal{C}} U^{\dagger} \tag{7.11}$$

with the reciprocal lattice vector $\mathbf{G}$ describing the winding of the loop $\mathcal{C}$. So the set of phases of the eigenvalues is related as $\{\phi_{O\mathcal{C}}\} = \{\phi_{\mathcal{C}} + (O\mathbf{G})\,\mathbf{t}\}$. This property is identical to the symmetry requirement for the projections of the atomic (Wyckoff) positions. The

set of atomic positions has to be invariant under the SG symmetry, $\{\mathbf{x}\} = \{O\mathbf{x} + \mathbf{t}\}$. Now consider the projection onto $O\mathbf{G}$, $\{(O\mathbf{G})\,\mathbf{x}\} = \{(O\mathbf{G})\,(O\mathbf{x} + \mathbf{t})\} = \{\mathbf{G}\mathbf{x} + (O\mathbf{G})\,\mathbf{t}\}$, same requirement as for the phases if we identify phases along a loop with winding $\mathbf{G}$ with the projections of atomic coordinates along $\mathbf{G}$. This picture is further supported by considering an atomic insulator with $\mathcal{P}_{\mathbf{k}}^{(\mathbf{x},l),(\mathbf{x}',l')} = \delta^{\mathbf{x},\mathbf{x}'} P_{\mathbf{x}}^{l,l'}$ where $P_{\mathbf{x}}^{l,l'}$ is the projector onto the occupied atomic levels at each site, same for all symmetry related sites. In this case $\mathcal{W}_{\mathcal{C}} = \mathcal{P} W_{-\mathbf{G}} \mathcal{P}$ whose eigenvalues are exactly the list of the projections of the atomic positions of the occupied orbitals onto $\mathbf{G}$.

7.3.2 TCI's from Wilson loop invariants

We emphasize that the WL eigenvalues are *not* the same as the projections of the polarization, the latter are obtained integrating the sum of the WL phases for all parallel lines in a given direction, thus contain less information. As already mentioned, for insulators on a given lattice, the polarization may characterize nontrivial TCI's if it is at a maximal symmetry Wyckoff position that is different from the underlying lattice.

The polarizations for individual bands are in general ill defined as WL eigenvalues can cross as moving the line $\mathcal{C}$ in the perpendicular direction. On the other hand, the above symmetry constraints on WL eigenvalues are weaker than those on Wyckoff positions, a symmetry preserving preimage of the projections as a set of 3D points may not exist, such a situation would signal a crystalline topological phase distinct from the trivial AI. This distinction also not stable, adding a sufficient number of trivial bands the eigenvalues may be continuously deformed to allow a preimage. We believe such phases can appear on a wide variety of simmorphic and nonsymmorphic lattices, explicite construction of models expressing this behavior is left for future work.

Symmorphic inversion symmetric systems were studied using similar methods in Ref. [30], there TCI's were identified by observing the nontrivial rearrangement of the WL eigenvalues as sweeping the WL across the BZ. Hourglass Fermions[43, 47] are also characterized by similar WL patterns.

7.3.3 Derivation of the Chern number formula with C_n symmetry

We briefly review the results of Ref. [31, 47] constraining the Chern number of insulators with discrete rotational symmetry. We use our notation for Wilson loop invariants (Sec. 7.3.1) and arrive at the same results.

As an example we detail the derivation for fourfold (C_4) rotations, the other cases can be obtained analogously. We are going to examine the Wilson loop operator along the contractible curve $\mathcal{C} = \Gamma X M Y$. As this curve is contractible, the enclosed Berry flux modulo 2π is given by the pseudodeterminant of $\mathcal{W}_{\mathcal{C}}$, and because of the symmetry properties of $\mathcal{F}$ this is exactly one quarter of the total flux through the BZ. This can be summarized as $\exp\left(\frac{2\pi i}{4} C\right) = \det{}_+ \mathcal{W}_{\mathcal{C}}$. We can break up the loop into 4 parts as $\mathcal{W}_{\mathcal{C}} = \mathcal{W}_{\Gamma \leftarrow Y} \mathcal{W}_{Y \leftarrow M} \mathcal{W}_{M \leftarrow X} \mathcal{W}_{X \leftarrow \Gamma}$ and analyze symmetry properties of its parts. We find

$\mathcal{W}_{\Gamma\leftarrow Y} = U\mathcal{W}_{\Gamma\leftarrow X}U = U\mathcal{W}^{-1}_{X\leftarrow\Gamma}U^\dagger$ as they are related by C_4 represented by U and reversal of the direction. Here and in the following by $()^{-1}$ we mean the Moore-Penrose pseudoinverse of singular operators, which in this case is the same as the inverse if we restrict both the domain and codomain to the occupied subspace. Similarly $\mathcal{W}_{Y\leftarrow M} = U^\dagger W_{-\mathbf{G}_x}\mathcal{W}^{-1}_{M\leftarrow X}W_{\mathbf{G}_x}U$ as now the necessary transformation is a rotation in the opposite direction combined with a translation by a reciprocal lattice vector and reversal of direction.

Substituting this we rearrange the WL operator as

$$\begin{aligned}\mathcal{W}_\mathcal{C} = &\left(\mathcal{P}_\Gamma U\mathcal{P}_\Gamma\right)\mathcal{W}^{-1}_{X\leftarrow\Gamma}\left(\mathcal{P}_X U^{-2}W_{-\mathbf{G}_x}\mathcal{P}_X\right)\mathcal{W}^{-1}_{M\leftarrow X}\times\\ &\left(\mathcal{P}_M W_{\mathbf{G}_x}U\mathcal{P}_M\right)\mathcal{W}_{M\leftarrow X}\mathcal{W}_{X\leftarrow\Gamma}.\end{aligned} \tag{7.12}$$

We inserted band projectors at the end points of the lines without changing the results and introduced parentheses to emphasize the structure. Every term in the product is a unitary when restricted to the occupied subspace at its domain and codomain. Thus the determinant multiplication theorem applies to the pseudodeterminant,

$$\begin{aligned}\det_+\mathcal{W}_\mathcal{C} = &\det_+\left(\mathcal{P}_\Gamma U\mathcal{P}_\Gamma\right)\det_+\left(\mathcal{P}_X U^{-2}W_{-\mathbf{G}_x}\mathcal{P}_X\right)\times\\ &\det_+\left(\mathcal{P}_M W_{\mathbf{G}_x}U\mathcal{P}_M\right).\end{aligned} \tag{7.13}$$

Each of these determinants is exactly the product of the occupied eigenvalues of a C_4 or C_2 rotation at a given point of the BZ,

$$\det_+\mathcal{W}_\mathcal{C} = \prod_{m\in\text{occ.}}\xi^\Gamma_m\left(C_4\right)\xi^M_m\left(C_4\right)\xi^X_m\left(C_4^{-2}\right) \tag{7.14}$$

where $\xi^\mathbf{k}_m\left(O\right)$ is the rotation eigenvalue of O in band m at momentum $\mathbf{k}$. Thus we reproduced the result for C_4 in Ref. [31] and Eqn. 6.5, results for C_2, C_3 and C_6 symmetry follow analogously:

$$e^{2\pi i\frac{C}{2}} = \prod_{m\in\text{occ.}}\xi^\Gamma_m\left(C_2\right)\xi^M_m\left(C_2\right)\xi^X_m\left(C_2^{-1}\right)\xi^Y_m\left(C_2^{-1}\right) \tag{7.15}$$

$$e^{2\pi i\frac{C}{3}} = \prod_{m\in\text{occ.}}\xi^\Gamma_m\left(C_3\right)\xi^K_m\left(C_3\right)\xi^{K'}_m\left(C_3^{-2}\right) \tag{7.16}$$

$$e^{2\pi i\frac{C}{6}} = \prod_{m\in\text{occ.}}\xi^\Gamma_m\left(C_6\right)\xi^K_m\left(C_6^{2}\right)\xi^M_m\left(C_6^{-3}\right). \tag{7.17}$$

Part IV

Topological response in metals

Chapter 8

Orbital magnetopiezoelectric effect in metals

The polarization of a material and its response to applied electric and magnetic fields are key solid-state properties with a long history in insulators, although a satisfactory theory required new concepts such as Berry-phase gauge fields. In metals, quantities such as static polarization and magnetoelectric θ-term cease to be well-defined. In polar metals there can be analogous dynamical current responses, which we study in a common theoretical framework. We find that current responses to dynamical strain in polar metals depend on both the first and second Chern forms, related to polarization and magnetoelectricity in insulators, as well as the orbital magnetization on the Fermi surface. We provide realistic estimates that predict that the latter contribution will dominate and investigate the feasibility of experimental detection of this effect.

8.1 Introduction

The importance of Berry phases and other geometrical properties of Bloch wavefunctions was first clearly understood in topological phases such as the integer quantum Hall effect [5, 12]. It rapidly became clear that many physical observables in solids are described by Berry phases even in ordinary insulators with no quantization; the electrical polarization in a crystal can be fully and concisely expressed via the Berry phase of Bloch states [186, 187]. Metallic systems present additional challenges: in the oldest example, the anomalous Hall effect [168], there are both Berry-phase "intrinsic" contributions and "extrinsic" contributions that depend on the details of scattering processes. Discrete symmetries underlie and restrict the emergence of these responses [188]; the anomalous Hall effect is enabled by the breaking of time-reversal symmetry and is observed in magnetic metals.

The goal of this paper is to analyze a class of transport effects enabled by the breaking of inversion symmetry in metals. The study of inversion breaking materials such as ferroelectric insulators with switchable polarization, has revealed several fundamental pieces of solid-state

physics and lead to a variety of applications [189, 190]. These advances have translated into a recent increasing interest in the more elusive *polar metals* [191–193]. While metals do not have a measurable electrical polarization–any surface charge density would be screened by the bulk conduction electrons–polar metals have a low enough symmetry group to support a static polarization were they insulators.

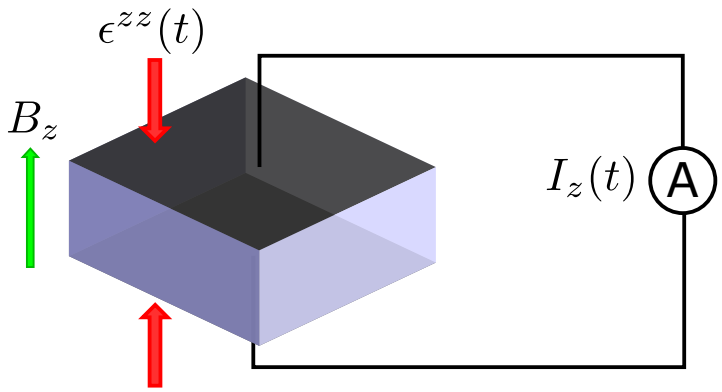

Figure 8.1: Schematic experimental setup. The sample is placed in static magnetic field and homogenous time-dependent strain is appiled. The top and bottom surfaces are contacted, short-circuited through a low impedance ammeter and the current parallel to the applied field is measured.

More precisely, we explain how the Berry phase and related quantities such as the orbital magnetic moments [194] determine multiple observable properties of polar metals with or without time reversal symmetry. Some of these observables can be viewed as generalizations to metals of Berry-phase properties in insulators such as electrical polarization and the orbital magnetoelectric effect, while others are Fermi-surface properties and hence specific to metals. The effects we discuss have important analogues in the corresponding insulating inversion-broken state, in the same way as the integer quantum Hall effect is connected to the intrinsic anomalous Hall effect [195, 196]. An additional motivation for the present work is the active theoretical discussion of when metals, such as Weyl semimetals [197, 198], can support a current that is induced by and is parallel to an applied magnetic field (the chiral magnetic effect) [199–206]. The answer is connected to the low-frequency limit of optical activity and involves the magnetic moment of Bloch electrons at the Fermi level [70, 71], which raises the question of what other properties of metals might involve such magnetic moments.

Table 8.1 compiles the requirements of the effects that are the focus of the present work. The first is referred to as piezoelectricity [185, 207, 208]; in a polar material, even in a metal, any time-dependent change of the material, such as a time-dependent strain, will induce a

current resulting from the change of polarization. In a metal, only changes in polarization are well-defined as these involve measurable bulk currents through the unit cell.

As a difference with the insulating case where the energy gap protects against process that do not excite electrons far from the ground state, we will require a slow evolution of strain relative to electronic time scales [1]. This assumption guarantees that the distribution function remains close to equilibrium. Additional effects from strongly non-equilibrium distributions and the scattering processes that restore equilibrium are left for future work.

	$\mathcal{T}$	$\mathcal{I}$	$\mathbf{m}$	Eq.
Piezoelectricity	Any	No	Any	(8.11)
MPE Fermi sea	No	No	Any	(8.12)
MPE Fermi surface	No	No	Nonzero	(8.13)

Table 8.1: The three effects considered in this work and their requirements in terms of time reversal ($\mathcal{T}$) and inversion ($\mathcal{I}$) symmetry and the orbital moment $\mathbf{m}$.

A second effect, which we call magnetopiezoelectricity (MPE), emerges when the material is magneticaly ordered and time-reversal symmetry is broken along with inversion symmetry. One contribution can be viewed as the generalization to metals of the orbital magnetoelectric effect in insulators [20, 27, 210, 211]. It involves the second Chern form of the Berry gauge fields [212, 213][2], a slightly more complicated geometrical object than the first Chern form that controls the polarization and Hall effect, and can be interpreted as a metallic version of the dynamical axion effect in antiferromagnets [214, 215].

We also find a second, purely Fermi-surface contribution to the MPE that is proportional to the orbital magnetic moment. Estimates for realistic systems predict that this part of the MPE unique to metals dominates the response. It is therefore the main prediction of this letter for a new experimental effect.

8.2 Methodology

To address the topological responses of metallic magneto-electrics we employ the semiclassical formalism [194, 195, 212, 216–218]. Our starting point is a three-dimensional Hamiltonian of a metal $H(\mathbf{k}, \theta)$ that is parametrized by a time dependent parameter $\theta(t)$. The microscopic origin of $\theta(t)$ can be diverse, it can for example parametrize ferromagnetic [47] or

[1] A different mechanism is considered in [209] that discusses a strain-induced chiral magnetic effect in Weyl semimetals. Unlike the near-equilibrium or adiabatic physics found here, it depends on a non-equilibrium electronic configuration created by straining faster than the intervalley relaxation time. This rapid strain can create a large current in a magnetic field.

[2] Refs. [212] and [213] discuss a different occurrence of the second Chern form in the response of metals to magnetic field in the presence of static spatial inhomogeneity rather than the purely dynamical effects studied here.

antiferromagnetic ordering [219]. Such a fluctuating magnetic order in insulating systems has been previously studied [220] and termed "dynamical axion field".

In this work we focus on the case where θ emerges from the coupling of homogeneous time-dependent strain to orbital degrees of freedom, which effectively renormalizes the hopping structure of $H(\mathbf{k})$ in a time-dependent fashion leading to $H(\mathbf{k},\theta)$. The parameter θ can refer to any strain component, or an arbitrary parametrization of some combination of strain components. Before proceeding, it is worth highlighting several relevant aspects of our calculation. First, strain is non-electromagnetic and acts as an independent external field. Second, although we allow for the time-reversal-breaking magnetic order required for the MPE to depend on θ, we assume it does not respond to external magnetic fields at the linear order of interest here. Thus we only focus on the orbital contribution. Finally, we assume the clamped ion limit; strain changes the hopping amplitudes for the electrons but the atomic coordinates remain fixed.

A compact way of dealing with $H(\mathbf{k},\theta)$ is to regard θ as an extra momentum coordinate k_θ and promote the semiclassical picture to a four-dimensional space. Its corresponding phase space is defined by an extended momentum and position vector, $k_\mu = (\mathbf{k},\theta)$ and $\mathbf{r}_\mu = (\mathbf{r}, r_\theta)$ respectively, with $\mu = x, y, z, \theta$. The semiclassical equations for such phase space read [194, 221]

$$\dot{r}^\mu = \frac{1}{\hbar}\frac{\partial\tilde{\mathcal{E}}_{\mathbf{k},\theta}}{\partial k_\mu} - \tilde{\mathcal{F}}^{\mu\nu}\dot{k}_\nu \tag{8.1}$$

$$\hbar\dot{k}_\mu = -eE_\mu - eB_{\mu\nu}\dot{r}^\nu \tag{8.2}$$

Here $E_\mu = \partial_0 A_\mu - \partial_\mu A_0$ and $B^{\mu\nu} = \partial_\mu A_\nu - \partial_\nu A_\mu$ are the generalization of the electric and magnetic fields constructed from the gauge field $A_\mu = (A_0, \mathbf{A}, A_\theta)$. By construction we impose that A_θ is uniform and time dependent while $\mathbf{A}$ is independent of θ. This constrains $B^{\nu\theta} = 0$ and, from (8.2), $\hbar\dot{\theta} = -eE_\theta$. We note that Eq. (8.1) includes two corrections due to the external fields [194, 222]. One modifies the band structure $\varepsilon_{\mathbf{k},\theta} \to \tilde{\mathcal{E}}_{\mathbf{k},\theta} = \varepsilon_{\mathbf{k},\theta} - \mathbf{m}_{\mathbf{k}}\cdot\mathbf{B}$ where $\mathbf{m}_{\mathbf{k},\theta} = \frac{e}{2\hbar}\mathrm{Im}\langle\partial_{\mathbf{k}}u_{\mathbf{k},\theta}|\times(H-\varepsilon_{\mathbf{k},\theta})|\partial_{\mathbf{k}}u_{\mathbf{k},\theta}\rangle$ is the magnetic orbital moment define through the Bloch wave-functions $|u_{\mathbf{k},\theta}\rangle$. Second, the Berry curvature $\mathcal{F}^{\mu\gamma} = \partial_{k_\mu}\mathcal{A}_{k_\gamma} - \partial_{k_\gamma}\mathcal{A}_{k_\mu}$ where $\mathcal{A}_{k_\mu} = i\langle u|\partial_{k_\mu}|u\rangle$ is the unperturbed Berry connection, is corrected as $\mathcal{F}^{\mu\gamma} \to \tilde{\mathcal{F}}^{\mu\gamma} = \mathcal{F}^{\mu\gamma} + \mathcal{F}_1^{\mu\gamma}$. The correcting $\mathcal{F}_1^{\mu\gamma} = \partial_{k_\mu}\mathcal{A}'_{k_\gamma} - \partial_{k_\gamma}\mathcal{A}'_{k_\mu}$ is defined by $\mathcal{A}'_{k_\mu} = i\langle u|\partial_{k_\mu}|u'\rangle + \text{c.c.}$ that incorporates the first-order correction from the *perturbing* electromagnetic fields to the Bloch wave-function $|u'_{\mathbf{k},\theta}\rangle$. The quantity a'_{k_μ} is gauge-invariant, and physically corresponds a shift of the wave-packet centre induced by interband mixing from the external fields [222].
Combining (8.1) and (8.2) and keeping terms to second order in the external fields results in [221]

$$\dot{r}^\mu = \frac{1}{\hbar}\frac{\partial\tilde{\mathcal{E}}_{\mathbf{k},\theta}}{\partial k_\mu} + \frac{e}{\hbar}\tilde{\mathcal{F}}^{\mu\nu}\left(E_\nu + \frac{1}{\hbar}B_{\nu\lambda}\frac{\partial\tilde{\mathcal{E}}_{\mathbf{k},\theta}}{\partial k_\lambda}\right) + \frac{e^2}{\hbar^2}\tilde{\mathcal{F}}^{\mu\nu}B_{\nu\lambda}\tilde{\mathcal{F}}^{\lambda\gamma}\left(E_\gamma + \frac{1}{\hbar}B_{\gamma\delta}\frac{\partial\tilde{\mathcal{E}}_{\mathbf{k},\theta}}{\partial k_\delta}\right) + \cdots,$$

which enters the current density

$$j^{\mu} = \int_{\mathbb{T}^3} \mathrm{d}^3k [\dot{r}^{\mu} D_{\mathbf{k},\theta}] f(\tilde{\mathcal{E}}_{\mathbf{k},\theta}, \mu). \tag{8.3}$$

Here $f(\tilde{\mathcal{E}}_{\mathbf{k},\theta}, \mu)$ is the Fermi-Dirac distribution for the perturbed band structure $\tilde{\mathcal{E}}_{\mathbf{k},\theta}$ at chemical potential μ and $D_{\mathbf{k},\theta}$ is the modified density of states defined as

$$D_{\mathbf{k},\theta} = \left[1 + \frac{1}{2}\frac{e}{\hbar} B_{\mu\nu} \tilde{\mathcal{F}}^{\mu\nu} + \mathcal{O}(B^2)\right]. \tag{8.4}$$

Using (8.3) and (8.3) the current density reads

$$\begin{aligned} j^{\mu} = e \int_{\mathbb{T}^3} \frac{\mathrm{d}^3k}{(2\pi)^3} \Bigg[& \frac{1}{\hbar}\frac{\partial \tilde{\mathcal{E}}_{\mathbf{k},\theta}}{\partial k_{\mu}} + \frac{e}{\hbar} \tilde{\mathcal{F}}^{\mu\nu} E_{\nu} + \frac{e^2}{\hbar^2} \left(\mathcal{F}^{\mu\nu} B_{\nu\gamma} \mathcal{F}^{\gamma\delta} E_{\delta} + \frac{1}{2} \mathcal{F}^{\delta\gamma} B_{\delta\gamma} \mathcal{F}^{\mu\nu} E_{\nu} \right) + \\ & + \frac{e}{\hbar^2} \left(\tilde{\mathcal{F}}^{\mu\nu} B_{\nu\gamma} \frac{\partial \tilde{\mathcal{E}}_{\mathbf{k},\theta}}{\partial k_{\gamma}} + \frac{1}{2} \tilde{\mathcal{F}}^{\gamma\nu} B_{\gamma\nu} \frac{\partial \tilde{\mathcal{E}}_{\mathbf{k},\theta}}{\partial k_{\mu}} \right) \Bigg] f(\tilde{\mathcal{E}}_{\mathbf{k},\theta}, \mu) + \cdots . \end{aligned} \tag{8.5}$$

We are interested in the spatial components of current density j^i with $i = x, y, z$ generated in the absence of an electric field $\mathbf{E} = 0$. Keeping terms potentially linear in magnetic field $B_i = \epsilon_{ijk} B_{jk}$ results in

$$\begin{aligned} j^i \approx e \int_{\mathbb{T}^3} \frac{\mathrm{d}^3k}{(2\pi)^3} \Bigg[& \left(\frac{1}{\hbar}\frac{\partial \tilde{\mathcal{E}}}{\partial k_i} + \dot{\theta} \tilde{\mathcal{F}}^{i\theta} \right) - \frac{1}{8}\frac{e}{\hbar} \left(\epsilon_{\mu\nu\gamma\delta} \mathcal{F}^{\mu\nu} \mathcal{F}^{\gamma\delta} \right) \dot{\theta} B_i \\ & + \frac{1}{2}\frac{e}{\hbar^2} \left(\epsilon_{lmn} \tilde{\mathcal{F}}^{lm} \frac{\partial \tilde{\mathcal{E}}}{\partial k_n} \right) B_i \Bigg] f(\tilde{\mathcal{E}}_{\mathbf{k},\theta}, \mu) + \cdots , \end{aligned} \tag{8.6}$$

which is of the form $j^i = j^i_a + j^i_b + j^i_c$. The last term, j^i_c can be proved to be zero (see supplementary material) and is consistent with the absence of the chiral magnetic effect in the static limit [70, 71]. In the second term, j^i_b, keeping only linear order corrections in B_i allows us to evaluate the distribution function at the unperturbed energy $\varepsilon_{\mathbf{k},\theta}$ leading to

$$j^i_b = -\frac{1}{8}\frac{e^2}{\hbar} \int_{\mathbb{T}^3} \frac{\mathrm{d}^3k}{(2\pi)^3} \left[\left(\epsilon_{\mu\nu\gamma\delta} \mathcal{F}^{\mu\nu} \mathcal{F}^{\gamma\delta} \right) \dot{\theta} \right] f(\varepsilon_{\mathbf{k},\theta}, \mu) B_i \,, \tag{8.7}$$

which is linear in magnetic field as desired and explicitly gauge invariant. To simplify j^i_a, we can expand the Fermi-Dirac distribution around its unperturbed form $f(\varepsilon_{\mathbf{k},\theta}, \mu)$

$$f(\tilde{\mathcal{E}}_{\mathbf{k},\theta}, \mu) \sim f(\varepsilon_{\mathbf{k},\theta}, \mu) + \frac{\partial f(\mathcal{E})}{\partial \mathcal{E}}\Big|_{\varepsilon_{\mathbf{k},\theta}} \tilde{\mathcal{E}}' + \cdots , \tag{8.8}$$

where $\tilde{\mathcal{E}}' = -\mathbf{m}_{\mathbf{k},\theta} \cdot \mathbf{B}$. We obtain

$$j^i_a = e \int_{\mathbb{T}^3} \frac{\mathrm{d}^3k}{(2\pi)^3} \left[\dot{\theta} \mathcal{F}^{i\theta} f(\varepsilon_{\mathbf{k},\theta}, \mu) + \dot{\theta} \mathcal{F}^{i\theta}_1 f(\varepsilon_{\mathbf{k},\theta}, \mu) - \dot{\theta} \mathcal{F}^{i\theta} \frac{\partial f(\mathcal{E})}{\partial \mathcal{E}}\Big|_{\varepsilon_{\mathbf{k},\theta}} \mathbf{m}_{\mathbf{k},\theta} \cdot \mathbf{B} \right] \tag{8.9}$$

using that the integral of the Fermi velocity over the Fermi sea vanishes. The correction $\mathcal{F}_1^{i\theta}$ to the Berry curvature results from interband mixing and vanishes as $1/\Delta^3$ where Δ is the separation between different bands [222]. Taking Δ to be large, the low temperature limit and recasting the last term in (8.9) as a Fermi surface contribution, the final response, which is the central result of this work, is given by

$$j^i = \beta^i \dot{\theta} + (\alpha_1^{ij} + \alpha_2^{ij}) \dot{\theta} B_j + \mathcal{O}(1/\Delta^3) \tag{8.10}$$

$$\beta^i = e \int_{\text{occ.}} \frac{\mathrm{d}^3 k}{(2\pi)^3} \mathcal{F}^{i\theta} \tag{8.11}$$

$$\alpha_1^{ij} = -\frac{\delta^{ij}}{8} \frac{e^2}{\hbar} \int_{\text{occ.}} \frac{\mathrm{d}^3 k}{(2\pi)^3} \epsilon_{\mu\nu\gamma\delta} \mathcal{F}^{\mu\nu} \mathcal{F}^{\gamma\delta} \tag{8.12}$$

$$\alpha_2^{ij} = -\frac{e}{\hbar} \int_{\text{FS}} \frac{\mathrm{d}^2 k}{(2\pi)^3} \frac{1}{|v_{\mathbf{k}}|} \mathcal{F}_{\mathbf{k}}^{i\theta} m_{\mathbf{k},\theta}^j \tag{8.13}$$

where $\hbar\,|v_{\mathbf{k}}| = |\partial \varepsilon_{\mathbf{k},\theta}/\partial \mathbf{k}|$.

The first term β^i is independent of the magnetic field and captures the piezoelectric effect [207] when θ corresponds to strain. For metals, the bulk current arises from the change in polarization involving occupied states.

The second term, α_1^{ij}, is the analogue of the isotropic magnetoelectric effect in insulators. Recall that in an insulating system a polarization in response to a static magnetic field is characterized by the momentum integral of a Chern-Simons three-form determined by the band structure [20, 27, 210, 211]. For the case of metals we find that the change in polarization depends on the variation with respect to θ and is determined by the integral of the second Chern-form, $\epsilon_{\mu\nu\gamma\delta}\,\mathrm{Tr}\,\mathcal{F}^{\mu\nu}\mathcal{F}^{\gamma\delta}$ over occupied states. It is exactly the derivative of the Chern-Simons three-form with respect to θ.

Two important remarks are in order. First, the semiclassical approach only incorporates single band effects and thus $\mathcal{F}^{\mu\nu}$ is an Abelian $U(1)$ curvature and we need not trace over its components. This yields an isotropic magnetoelectric effect in our semiclassical treatment, which neglects terms resulting from cross-gap contributions, which vanish as $1/\Delta$ [223]. Second, the current generated by finite deformations is well defined since it is the integral of the second Chern-form. The Chern-Simons three-form is only gauge-invariant if integrated over a closed manyfold, so it does not correspond to a measurable quantity in metals; the static polarization is ill defined in metals.

Finally, the third term, α_2^{ij}, is a novel Fermi surface contribution that is unique to metals. It is the correction to the piezoelectric response at linear order in the magnetic field due to the orbital moment of the Bloch states. In what follows, we estimate the magnitude of all three terms contributing to the current to find that the Fermi surface contribution dominates the response.

8.3 Experimental feasibility

An estimate of the observability of the current in Eq. (8.10) relies on the magnitude of the Berry curvature $\mathcal{F}^{\mu\nu}$, which is common to all its terms. We distinguish two contributions to $\mathcal{F}^{\mu\nu}$ of distinct physical origin: the purely spatial part $\mathcal{F}^{ij}$ and the mixed $\mathcal{F}^{i\theta}$ terms. The former defines the Hall conductivity $\sigma_{ij} = C_{ij}e^2/h$ in the (i,j) plane through the Chern number $C_{ij} = \frac{1}{2\pi}\int d^2k\mathcal{F}^{ij}$. Since C_{ij} is of the order of unity [13] or higher [224, 225], we expect $\mathcal{F}^{ij} \gtrsim \frac{a^2}{2\pi}$ where we estimate the cross sectional area of the unit cell in the (i,j) plane using the lattice spacing a. To estimate $\mathcal{F}^{i\theta}$ we use previously known facts about the piezoelectric effect. Identifying θ with a specific strain component ϵ^{jk} ($\theta = \epsilon^{jk}$), the piezoelectric constant reads [185]

$$\beta^i_{jk} = \frac{\partial P^i}{\partial \epsilon^{jk}} = -e\int_{\text{occ.}} \frac{d^3k}{(2\pi)^3}\mathcal{F}^{i\theta}. \tag{8.14}$$

This formula only contains the electronic (clamped ion) contribution to the polarization response, typically smaller than the dominant contribution from the rearrangement of the ions. The electronic contribution can nonetheless be accessed independently in *ab initio* calculations that estimate $\beta^i \sim 1\,\mathrm{C/m^2}$ [226] (suppressing the strain component indices for clarity). It follows that $\mathcal{F}^{i\theta} \sim \beta^i\,\frac{a^3}{e}$ using the inverse cube of the lattice spacing as an approximate volume of the Fermi sea.

From the above estimate of the piezoelectric effect we now can now approximate the magnitude of the remaining terms in Eq. (8.10), $\alpha^{ij}_{1,2}$ given by Eqs. (8.12) and (8.13) that are novel to this work. The magnitude of the Fermi sea contribution α_1 amounts to

$$\alpha_1 \sim \frac{e}{\hbar}a^2 C_{ij}\beta^k, \tag{8.15}$$

for a particular set of $i \neq j \neq k$ and neglecting the order one factor arising from the difference between a Fermi sea integral and a Brillouin zone integral. Inserting $\beta^k \sim 1\,\mathrm{C/m^2}$, $a \sim 10^{-10}\mathrm{m}$, $C_{ij} = 1$ we get $\alpha_1 \sim 10^{-5}\frac{\mathrm{A\,s}}{\mathrm{T\,m^2}}$.

The estimate of the magnitude of the Fermi surface term α_2, unique to metals, requires the magnitude of the orbital magnetic moment $|\mathbf{m}|$. A conservative estimate results in $|\mathbf{m}| \sim \mu_B \sim 10^{-23}\mathrm{J/T}$ where μ_B is the Bohr magneton but it can be as large as $|\mathbf{m}| \sim 30\mu_B$ [194]. The area of the Fermi surface can be estimated as $1/a^2$, the cross section of the BZ which is the inverse of the cross section of the real space unit cell. Taking $v_F \sim 10^6\mathrm{m/s}$, which is typical for metals but can be significantly smaller for lightly doped insulators near the band bottom, and using our above estimate for $\mathcal{F}^{i\theta}$ we obtain

$$\alpha_2 \sim \frac{\beta^i m^j a}{\hbar v_F} \sim 10^{-4}\frac{\mathrm{A\,s}}{\mathrm{T\,m^2}}. \tag{8.16}$$

Therefore we conclude that $\alpha_2 \gtrsim \alpha_1$, and the Fermi surface contribution specific to metallic systems is dominant.

In addition, it is relevant to emphasize the following important points regarding experimental detection. Firstly strain rates at the order of $10^{-2}\mathrm{s}^{-1}$ are achievable in the elastic regime using ultrasonic techniques [227, 228]. For a sample at the cm scale, with cross sectional area $A_s \sim 10^{-4}\mathrm{m}^2$ and a magnetic field of 1T [3], the current signal is of the order of $I_i = A_s j_i \sim 100$ pA. Conventional ammeters have sensitivity extending to the pA range that is further improved in SQUID devices.

Second, the magnetopiezoelectric effect is expected to coexist with the piezoelectric contribution, so accurate measurements over a range of magnetic fields are necessary for its detection. In our estimates α_2 is proportional to and much smaller than β. However, β gets contributions from the entire Fermi sea, while α_2 only depends on Fermi surface properties. This allows suppression of β without changing α_2 in appropriately engineered band structures.

Third, the movement of the ions and the polarization of electrons in the valence bands induces a bound surface charge density. Part of the bulk current can be trapped screening it, possibly preventing its detection in our proposed setup (Fig. 8.1), but there is no reason to expect full cancellation. We note as well that pumping DC current is also possible by out-of-phase modulation of different strain components. Such a deformation path encircles a finite area in parameter space; the integral of the current for a pumping cycle is in general a non-vanishing, non-quantized value.

Finally, from the materials perspective we find that MnSi satisfies most requirements for these effects to manifest. It is a magnetically ordered, inversion breaking metal with complex Berry curvature patterns in the conduction bands that is very susceptible to strain [229–232]. The magnetic order, however, is incommensurate and very sensitive to external magnetic field. An ideal candidate material would have simple easy axis ferromagnetic or Néel order that has vanishing susceptibility for magnetic fields in the ordering direction in the low temperature limit. The recently studied polar metals [192, 193], while non-magnetic, would provide a platform to realize the field-independent piezoelectric response β. Cold-atomic systems also offer an alternative; the current is related to an easily accesible observable, the center-of-mass velocity $\mathbf{v}_{c.m.}$ through $\mathbf{v}_{c.m.} = \mathbf{j}/n$ where n is the density of the atomic cloud. Recently, $\mathbf{v}_{c.m.}$ has been exploited as a probe of topological properties [233] and it is therefore plausible that the effects we discuss here can be observed in these systems as well.

[3] The semiclassical approach is applicable if $\hbar\mathcal{F}_c = \hbar eB/m \ll \min(h/\tau_{MF}, k_B T)$ where $\tau_{MF} = l/v_F$ is the mean free time between scattering events and l is the average distance between impurities. For $B = 1$T the Landau level splitting is $\hbar\mathcal{F}_c \sim 7.27 \times 10^{-4}$eV, a broadening similar to that achieved at a temperature of $T = 8.44$K. Assuming a relatively pure material with $l \sim 10^{-7}$m with $v_F \sim 10^6$m/s, the broadening from scattering is $h/\tau_{MF} \sim 10^{-2}$eV, which is two orders of magnitude larger than $\hbar\mathcal{F}_c$, establishing the applicability of our approach.

8.4 Conclusion

We have calculated a novel magnetopiezoelectric response in inversion and time reversal breaking metals subjected to static magnetic field and dynamic strain. Similar to the anomalous Hall effect in metals which can be viewed as a generalization of the quantized anomalous Hall effect in insulators, our results for magnetopiezoelectricity generalize the magnetoelectric response of insulators to metals. As a key difference, we find an additional Fermi surface contribution that relies on a finite orbital moment of the electrons, that is unique to metals and likely dominates the effect in real systems.

8.5 Acknowledgements

The author thanks Adolfo G. Grushin, Roni Ilan and Joel E. Moore for the collaboration on this project. We are grateful to Fernando de Juan and Hannah Price for enlightening discussions and correspondence. We acknowledge financial support from the Marie Curie Programme under EC Grant agreement No. 653846. (A.G.G.), NSF Grant No. DMR-1507141 (D.V.), AFOSR MURI (R.I.), and the Quantum Materials program of LBNL (J.E.M.). JEM acknowledges travel support from the Simons Center for Geometry and Physics and a Simons Investigatorship.

Appendix

8.A Vanishing of j_c^i

In this section we prove that j_c^i, defined as

$$j_c^i = e \int_{\mathbb{T}^3} \frac{\mathrm{d}^3 k}{(2\pi)^3} \frac{1}{2} \frac{e}{\hbar^2} \left(\epsilon_{lmn} \tilde{\mathcal{F}}^{lm} \frac{\partial \tilde{\mathcal{E}}}{\partial k_n} \right) B_i f(\tilde{\mathcal{E}}_{\mathbf{k},\theta}, \mu) \,,$$

in the main text is zero. The last term, corresponding to j_c^z, can be integrated by parts to give

$$j_c^i = \frac{1}{2} \frac{e}{\hbar^2} \int_{\mathbb{T}^3} \frac{\mathrm{d}^3 k}{(2\pi)^3} \left[-\tilde{\mathcal{E}} \left(\epsilon_{lmn} \frac{\partial \tilde{\mathcal{F}}^{lm}}{\partial k_n} \right) f(\tilde{\mathcal{E}}_{\mathbf{k},\theta}, \mu) - \tilde{\mathcal{E}} \left(\epsilon_{lmn} \tilde{\mathcal{F}}^{lm} \frac{\partial f(\tilde{\mathcal{E}}_{\mathbf{k},\theta}, \mu)}{\partial k_n} \right) \right] B_i \qquad (8.17)$$

The first term is the divergence of the Berry field strength and vanishes. The second term in the low temperature limit can be rewritten as the total the Berry flux over all Fermi surfaces, which vanishes as well. This results is consistent with the absence of the chiral magnetic effect in the static limit [70, 71].

Bibliography

[1] L. D. Landau and E. M. Lifshitz. *Statistical physics. Pt.1, Pt.2.* 1980.

[2] K. V. Klitzing, G. Dorda, and M. Pepper. "New Method for High-Accuracy Determination of the Fine-Structure Constant Based on Quantized Hall Resistance". In: *Physical Review Letters* 45 (1980), pp. 494–497.

[3] R. B. Laughlin. "Quantized Hall conductivity in two dimensions". In: *Phys. Rev. B* 23 (1981), pp. 5632–5633.

[4] F. D. M. Haldane. "Model for a Quantum Hall Effect without Landau Levels: Condensed-Matter Realization of the "Parity Anomaly"". In: *Phys. Rev. Lett.* 61 (1988), pp. 2015–2018.

[5] D. J. Thouless et al. "Quantized Hall Conductance in a Two-Dimensional Periodic Potential". In: *Phys. Rev. Lett.* 49.6 (1982), pp. 405–408.

[6] D. C. Tsui, H. L. Stormer, and A. C. Gossard. "Two-Dimensional Magnetotransport in the Extreme Quantum Limit". In: *Physical Review Letters* 48 (1982), pp. 1559–1562.

[7] R. B. Laughlin. "Anomalous Quantum Hall Effect: An Incompressible Quantum Fluid with Fractionally Charged Excitations". In: *Phys. Rev. Lett.* 50 (1983), pp. 1395–1398.

[8] X. Chen et al. "Symmetry protected topological orders and the group cohomology of their symmetry group". In: *Phys. Rev. B* 87.15, 155114 (2013), p. 155114.

[9] J. E. Moore and L. Balents. "Topological invariants of time-reversal-invariant band structures". In: *Phys. Rev. B* 75.12, 121306 (2007), p. 121306.

[10] J. C. Y. Teo, L. Fu, and C. L. Kane. "Surface states and topological invariants in three-dimensional topological insulators: Application to $Bi_{1-x}Sb_x$". In: *Phys. Rev. B* 78.4, 045426 (2008), p. 045426.

[11] A. Kitaev. "Periodic table for topological insulators and superconductors". In: *American Institute of Physics Conference Series*. Ed. by V. Lebedev and M. Feigel'Man. Vol. 1134. American Institute of Physics Conference Series. 2009, pp. 22–30.

[12] J. E. Avron, R. Seiler, and B. Simon. "Homotopy and Quantization in Condensed Matter Physics". In: *Phys. Rev. Lett.* 51 (1983), p. 51.

[13] Cui-Zu Chang et al. "Experimental Observation of the Quantum Anomalous Hall Effect in a Magnetic Topological Insulator". In: *Science* 340.6129 (2013), pp. 167–170.

[14] Y.-M. Lu and D.-H. Lee. "Inversion symmetry protected topological insulators and superconductors". In: *ArXiv preprint arXiv:1403.5558* (2014).

[15] Andreas P. Schnyder et al. "Classification of topological insulators and superconductors in three spatial dimensions". In: *Phys. Rev. B* 78 (2008), p. 195125.

[16] A. Altland and M. R. Zirnbauer. "Nonstandard symmetry classes in mesoscopic normal-superconducting hybrid structures". In: *Phys. Rev. B* 55 (1997), pp. 1142–1161.

[17] B. Andrei Bernevig and Shou-Cheng Zhang. "Quantum Spin Hall Effect". In: *Phys. Rev. Lett.* 96 (2006), p. 106802.

[18] C. L. Kane and E. J. Mele. "Z_2 Topological Order and the Quantum Spin Hall Effect". In: *Physical Review Letters* 95.14, 146802 (2005), p. 146802.

[19] B. Andrei Bernevig, Taylor L. Hughes, and Shou-Cheng Zhang. "Quantum Spin Hall Effect and Topological Phase Transition in HgTe Quantum Wells". In: *Science* 314.5806 (2006), pp. 1757–1761.

[20] Xiao-Liang Qi, Taylor L. Hughes, and Shou-Cheng Zhang. "Topological field theory of time-reversal invariant insulators". In: *Phys. Rev. B* 78.19 (2008), pp. 195424–.

[21] Shinsei Ryu, Joel E. Moore, and Andreas W. W. Ludwig. "Electromagnetic and gravitational responses and anomalies in topological insulators and superconductors". In: *Phys. Rev. B* 85.4 (2012), pp. 045104–.

[22] Lukasz Fidkowski and Alexei Kitaev. "Effects of interactions on the topological classification of free fermion systems". In: *Phys. Rev. B* 81 (2010), p. 134509.

[23] R. Queiroz, E. Khalaf, and A. Stern. "Classification of interacting fermionic phases by dimensional reduction". In: *ArXiv preprint arXiv:1601.01596* (2016).

[24] Markus König et al. "Quantum Spin Hall Insulator State in HgTe Quantum Wells". In: *Science* 318.5851 (2007), pp. 766–770.

[25] Y. Xia et al. "Observation of a large-gap topological-insulator class with a single Dirac cone on the surface". In: *Nature Physics* 5 (2009), pp. 398–402.

[26] Y. L. Chen et al. "Experimental Realization of a Three-Dimensional Topological Insulator, Bi2Te3". In: *Science* 325.5937 (2009), pp. 178–181.

[27] Andrew M. Essin, Joel E. Moore, and David Vanderbilt. "Magnetoelectric Polarizability and Axion Electrodynamics in Crystalline Insulators". In: *Phys. Rev. Lett.* 102.14 (2009), pp. 146805–.

[28] Liang Fu. "Topological Crystalline Insulators". In: *Phys. Rev. Lett.* 106.10 (2011), pp. 106802–.

[29] Y. Ando and L. Fu. "Topological Crystalline Insulators and Topological Superconductors: From Concepts to Materials". In: *Annual Review of Condensed Matter Physics* 6 (2015), pp. 361–381.

[30] A. Alexandradinata, Xi Dai, and B. Andrei Bernevig. "Wilson-loop characterization of inversion-symmetric topological insulators". In: *Phys. Rev. B* 89 (2014), p. 155114.

[31] Chen Fang, Matthew J. Gilbert, and B. Andrei Bernevig. "Bulk topological invariants in noninteracting point group symmetric insulators". In: *Phys. Rev. B* 86 (2012), p. 115112.

[32] A. Alexandradinata et al. "Spin-Orbit-Free Topological Insulators without Time-Reversal Symmetry". In: *Physical Review Letters* 113.11, 116403 (2014), p. 116403.

[33] Taylor L. Hughes, Emil Prodan, and B. Andrei Bernevig. "Inversion-symmetric topological insulators". In: *Phys. Rev. B* 83.24 (2011), pp. 245132–.

[34] J. C. Y. Teo and T. L. Hughes. "Existence of Majorana-Fermion Bound States on Disclinations and the Classification of Topological Crystalline Superconductors in Two Dimensions". In: *Physical Review Letters* 111.4, 047006 (2013), p. 047006.

[35] R.-J. Slager et al. "The space group classification of topological band-insulators". In: *Nature Physics* 9 (2013), pp. 98–102.

[36] C.-K. Chiu, H. Yao, and S. Ryu. "Classification of topological insulators and superconductors in the presence of reflection symmetry". In: *Phys. Rev. B* 88.7, 075142 (2013), p. 075142.

[37] T. Morimoto and A. Furusaki. "Topological classification with additional symmetries from Clifford algebras". In: *Phys. Rev. B* 88.12, 125129 (2013), p. 125129.

[38] Priyamvada Jadaun et al. "Topological classification of crystalline insulators with space group symmetry". In: *Physical Review B* 88.8 (2013), p. 085110.

[39] Wladimir A. Benalcazar, Jeffrey C. Y. Teo, and Taylor L. Hughes. "Classification of two-dimensional topological crystalline superconductors and Majorana bound states at disclinations". In: *Phys. Rev. B* 89 (2014), p. 224503.

[40] C. Fang and L. Fu. "New classes of three-dimensional topological crystalline insulators: Nonsymmorphic and magnetic". In: *Phys. Rev. B* 91.16, 161105 (2015), p. 161105.

[41] K. Shiozaki and M. Sato. "Topology of crystalline insulators and superconductors". In: *Phys. Rev. B* 90.16, 165114 (2014), p. 165114.

[42] K. Shiozaki, M. Sato, and K. Gomi. "Z_2 topology in nonsymmorphic crystalline insulators: Möbius twist in surface states". In: *Phys. Rev. B* 91.15, 155120 (2015), p. 155120.

[43] K. Shiozaki, M. Sato, and K. Gomi. "Topology of nonsymmorphic crystalline insulators and superconductors". In: *Phys. Rev. B* 93.19, 195413 (2016), p. 195413.

[44] R. S. K. Mong, A. M. Essin, and J. E. Moore. "Antiferromagnetic topological insulators". In: *Phys. Rev. B* 81.24, 245209 (2010), p. 245209.

[45] C.-X. Liu, R.-X. Zhang, and B. K. VanLeeuwen. "Topological nonsymmorphic crystalline insulators". In: *Phys. Rev. B* 90.8, 085304 (2014), p. 085304.

[46] Ari M. Turner et al. "Quantized response and topology of magnetic insulators with inversion symmetry". In: *Phys. Rev. B* 85.16 (2012), pp. 165120–.

[47] Z. Wang et al. "Hourglass fermions". In: *Nature* 532 (2016), pp. 189–194.

[48] Dániel Varjas, Fernando de Juan, and Yuan-Ming Lu. "Bulk invariants and topological response in insulators and superconductors with nonsymmorphic symmetries". In: *Phys. Rev. B* 92 (2015), p. 195116.

[49] D. Varjas, F. de Juan, and Y.-M. Lu. "Space group constraints on weak indices in topological insulators". In: *ArXiv preprint arXiv:1603.04450* (2016).

[50] H. Watanabe et al. "Lieb-Schultz-Mattis theorems in the presence of spin-orbit coupling: filling constraints for insulators in symmorphic and non-symmorphic crystals". In: *ArXiv preprint arXiv:1505.04193* (2015).

[51] H. Watanabe et al. "Filling constraints for spin-orbit coupled insulators in symmorphic and nonsymmorphic crystals". In: *Proceedings of the National Academy of Science* 112 (2015), pp. 14551–14556.

[52] H. C. Po et al. "Filling-enforced quantum band insulators in spin-orbit coupled crystals". In: *Science Advances* 2 (2016), e1501782–e1501782.

[53] Q.-Z. Wang and C.-X. Liu. "Topological nonsymmorphic crystalline superconductors". In: *Phys. Rev. B* 93.2, 020505 (2016), p. 020505.

[54] Hao Song et al. "Topological phases protected by point group symmetry". In: *arXiv preprint arXiv:1604.08151* (2016).

[55] Roger S. K. Mong, Jens H. Bardarson, and Joel E. Moore. "Quantum Transport and Two-Parameter Scaling at the Surface of a Weak Topological Insulator". In: *Phys. Rev. Lett.* 108 (2012), p. 076804.

[56] Zohar Ringel, Yaacov E. Kraus, and Ady Stern. "Strong side of weak topological insulators". In: *Phys. Rev. B* 86 (2012), p. 045102.

[57] Yukinori Yoshimura et al. "Perfectly conducting channel on the dark surface of weak topological insulators". In: *Phys. Rev. B* 88 (2013), p. 045408.

[58] Takahiro Morimoto and Akira Furusaki. "Stability of surface states of weak $\mathbb{Z}_2$ topological insulators and superconductors". In: *Phys. Rev. B* 89 (2014), p. 035117.

[59] David F. Mross et al. "Anomalous Quasiparticle Symmetries and Non-Abelian Defects on Symmetrically Gapped Surfaces of Weak Topological Insulators". In: *Phys. Rev. Lett.* 116 (2016), p. 036803.

[60] Y. Ran, Y. Zhang, and A. Vishwanath. "One-dimensional topologically protected modes in topological insulators with lattice dislocations". In: *Nature Physics* 5 (2009), pp. 298–303.

[61] Ying Ran. "Weak indices and dislocations in general topological band structures". In: *arXiv preprint arXiv:1006.5454* (2010).

[62] Robert-Jan Slager et al. "Interplay between electronic topology and crystal symmetry: Dislocation-line modes in topological band insulators". In: *Phys. Rev. B* 90 (2014), p. 241403.

[63] I. C. Fulga et al. "Coupled-layer description of topological crystalline insulators". In: *ArXiv preprint arXiv:1605.00652* (2016).

[64] Shunji Matsuura et al. "Protected boundary states in gapless topological phases". In: *New Journal of Physics* 15.6 (2013), p. 065001.

[65] Xiangang Wan et al. "Topological semimetal and Fermi-arc surface states in the electronic structure of pyrochlore iridates". In: *Physical Review B* 83.20 (2011), p. 205101.

[66] Su-Yang Xu et al. "Discovery of a Weyl fermion semimetal and topological Fermi arcs". In: *Science* 349.6248 (2015), pp. 613–617.

[67] BQ Lv et al. "Experimental discovery of Weyl semimetal TaAs". In: *Physical Review X* 5.3 (2015), p. 031013.

[68] Hongming Weng et al. "Weyl semimetal phase in noncentrosymmetric transition-metal monophosphides". In: *Physical Review X* 5.1 (2015), p. 011029.

[69] Andrew C Potter, Itamar Kimchi, and Ashvin Vishwanath. "Quantum oscillations from surface Fermi arcs in Weyl and Dirac semimetals". In: *Nature communications* 5 (2014).

[70] Jing Ma and D. A. Pesin. "Chiral magnetic effect and natural optical activity in metals with or without Weyl points". In: *Phys. Rev. B* 92 (2015), p. 235205.

[71] Shudan Zhong, Joel E. Moore, and Ivo Souza. "Gyrotropic Magnetic Effect and the Magnetic Moment on the Fermi Surface". In: *Phys. Rev. Lett.* 116 (2016), p. 077201.

[72] DT Son and BZ Spivak. "Chiral anomaly and classical negative magnetoresistance of Weyl metals". In: *Physical Review B* 88.10 (2013), p. 104412.

[73] Xiaochun Huang et al. "Observation of the chiral-anomaly-induced negative magnetoresistance in 3D Weyl semimetal TaAs". In: *Physical Review X* 5.3 (2015), p. 031023.

[74] F. D. M. Haldane. "Fractional Quantization of the Hall Effect: A Hierarchy of Incompressible Quantum Fluid States". In: *Phys. Rev. Lett.* 51 (1983), pp. 605–608.

[75] Jainendra K Jain. "Composite-fermion approach for the fractional quantum Hall effect". In: *Physical review letters* 63.2 (1989), p. 199.

[76] Ana Lopez and Eduardo Fradkin. "Fractional quantum Hall effect and Chern-Simons gauge theories". In: *Phys. Rev. B* 44 (1991), pp. 5246–5262.

[77] X. G. Wen. "Topological orders and edge excitations in fractional quantum hall states". In: *Field Theory, Topology and Condensed Matter Physics*. Ed. by HendrikB. Geyer. Vol. 456. Lecture Notes in Physics. Springer Berlin Heidelberg, 1995, pp. 155–176.

[78] G. Moore and N. Read. "Nonabelions in the fractional quantum hall effect". In: *Nuclear Physics B* 360 (1991), pp. 362–396.

[79] A. M. Chang, L. N. Pfeiffer, and K. W. West. "Observation of Chiral Luttinger Behavior in Electron Tunneling into Fractional Quantum Hall Edges". In: *Phys. Rev. Lett.* 77 (1996), pp. 2538–2541.

[80] W. Kang et al. "Tunnelling between the edges of two lateral quantum Hall systems". In: *Nature* 403.6765 (2000), pp. 59–61.

[81] C. L. Kane and Matthew P. A. Fisher. "Nonequilibrium noise and fractional charge in the quantum Hall effect". In: *Phys. Rev. Lett.* 72 (1994), pp. 724–727.

[82] R. de Picciotto et al. "Direct observation of a fractional charge". In: *Nature* 389 (1997), pp. 162–164.

[83] L. Saminadayar et al. "Observation of the $e/3$ Fractionally Charged Laughlin Quasiparticle". In: *Phys. Rev. Lett.* 79 (1997), pp. 2526–2529.

[84] R Walter Ogburn and John Preskill. "Topological quantum computation". In: *Quantum Computing and Quantum Communications*. Springer, 1999, pp. 341–356.

[85] Michael Freedman et al. "Topological quantum computation". In: *Bulletin of the American Mathematical Society* 40.1 (2003), pp. 31–38.

[86] C. Nayak et al. "Non-Abelian anyons and topological quantum computation". In: *Reviews of Modern Physics* 80 (2008), pp. 1083–1159.

[87] A Yu Kitaev. "Unpaired Majorana fermions in quantum wires". In: *Physics-Uspekhi* 44.10S (2001), p. 131.

[88] Yuval Oreg, Gil Refael, and Felix von Oppen. "Helical liquids and Majorana bound states in quantum wires". In: *Physical review letters* 105.17 (2010), p. 177002.

[89] Vincent Mourik et al. "Signatures of Majorana fermions in hybrid superconductor-semiconductor nanowire devices". In: *Science* 336.6084 (2012), pp. 1003–1007.

[90] Jason Alicea et al. "Non-Abelian statistics and topological quantum information processing in 1D wire networks". In: *Nature Physics* 7.5 (2011), pp. 412–417.

[91] A. C. Potter and A. Vishwanath. "Protection of topological order by symmetry and many-body localization". In: *ArXiv e-prints arXiv:1506.00592* (2015).

[92] D. Varjas, M. P. Zaletel, and J. E. Moore. "Chiral Luttinger liquids and a generalized Luttinger theorem in fractional quantum Hall edges via finite-entanglement scaling". In: *Phys. Rev. B* 88.15, 155314 (2013), p. 155314.

[93] D. Varjas et al. "Dynamical piezoelectric and magnetopiezoelectric effects in polar metals from Berry phases and orbital moments". In: *ArXiv e-prints arXiv:1607.05278* (2016).

[94] J.M. Leinaas and J. Myrheim. "On the theory of identical particles". English. In: *Il Nuovo Cimento B Series 11* 37.1 (1977), pp. 1–23.

[95] D. C. Glattli et al. "Dynamical Hall Effect in a Two-Dimensional Classical Plasma". In: *Phys. Rev. Lett.* 54 (1985), pp. 1710–1713.

[96] Yaron Gross et al. "Upstream Neutral Modes in the Fractional Quantum Hall Effect Regime: Heat Waves or Coherent Dipoles". In: *Phys. Rev. Lett.* 108 (2012), p. 226801.

[97] N. Goldman et al. "Direct imaging of topological edge states in cold-atom systems". In: *Proceedings of the National Academy of Sciences* 110.17 (2013), pp. 6736–6741.

[98] C. de C. Chamon and X. G. Wen. "Sharp and smooth boundaries of quantum Hall liquids". In: *Phys. Rev. B* 49 (1994), pp. 8227–8241.

[99] X. G. Wen. "Chiral Luttinger liquid and the edge excitations in the fractional quantum Hall states". In: *Phys. Rev. B* 41 (1990), pp. 12838–12844.

[100] J. M. Luttinger. "Fermi Surface and Some Simple Equilibrium Properties of a System of Interacting Fermions". In: *Phys. Rev.* 119 (1960), pp. 1153–1163.

[101] Kiaran B. Dave, Philip W. Phillips, and Charles L. Kane. "Absence of Luttinger's Theorem due to Zeros in the Single-Particle Green Function". In: *Phys. Rev. Lett.* 110 (2013), p. 090403.

[102] F. D. M. Haldane. "Luttinger's Theorem and Bosonization of the Fermi Surface". In: *ArXiv eprints arXiv:cond-mat/0505529* (2005).

[103] F. D. M. Haldane. ""Hall viscosity" and intrinsic metric of incompressible fractional Hall fluids". In: *ArXiv e-prints arXiv:0906.1854* (2009).

[104] Elliott Lieb, Theodore Schultz, and Daniel Mattis. "Two soluble models of an antiferromagnetic chain". In: *Annals of Physics* 16.3 (1961), pp. 407 –466.

[105] Masanori Yamanaka, Masaki Oshikawa, and Ian Affleck. "Nonperturbative Approach to Luttinger's Theorem in One Dimension". In: *Phys. Rev. Lett.* 79 (1997), pp. 1110–1113.

[106] Steven R. White. "Density matrix formulation for quantum renormalization groups". In: *Phys. Rev. Lett.* 69.19 (1992), pp. 2863–2866.

[107] I. P. McCulloch. "Infinite size density matrix renormalization group, revisited". In: *ArXiv e-prints arXiv:0804.2509* (2008).

[108] Frank Pollmann et al. "Theory of Finite-Entanglement Scaling at One-Dimensional Quantum Critical Points". In: *Phys. Rev. Lett.* 102 (2009), p. 255701.

[109] C. Holzhey, F. Larsen, and F. Wilczek. "Geometric and renormalized entropy in conformal field-theory". In: *Nucl. Phys. B* 424 (1994), pp. 443–467.

[110] M. Zwolak and G. Vidal. "Mixed-State Dynamics in One-Dimensional Quantum Lattice Systems: A Time-Dependent Superoperator Renormalization Algorithm". In: *Phys. Rev. Lett.* 93 (2004), p. 207205.

[111] Pasquale Calabrese and John Cardy. "Entanglement entropy and quantum field theory". In: *Journal of Statistical Mechanics: Theory and Experiment* 2004.06 (2004), P06002.

[112] J. J. Palacios and A. H. MacDonald. "Numerical Tests of the Chiral Luttinger Liquid Theory for Fractional Hall Edges". In: *Phys. Rev. Lett.* 76 (1996), pp. 118–121.

[113] Sudhansu S. Mandal and J.K. Jain. "How universal is the fractional-quantum-Hall edge Luttinger liquid?" In: *Solid State Communications* 118.10 (2001), pp. 503 –507.

[114] U. Zülicke, J. J. Palacios, and A. H. MacDonald. "Fractional-quantum-Hall edge electrons and Fermi statistics". In: *Phys. Rev. B* 67 (2003), p. 045303.

[115] Xin Wan, E. H. Rezayi, and Kun Yang. "Edge reconstruction in the fractional quantum Hall regime". In: *Phys. Rev. B* 68 (2003), p. 125307.

[116] Shivakumar Jolad, Chia-Chen Chang, and Jainendra K. Jain. "Electron operator at the edge of the 1/3 fractional quantum Hall liquid". In: *Phys. Rev. B* 75 (2007), p. 165306.

[117] Zi-Xiang Hu et al. "Ground state and edge excitations of a quantum Hall liquid at filling factor 2/3". In: *Phys. Rev. B* 78 (2008), p. 235315.

[118] Shivakumar Jolad and Jainendra K. Jain. "Testing the Topological Nature of the Fractional Quantum Hall Edge". In: *Phys. Rev. Lett.* 102 (2009), p. 116801.

[119] Shivakumar Jolad, Diptiman Sen, and Jainendra K. Jain. "Fractional quantum Hall edge: Effect of nonlinear dispersion and edge roton". In: *Phys. Rev. B* 82 (2010), p. 075315.

[120] G. J. Sreejith et al. "Microscopic study of the $\frac{2}{5}$ fractional quantum Hall edge". In: *Phys. Rev. B* 84 (2011), p. 245104.

[121] A. Sterdyniak et al. "Real-space entanglement spectrum of quantum Hall states". In: *Phys. Rev. B* 85.12, 125308 (2012), p. 125308.

[122] N. Read. "Conformal invariance of chiral edge theories". In: *Phys. Rev. B* 79 (2009), p. 245304.

[123] Sudhansu S. Mandal and Jainendra K. Jain. "Relevance of Inter-Composite-Fermion Interaction to the Edge Tomonaga-Luttinger Liquid". In: *Phys. Rev. Lett.* 89 (2002), p. 096801.

[124] E. H. Rezayi and F. D. M. Haldane. "Laughlin state on stretched and squeezed cylinders and edge excitations in the quantum Hall effect". In: *Phys. Rev. B* 50 (1994), pp. 17199–17207.

[125] Emil J. Bergholtz and Anders Karlhede. "Half-Filled Lowest Landau Level on a Thin Torus". In: *Phys. Rev. Lett.* 94 (2005), p. 026802.

[126] Alexander Seidel et al. "Incompressible Quantum Liquids and New Conservation Laws". In: *Phys. Rev. Lett.* 95 (2005), p. 266405.

[127] Michael P. Zaletel, Roger S. K. Mong, and Frank Pollmann. "Topological Characterization of Fractional Quantum Hall Ground States from Microscopic Hamiltonians". In: *Phys. Rev. Lett.* 110 (2013), p. 236801.

[128] F. D. M. Haldane and E. H. Rezayi. "Spin-singlet wave function for the half-integral quantum Hall effect". In: *Phys. Rev. Lett.* 60 (1988), pp. 956–959.

[129] Naokazu Shibata and Daijiro Yoshioka. "Ground-State Phase Diagram of 2D Electrons in a High Landau Level: A Density-Matrix Renormalization Group Study". In: *Phys. Rev. Lett.* 86 (2001), pp. 5755–5758.

[130] E. J. Bergholtz and A. Karlhede. "Density Matrix Renormalization Group Study of a Lowest Landau Level Electron Gas on a Thin Cylinder". In: *ArXiv eprints arXiv:cond-mat/0304517* (2003).

[131] L. Tagliacozzo et al. "Scaling of entanglement support for matrix product states". In: *Phys. Rev. B* 78 (2008), p. 024410.

[132] B. Pirvu et al. "Matrix product states for critical spin chains: Finite-size versus finite-entanglement scaling". In: *Phys. Rev. B* 86 (2012), p. 075117.

[133] Jonas A. Kjäll et al. "Phase diagram of the anisotropic spin-2 XXZ model: Infinite-system density matrix renormalization group study". In: *Phys. Rev. B* 87 (2013), p. 235106.

[134] Joel E. Moore and X. G. Wen. "Classification of disordered phases of quantum Hall edge states". In: *Phys. Rev. B* 57 (1998), pp. 10138–10156.

[135] Paul Soulé and Thierry Jolicoeur. "Edge properties of principal fractional quantum Hall states in the cylinder geometry". In: *Phys. Rev. B* 86 (2012), p. 115214.

[136] S. E. Yang et al. "Momentum Distribution Function of a Narrow Hall Bar in the FQHE Regime". In: (2002).

[137] C. L. Kane, Matthew P. A. Fisher, and J. Polchinski. "Randomness at the edge: Theory of quantum Hall transport at filling $\nu = 2/3$". In: *Phys. Rev. Lett.* 72 (1994), pp. 4129–4132.

[138] C. L. Kane and Matthew P. A. Fisher. "Impurity scattering and transport of fractional quantum Hall edge states". In: *Phys. Rev. B* 51 (1995), pp. 13449–13466.

[139] C. de C. Chamon et al. "Two point-contact interferometer for quantum Hall systems". In: *Phys. Rev. B* 55 (1997), pp. 2331–2343.

[140] Ho N. Phien, Guifré Vidal, and Ian P. McCulloch. "Infinite boundary conditions for matrix product state calculations". In: *Phys. Rev. B* 86 (2012), p. 245107.

[141] Xin Wan, Kun Yang, and E. H. Rezayi. "Edge Excitations and Non-Abelian Statistics in the Moore-Read State: A Numerical Study in the Presence of Coulomb Interaction and Edge Confinement". In: *Phys. Rev. Lett.* 97 (2006), p. 256804.

[142] Xin Wan et al. "Fractional quantum Hall effect at $\nu = 5/2$: Ground states, non-Abelian quasiholes, and edge modes in a microscopic model". In: *Phys. Rev. B* 77 (2008), p. 165316.

[143] S. A. Parameswaran et al. "Topological order and absence of band insulators at integer filling in non-symmorphic crystals". In: *Nature Physics* 9 (2013), pp. 299–303.

[144] Raffaele Resta. "Manifestations of Berry's phase in molecules and condensed matter". In: *Journal of Physics: Condensed Matter* 12.9 (2000), R107.

[145] J. M. Luttinger. "The Effect of a Magnetic Field on Electrons in a Periodic Potential". In: *Phys. Rev.* 84 (1951), pp. 814–817.

[146] Mikio Nakahara. *Geometry, topology, and physics*. Graduate student series in physics. Bristol, Philadelphia: Institute of Physics Publishing, 2003.

[147] Shinsei Ryu et al. "Topological insulators and superconductors: tenfold way and dimensional hierarchy". In: *New Journal of Physics* 12.6 (2010), p. 065010.

[148] M. Z. Hasan and C. L. Kane. "Colloquium: Topological insulators". In: *Rev. Mod. Phys.* 82.4 (2010), pp. 3045–.

[149] M. Zahid Hasan and Joel E. Moore. "Three-Dimensional Topological Insulators". In: *Annu. Rev. Condens. Matter Phys.* 2.1 (2011), pp. 55–78.

[150] Xiao-Liang Qi and Shou-Cheng Zhang. "Topological insulators and superconductors". In: *Rev. Mod. Phys.* 83.4 (2011), pp. 1057–1110.

[151] Ying Ran. "Weak indices and dislocations in general topological band structures". In: *ArXiv e-prints 1006.5454* (2010).

[152] Liang Fu and C. L. Kane. "Topological insulators with inversion symmetry". In: *Phys. Rev. B* 76 (2007), p. 045302.

[153] Sinisa Coh and David Vanderbilt. "Electric Polarization in a Chern Insulator". In: *Phys. Rev. Lett.* 102 (2009), p. 107603.

[154] Timothy H Hsieh et al. "Topological crystalline insulators in the SnTe material class". In: *Nat. Commun.* 3 (2012), p. 982.

[155] G. P. Lepage. "A New Algorithm for Adaptive Multidimensional Integration". In: *Journal of Computational Physics* 27 (1978), p. 192.

[156] I. C. Fulga et al. "Statistical topological insulators". In: *Phys. Rev. B* 89.15, 155424 (2014), p. 155424.

[157] C. L. Kane and Matthew P. A. Fisher. "Thermal Transport in a Luttinger Liquid". In: *Phys. Rev. Lett.* 76.17 (1996), pp. 3192–3195.

[158] T. Senthil, J. B. Marston, and Matthew P. A. Fisher. "Spin quantum Hall effect in unconventional superconductors". In: *Phys. Rev. B* 60 (1999), pp. 4245–4254.

[159] N. Read and D. Green. "Paired states of fermions in two dimensions with breaking of parity and time-reversal symmetries and the fractional quantum Hall effect". In: *Phys. Rev. B* 61 (2000), p. 10267.

[160] J. C. Y. Teo and C. L. Kane. "Topological defects and gapless modes in insulators and superconductors". In: *Phys. Rev. B* 82.11, 115120 (2010), p. 115120.

[161] A. A. Soluyanov and D. Vanderbilt. "Computing topological invariants without inversion symmetry". In: *Phys. Rev. B* 83.23, 235401 (2011), p. 235401.

[162] Yang Qi and Liang Fu. "Anomalous Crystal Symmetry Fractionalization on the Surface of Topological Crystalline Insulators". In: *Phys. Rev. Lett.* 115 (2015), p. 236801.

[163] Bertold Rasche et al. "Stacked topological insulator built from bismuth-based graphene sheet analogues". In: *Nat. Mater.* 12.5 (2013), pp. 422–425.

[164] Binghai Yan, Lukas Müchler, and Claudia Felser. "Prediction of Weak Topological Insulators in Layered Semiconductors". In: *Phys. Rev. Lett.* 109 (2012), p. 116406.

[165] Peizhe Tang et al. "Weak topological insulators induced by the interlayer coupling: A first-principles study of stacked Bi_2TeI". In: *Phys. Rev. B* 89 (2014), p. 041409.

[166] Gang Yang et al. "Weak topological insulators in PbTe/SnTe superlattices". In: *Phys. Rev. B* 89 (2014), p. 085312.

[167] Cheng-Cheng Liu et al. "Weak Topological Insulators and Composite Weyl Semimetals: β-Bi_4X_4 (X = Br, I)". In: *Phys. Rev. Lett.* 116 (2016), p. 066801.

[168] Naoto Nagaosa et al. "Anomalous Hall effect". In: *Rev. Mod. Phys.* 82.2 (2010), pp. 1539–1592.

[169] Bertrand I. Halperin. "Possible States for a Three-Dimensional Electron Gas in a Strong Magnetic Field". In: *Japanese Journal of Applied Physics* 26.S3-3 (1987), p. 1913.

[170] P Streda. "Quantised Hall effect in a two-dimensional periodic potential". In: *Journal of Physics C: Solid State Physics* 15.36 (1982), p. L1299.

[171] Liang Fu, C. L. Kane, and E. J. Mele. "Topological Insulators in Three Dimensions". In: *Phys. Rev. Lett.* 98 (2007), p. 106803.

[172] H. Wondratschek and U. Müller. *International Tables for Crystallography, Volume A1.* 2008.

[173] M. I. Aroyo et al. "Bilbao Crystallographic Server: I. Databases and crystallographic computing programs". In: *Zeitschrift fur Kristallographie* 221 (2006), pp. 15–27.

[174] Mois I. Aroyo et al. "Brillouin-zone database on the *Bilbao Crystallographic Server*". In: *Acta Crystallographica Section A* 70.2 (2014), pp. 126–137.

[175] Fernando de Juan, Andreas Rüegg, and Dung-Hai Lee. "Bulk-defect correspondence in particle-hole symmetric insulators and semimetals". In: *Phys. Rev. B* 89 (2014), p. 161117.

[176] J. E. Moore, Y. Ran, and X.-G. Wen. "Topological Surface States in Three-Dimensional Magnetic Insulators". In: *Physical Review Letters* 101.18, 186805 (2008), p. 186805.

[177] Eric Yue Ma et al. "Mobile metallic domain walls in an all-in-all-out magnetic insulator". In: *Science* 350.6260 (2015), pp. 538–541.

[178] Youhei Yamaji and Masatoshi Imada. "Metallic interface emerging at magnetic domain wall of antiferromagnetic insulator: Fate of extinct Weyl electrons". In: *Physical Review X* 4.2 (2014), p. 021035.

[179] Joshua Zak. *The irreducible representations of space groups*. WA Benjamin Advanced Book Program, 1969.

[180] J. Zak. "Topologically unavoidable points and lines of crossings in the band structure of solids". In: *Journal of Physics A Mathematical General* 35 (2002), pp. 6509–6516.

[181] L. Michel and J. Zak. "Connectivity of energy bands in crystals". In: *Phys. Rev. B* 59 (1999), pp. 5998–6001.

[182] Conyers Herring. "Effect of time-reversal symmetry on energy bands of crystals". In: *Physical Review* 52.4 (1937), p. 361.

[183] L. D. Landau and E. M. Lifshitz. *Electrodynamics of continuous media*. 1960.

[184] Anja König and N David Mermin. "Electronic level degeneracy in nonsymmorphic periodic or aperiodic crystals". In: *Physical Review B* 56.21 (1997), p. 13607.

[185] Raffaele Resta and David Vanderbilt. "Physics of Ferroelectrics: A Modern Perspective". In: Berlin, Heidelberg: Springer Berlin Heidelberg, 2007. Chap. Theory of Polarization: A Modern Approach, pp. 31–68.

[186] D. J. Thouless. "Quantization of particle transport". In: *Phys. Rev. B* 27 (1983), pp. 6083–6087.

[187] R. D. King-Smith and D. Vanderbilt. "Theory of polarization of crystalline solids". In: *Phys. Rev. B* 47 (1993), p. 1651.

[188] F. D. M. Haldane. "Berry Curvature on the Fermi Surface: Anomalous Hall Effect as a Topological Fermi-Liquid Property". In: *Phys. Rev. Lett.* 93 (2004), p. 206602.

[189] M. Dawber, K. M. Rabe, and J. F. Scott. "Physics of thin-film ferroelectric oxides". In: *Rev. Mod. Phys.* 77 (2005), pp. 1083–1130.

[190] Karin M. Rabe et al. "Modern Physics of Ferroelectrics: Essential Background". In: *Physics of Ferroelectrics: A Modern Perspective*. Berlin, Heidelberg: Springer Berlin Heidelberg, 2007, pp. 1–30.

[191] P. W. Anderson and E. I. Blount. "Symmetry Considerations on Martensitic Transformations: "Ferroelectric" Metals?" In: *Phys. Rev. Lett.* 14 (1965), pp. 217–219.

[192] Youguo Shi et al. "A ferroelectric-like structural transition in a metal". In: *Nat Mater* 12.11 (2013), pp. 1024–1027.

[193] TH Kim et al. "Polar metals by geometric design". In: *Nature* 533.7601 (2016), pp. 68–72.

[194] Di Xiao, Ming-Che Chang, and Qian Niu. "Berry phase effects on electronic properties". In: *Rev. Mod. Phys.* 82 (2010), pp. 1959–2007.

[195] G. Sundaram and Q. Niu. "Wave-packet dynamics in slowly perturbed crystals: Gradient corrections and Berry-phase effects". In: *Phys. Rev. B* 59 (1999), p. 14915.

[196] J. Dahlhaus et al. "Pumping conductance, the intrinsic anomalous Hall effect, and statistics of topological invariants". In: *Phys. Rev. B* 91.24, 245107 (2015), p. 245107.

[197] Ari M Turner and Ashvin Vishwanath. "Beyond Band Insulators: Topology of Semimetals and Interacting Phases". In: *ArXiv preprints arXiv:1301.0330* ().

[198] Pavan Hosur and Xiaoliang Qi. "Recent developments in transport phenomena in Weyl semimetals". In: *C. R. Phys.* 14.910 (2013), pp. 857–870.

[199] Kenji Fukushima, Dmitri E. Kharzeev, and Harmen J. Warringa. "Chiral magnetic effect". In: *Phys. Rev. D* 78 (2008), p. 074033.

[200] Dmitri E. Kharzeev. "The Chiral Magnetic Effect and anomaly-induced transport". In: *Progress in Particle and Nuclear Physics* 75 (2014), pp. 133 –151.

[201] Vivek Aji. "Adler-Bell-Jackiw anomaly in Weyl semimetals: Application to pyrochlore iridates". In: *Phys. Rev. B* 85 (2012), p. 241101.

[202] AA Zyuzin and AA Burkov. "Topological response in Weyl semimetals and the chiral anomaly". In: *Physical Review B* 86.11 (2012), p. 115133.

[203] Adolfo G. Grushin. "Consequences of a condensed matter realization of Lorentz-violating QED in Weyl semi-metals". In: *Phys. Rev. D* 86 (2012), p. 045001.

[204] Pallab Goswami and Sumanta Tewari. "Chiral magnetic effect of Weyl fermions and its applications to cubic noncentrosymmetric metals". In: *arXiv preprint arXiv:1311.1506* (2013).

[205] M. M. Vazifeh and M. Franz. "Electromagnetic Response of Weyl Semimetals". In: *Phys. Rev. Lett.* 111 (2013), p. 027201.

[206] Ming-Che Chang and Min-Fong Yang. "Chiral magnetic effect in a two-band lattice model of Weyl semimetal". In: *Physical Review B* 91.11 (2015), p. 115203.

[207] David Vanderbilt. "Berry-phase theory of proper piezoelectric response". In: *Journal of Physics and Chemistry of Solids* 61.2 (2000), pp. 147–151.

[208] Raffaele Resta. "Macroscopic polarization in crystalline dielectrics: the geometric phase approach". In: *Rev. Mod. Phys.* 66 (1994), pp. 899–915.

[209] A. Cortijo et al. "Strain induced Chiral Magnetic Effect in Weyl semimetals". In: *ArXiv e-prints arXiv:1607.03491* (2016).

[210] A. M. Essin, J. E. Moore, and D. Vanderbilt. "Magnetoelectric Polarizability and Axion Electrodynamics in Crystalline Insulators". In: *Physical Review Letters* 102.14, 146805 (2009), p. 146805.

[211] A. Malashevich et al. "Theory of orbital magnetoelectric response". In: *New Journal of Physics* 12 (2010), p. 053032.

[212] Zhou Jian-Hui et al. "Topological invariants of metals and the related physical effects". In: *Chinese Physics Letters* 30.2 (2013), p. 027101.

[213] Maissam Barkeshli and Xiao-Liang Qi. "Topological Response Theory of Doped Topological Insulators". In: *Phys. Rev. Lett.* 107 (2011), p. 206602.

[214] Rundong Li et al. "Dynamical axion field in topological magnetic insulators". In: *Nature Physics* 6.4 (2010), pp. 284–288.

[215] Akihiko Sekine and Kentaro Nomura. "Chiral Magnetic Effect and Anomalous Hall Effect in Antiferromagnetic Insulators with Spin-Orbit Coupling". In: *Phys. Rev. Lett.* 116 (2016), p. 096401.

[216] Di Xiao et al. "Theory of electric polarization induced by inhomogeneity in crystals". In: *arXiv preprints arXiv:0711.1855* (2007).

[217] Di Xiao et al. "Polarization and adiabatic pumping in inhomogeneous crystals". In: *Physical review letters* 102.8 (2009), p. 087602.

[218] Yang Gao, Shengyuan A Yang, and Qian Niu. "Geometrical effects in orbital magnetic susceptibility". In: *Physical Review B* 91.21 (2015), p. 214405.

[219] R. Li et al. "Dynamical axion field in topological magnetic insulators". In: *Nature Physics* 6 (2010), pp. 284–288.

[220] Hirosi Ooguri and Masaki Oshikawa. "Instability in Magnetic Materials with a Dynamical Axion Field". In: *Phys. Rev. Lett.* 108 (2012), p. 161803.

[221] H. M. Price et al. "Four-Dimensional Quantum Hall Effect with Ultracold Atoms". In: *Phys. Rev. Lett.* 115 (2015), p. 195303.

[222] Yang Gao, Shengyuan A. Yang, and Qian Niu. "Field Induced Positional Shift of Bloch Electrons and Its Dynamical Implications". In: *Phys. Rev. Lett.* 112 (2014), p. 166601.

[223] Andrew M. Essin et al. "Orbital magnetoelectric coupling in band insulators". In: *Phys. Rev. B* 81 (2010), p. 205104.

[224] Chen Fang, Matthew J Gilbert, and B Andrei Bernevig. "Large-Chern-number quantum anomalous Hall effect in thin-film topological crystalline insulators". In: *Physical review letters* 112.4 (2014), p. 046801.

[225] Jing Wang et al. "Quantum anomalous Hall effect with higher plateaus". In: *Physical review letters* 111.13 (2013), p. 136801.

[226] Gotthard Sághi-Szabó, Ronald E. Cohen, and Henry Krakauer. "First-Principles Study of Piezoelectricity in $PbTiO_3$". In: *Phys. Rev. Lett.* 80 (1998), pp. 4321–4324.

[227] B. Langenecker. "Dislocation Damping in Macrosonic Fields". In: *Phys. Rev.* 145 (1966), pp. 487–491.

[228] R.E. Green. "Non-linear effects of high-power ultrasonics in crystalline solids". In: *Ultrasonics* 13.3 (1975), pp. 117 –127.

[229] A. Neubauer et al. "Topological Hall Effect in the *A* Phase of MnSi". In: *Phys. Rev. Lett.* 102 (2009), p. 186602.

[230] Minhyea Lee et al. "Unusual Hall Effect Anomaly in MnSi under Pressure". In: *Phys. Rev. Lett.* 102 (2009), p. 186601.

[231] B Fåk et al. "Pressure dependence of the magnetic structure of the itinerant electron magnet MnSi". In: *Journal of Physics: Condensed Matter* 17.10 (2005), p. 1635.

[232] K Shibata et al. "Large anisotropic deformation of skyrmions in strained crystal". In: *Nature nanotechnology* 10.7 (2015), pp. 589–592.

[233] H. M. Price et al. "Measurement of Chern numbers through center-of-mass responses". In: *Phys. Rev. B* 93 (2016), p. 245113.